JOINT TRANSPORTATION
RESEARCH PROGRAM
INDIANA DEPARTMENT OF TRANSPORTATION
AND PURDUE UNIVERSITY

Post-Fire Assessment of Prestressed Concrete Bridges in Indiana

Amit H. Varma, Jan Olek, Christopher S. Williams,
Tzu-Chun Tseng, Sijia Wang, Dan Huang, Tom Bradt

SPR-4221 • Report Number: FHWA/IN/JTRP-2021/05 • DOI: 10.5703/1288284317290

RECOMMENDED CITATION

Varma, A. H., Olek, J., Williams, C. S., Tseng, T.-C., Wang, S., Huang, D., & Bradt, T. (2021). *Post-fire assessment of prestressed concrete bridges in Indiana* (Joint Transportation Research Program Publication No. FHWA/IN/JTRP-2021/05). West Lafayette, IN: Purdue University. https://doi.org/10.5703/1288284317290

AUTHORS

Amit H. Varma, PhD
Karl H. Kettelhut Professor of Civil Engineering
Director of Bowen Laboratory of Large-Scale CE Research
Lyles School of Civil Engineering
Purdue University
Principle Investigator

Jan Olek, PhD
James H. and Carol H. Cure Professor in Civil Engineering
Lyles School of Civil Engineering
Purdue University
Principle Investigator

Christopher S. Williams
Assistant Professor of Civil Engineering
Lyles School of Civil Engineering
Purdue University
(765) 494-5828
csw@purdue.edu
Corresponding Author

Tzu-Chun Tseng
Sijia Wang
Dan Huang
Graduate Research Assistants
Lyles School of Civil Engineering
Purdue University

Tom Bradt
Senior Research Engineer
Bowen Laboratory
Purdue University

JOINT TRANSPORTATION RESEARCH PROGRAM

The Joint Transportation Research Program serves as a vehicle for INDOT collaboration with higher education institutions and industry in Indiana to facilitate innovation that results in continuous improvement in the planning, design, construction, operation, management and economic efficiency of the Indiana transportation infrastructure. https://engineering.purdue.edu/JTRP/index_html

Published reports of the Joint Transportation Research Program are available at http://docs.lib.purdue.edu/jtrp/.

NOTICE

TECHNICAL REPORT DOCUMENTATION PAGE

1. Report No. FHWA/IN/JTRP-2021/05	**2. Government Accession No.**	**3. Recipient's Catalog No.**
4. Title and Subtitle Post-Fire Assessment of Prestressed Concrete Bridges in Indiana		**5. Report Date** January 2021 **6. Performing Organization Code**
7. Author(s) Amit H. Varma, Jan Olek, Christopher S. Williams, Tzu-Chun Tseng, Sijia Wang, Dan Huang, and Tom Bradt		**8. Performing Organization Report No.** FHWA/IN/JTRP-2021/05
9. Performing Organization Name and Address Joint Transportation Research Program Hall for Discovery and Learning Research (DLR), Suite 204 207 S. Martin Jischke Drive West Lafayette, IN 47907		**10. Work Unit No.** **11. Contract or Grant No.** SPR-4221
12. Sponsoring Agency Name and Address Indiana Department of Transportation (SPR) State Office Building 100 North Senate Avenue Indianapolis, IN 46204		**13. Type of Report and Period Covered** Final Report **14. Sponsoring Agency Code**

15. Supplementary Notes

Conducted in cooperation with the U.S. Department of Transportation, Federal Highway Administration.

16. Abstract

This project focused on evaluating the effects of fire-induced damage on concrete bridge elements, including prestressed concrete bridge girders. A series of controlled heating experiments, pool fire tests, material tests, and structural loading tests were conducted. Experimental results indicate that the portion of concrete subjected to temperatures higher than 400°C loses significant amounts of calcium hydroxide (CH). Decomposition of CH increases porosity and causes significant cracking. The portion of concrete exposed to temperatures higher than 400°C should be repaired or replaced. When subjected to ISO-834 standard fire heating, approximately 0.25 in. and 0.75 in. of concrete from the exposed surface are damaged after 40 minutes and 80 minutes of heating, respectively. Prestressed concrete girders exposed to about 50 minutes of hydrocarbon fire undergo superficial concrete material damage with loss of CH and extensive cracking and spalling extending to the depth of 0.75–1.0 in. from the exposed surface. These girders do not undergo significant reduction in flexural strength or shear strength. The reduction in the initial stiffness may be notable due to concrete cracking and spalling. Bridge inspectors can use these findings to infer the extent of material and structural damage to prestressed concrete bridge girders in the event of a fire and develop a post-fire assessment plan.

17. Key Words prestressed concrete, bridge girder, fire, post-fire, damage, assessment	**18. Distribution Statement** No restrictions. This document is available through the National Technical Information Service, Springfield, VA 22161.

19. Security Classif. (of this report) Unclassified	**20. Security Classif. (of this page)** Unclassified	**21. No. of Pages** 87 including appendices	**22. Price**

EXECUTIVE SUMMARY

Introduction

This project focused on evaluating the effects of fire-induced damage on concrete bridge elements, including prestressed concrete bridge girders. A series of controlled heating experiments, pool fire tests, material tests, and structural loading tests were conducted. The results were used to establish the effects of heating due to standard ISO-834 and hydrocarbon fires on (1) temperature profiles through the concrete depth, (2) concrete material degradation due to decomposition of calcium hydroxide (CH), (3) concrete spalling and cracking through the depth, and (4) flexural and shear strength of prestressed concrete girders. The findings were used to develop guidelines for post-fire assessment of prestressed concrete bridges.

Findings

Two concrete bridge deck specimens from the I-469 bridge over Feighner Road were heated for different time durations (40–80 minutes) following the ISO-834 standard fire curve. Six prismatic specimens were designed and built to simulate the bottom flanges of prestressed bridge girders with different section layouts (two-strand and six-strand). Four (of the six) prismatic specimens were heated in the laboratory following the ISO-834 standard fire curve for different durations (30, 40, and 80 minutes) and heating conditions (two-sided and four-sided). Two (of the six) prismatic specimens built in the laboratory, and two AASHTO Type I girders, decommissioned from the bridge carrying I-469 over Feighner Road, were subjected to hydrocarbon pool fire tests conducted in the field for a duration of 48 minutes using approximately 135 gallons of kerosene.

The temperature profiles through the depths of all the specimens were measured during heating and natural cooling. After cooling, concrete samples were cored from the specimens for material analysis. Different types of material tests such as scanning electron microscopy (SEM), energy dispersive spectroscopy (EDS), and differential scanning calorimetry (DSC) were conducted to evaluate the extent of calcium hydroxide decomposition and the extent of concrete microstructure cracking through the depth of the concrete. For the AASHTO Type I prestressed girders, structural loading tests were conducted on control beams (without fire damage) and beams with extensive fire damage. After structural testing, material tests were also conducted on concrete cores taken from the girders.

The results from the experimental investigations indicate that the duration of heating determines the temperature profile through the thickness of concrete. If the fire lasts for a longer duration, the temperature through the depth of the concrete increases. The portion of concrete subjected to temperatures higher than 752°F (400°C) loses significant amounts of calcium hydroxide (CH), which decomposes by losing water and converting to calcium oxide (lime). The decomposition of CH increases porosity of the affected area. The portion of the concrete affected by CH decomposition also developed significant cracking, which further reduces the strength and increases permeability. It is highly recommended that the portion of concrete exposed to temperatures higher than 752°F (400°C) be considered fully damaged, and therefore repaired or replaced with new material.

When concrete components are heated following the ISO-834 standard fire curve, 0.25 in. of concrete from the exposed surface is compromised after approximately 40 minutes due to loss of CH and extensive cracking. After about 80 minutes of ISO-834 standard fire heating, 0.75 in. of concrete from the exposed surface is compromised by the loss of CH and extensive cracking. After about 50 minutes of an intense hydrocarbon fire, 0.75–1.0 in. of concrete from the exposed surface is compromised by the loss of CH and extensive cracking.

Prestressed concrete girders exposed to about 50 minutes of intense hydrocarbon fire undergo superficial concrete material damage with loss of CH and extensive cracking and spalling extending to the depth of 0.75–1.0 in. from the exposed surface. The reduction in the initial stiffness of the specimens may be notable due to concrete material damage, cracking, and spalling. In spite of the superficial concrete material damage, cracking, and spalling, these prestressed concrete girders do not undergo significant reduction in flexural strength or shear strength. Additionally, there does not seem to be significant influence on the bond between strands and concrete, and the prestressing force (or losses) in steel strands.

Implementation

Based on these conclusions, guidelines for post-fire assessment of prestressed concrete bridges are included in this report along with a step-by-step checklist. Bridge inspectors can infer the extent of damage to prestressed concrete bridge girders in the event of a fire and develop a post-fire assessment plan cognizant of the findings. In most cases, no more than 1.0 in. of the concrete from the exposed surface undergoes material damage/deterioration due to loss of CH, cracking, and spalling. The impact on the strength of prestressed concrete girders is relatively minor based on experimental results. Their initial stiffness, however, will likely be reduced. Recommendations for future work including research on long-term durability of fire damaged girders, and development of long-term repair methods are also included in the report.

CONTENTS

TABLE LIST

FIGURE LIST

1. INTRODUCTION

1.1 Background

Several fire events (Graybeal, 2007; Stoddard, 2004) in the United States involving highway bridge structures within the recent past have highlighted the need to gain a better understanding of the impact of fire on concrete bridge components. After a fire event, it is difficult for bridge inspectors to establish the intensity of the fire, the concrete surface temperatures that were experienced, and the associated damage at both the material and structural level. Research-based guidance is needed for bridge inspectors to accurately assess and evaluate the structural components exposed to fire. This guidance should address the extent of damage, the potential for repair, and the need for partial or complete replacement of concrete components subjected to fire events. The focus of the study presented in this report is the post-fire assessment of structural concrete of bridge components with the goal of providing guidance for evaluating material condition and structural integrity after a significant fire event.

1.2 Project Objectives

The main objectives of this project were to do the following:

- Conduct a literature review of the current state-of-knowledge regarding the assessment of concrete bridge components damaged by a fire event.
- Evaluate the effects of fire-induced damage on concrete bridge elements, including color change, cracking, and spalling.
- Measure the surface temperature and through-depth temperature profiles of concrete members exposed to heating with temperatures based on the ISO-834 (ISO, 2002) fire temperature-time curve.
- Evaluate the effects of fire-induced damage on the concrete microstructure and correlate the microstructure degradation with the through-depth temperature profiles of concrete specimens.
- Determine the impact of fire on the moment and shear capacities of prestressed concrete bridge girders.
- Develop recommendations and guidance for bridge inspectors to assess the quality of concrete bridge components subjected to a fire event.

2. LITERATURE REVIEW

2.1 Case Study–Prestressed Bridge Under Fire

In 2002, a railroad tanker collided on a prestressed girder bridge and caused a fire under the bridge, and the incident was inspected by the Washington State Department of Transportation (WSDOT) and reported by Stoddard (2004). About 30,000 gallons of methanol was consumed during the fire. The flame temperature of the fire was estimated to be around 3,000°F (1,649°C). According to Stoddard (2004), it is likely that the temperature of the bottom of the girders reached to almost 2,700°F (1,482°C) after only 30 minutes.

Inspections and evaluations have been conducted by WSDOT, showing that the surface temperature on the soffit of the prestressed girders was estimated to be around 1,700°F (927°C), with the internal temperature in the bottom flanges and webs ranging from 500°F to 1,100°F (260°C to 593°C). The damage of the concrete in the girders and columns was caused by the rapid heating and cooling rates. The outer part of concrete spalled and fell off, but the compressive strengths still exceeded 9,000 psi, which indicates the residual strengths for remaining concrete are still adequate.

An accident involving truck fire in Connecticut was reported by Graybeal (2007). In 2005, a gasoline tanker truck overturned and exploded causing significant damage to a box-beam bridge in southwestern Connecticut. About 8,000 gallons of burning fuel flowed over the bridge, and the temperature of the truck could have been over 4,472°F (2,467°C). Four beams were selected from different areas in the bridge and used to conduct flexural capacity tests. The results from those four beams showed that even the most damaged beam had the ultimate flexural capacity that was more than 10% higher than the analytically determined flexural capacity of the unburned beam. This indicates that the post-fire flexural capacity of beams was adequate. However, the long-term viability of the fire-damaged beams was more questionable, as the bottom flange concrete and strands may have experienced accelerated deterioration which can cause a long-term decrease in the flexural capacity of the beams.

A fire that damaged Chase Street Bridge in Indiana was evaluated by Ashraf and Olek (2016). In 2015, the truck fire under the Chase Street overpass near Gary, Indiana caused damage to several girders of the bridge, due to the collision of a semi-truck with the bridge in Indiana. An investigation was performed by Ashraf and Olek (2016) on the concrete samples extracted from the girders. The evaluation of concrete includes visual assessment of general conditions of concrete, detailed examination of the microstructure using Scanning Electron Microscopy (SEM) and Energy Dispersive Spectroscopy (EDS) techniques, and determination of change in the amount of calcium hydroxide (CH) in hydrated cement paste using Thermogravimetric Analysis (TGA) technique. Based on the results of investigations, cracking, debonding of aggregate, and increased micro porosity could be found near the surface of the concrete sample, which indicated that CH and calcium-silicate-hydrate (C-S-H) matrix were partially or fully decomposed and that the temperature around this area could be in the range of 752°F to 1,112°F (400°C to 600°C), and this range of temperature indicated that the concrete could lose as much as 60% of its original strength. With increase of the distance from the surface towards the interior of the sample, it seems that the inner region of the sample also had some levels of microstructural cracking that can be due to the decomposition of C-S-H, which suggested

that the inner region exposed to the fire temperature in the range of 212°F to 572°F (100°C to 300°C). The loss of the evaporable water caused the reduction of stiffness of C-S-H when temperature reaches to around 302°F (150°C), 60% of its stiffness was estimated to be lost based on the corresponding temperature range, according to Ashraf et al. (2016).

2.2 Concrete Exposed to High Temperature

2.2.1 Microstructure of Concrete

Increase in temperature can cause the change in the microstructures of both cement paste and aggregate in the concrete. According to Hager (2013), with temperature increasing, cement paste results in losing moisture, starting with free water, followed by capillary water, then physically bound water, and eventually water chemically bound with cement hydrates, which affects the mechanical properties of cement paste. For calcium hydroxide (CH), which is normally found in the transition zones between aggregate and cement paste, it starts to dehydrate at 752°F (400°C). For carbonates in coarse aggregate (e.g., limestone and dolomite), it decomposes into lime and gas at around 1,292°F (700°C). The gas can cause additional cracking and spalling. A summary table with the list of changes in concrete during heating is summarized by Hager (2013) and shown in Figure 2.1.

2.2.2 Properties of Concrete

According to Griffin and Beavis (1992), concrete exposed to high temperature will experience reduction of its compressive strength, modulus of elasticity, and stiffness. Degradation of concrete properties depends on the type of aggregate. Aggregates are mainly divided into two types: carbonate aggregates and siliceous aggregates. Carbonate aggregates include limestone, lime rock, and dolomite, all of which contain calcium and/or magnesium carbonate. The carbonate aggregate will undergo a thermal decomposition in the temperature range of about 1,110°F to 1,470°F (600°C to 800°C). This decomposition releases carbon dioxide which can cause considerable volume contraction and cracking of concrete, according to Ingham (2009).

Siliceous aggregates include silicon dioxide. For siliceous aggregates, they do not undergo any chemical changes within the temperature range of fire tests. Figure 2.2 also shows the change of compressive strength at elevated temperature for concrete using different types of aggregate. As shown in Figure 2.2, the strength of concrete with all types of aggregates starts to reduce when temperature reaches to about 800°F (about 400°C), which is also the temperature that calcium hydroxide (CH) in concrete decomposes.

When the temperature is at 410°F (210°C), modulus of elasticity decreases to 70% of original value. When the temperature is at 788°F (420°C), modulus of elasticity decreases to 50% of original value. When the

Temperature range	Changes
20–200°C	slow capillary water loss and reduction in cohesive forces as water expands; 80–150°C ettringite dehydration; C-S-H gel dehydration; 150–170°C gypsum decomposition ($CaSO_4 \cdot 2H_2O$); physically bound water loss;
300–400°C	approx. 350°C break up of some siliceous aggregates (flint); 374°C critical temperature of water;
400–500°C	460–540°C portlandite decomposition $Ca(OH)_2 \rightarrow CaO + H_2O$;
500–600°C	573°C quartz phase change $\beta - \alpha$ in aggregates and sands;
600–800°C	second phase of the C-S-H decomposition, formation of β-C_2S;
800–1000°C	840°C dolomite decomposition; 930–960°C calcite decomposition $CaCO_3 \rightarrow CaO + CO_2$, carbon dioxide release; ceramic binding initiation which replaces hydraulic bonds;
1000–1200°C	1050°C basalt melting;
1300°C	total decomposition of concrete, melting.

Figure 2.1 The list of changes taking place in concrete during heating (Hager, 2013).

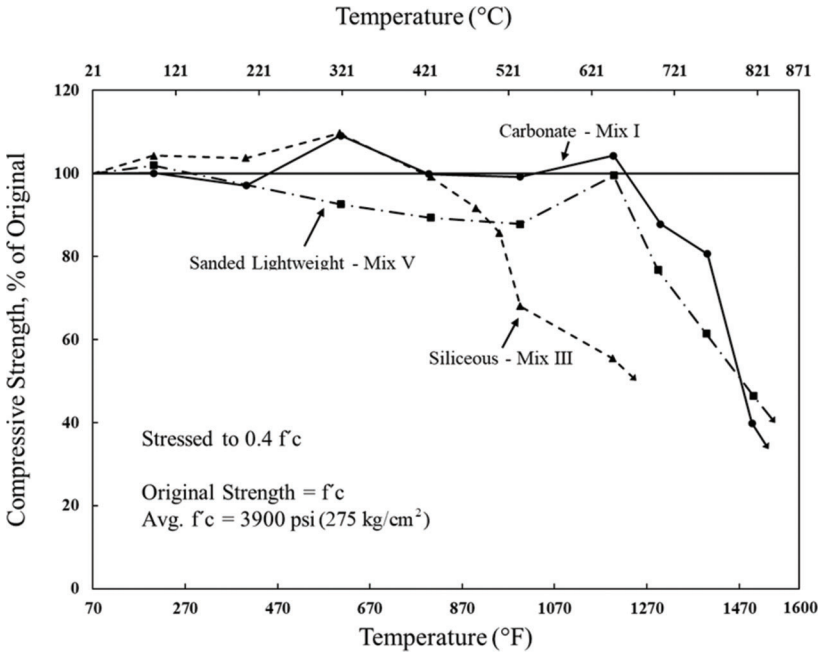

Figure 2.2 Compressive strength of concrete at high temperatures (Griffin & Beavis, 1992).

temperature is at 1,166°F (630°C), modulus of elasticity decreases to 30% of original value.

Griffin and Beavis (1992) also explained that the thermal stresses become higher than the compressive stresses when bridge deck is exposed to fire on one side. Also, rising temperature can cause further hydration of the cement and eventually a degradation in bond.

2.2.3 Color Change

According to Lee, Choi, and Hong (2010), high temperature can cause a change in color and reduce the residual compressive strength of concrete. The color of concrete changes to red in the temperature range from 572°F to 1,112°F (300°C to 600°C), to whitish grey in the temperature range from 1,112°F to 1,652°F (600°C to 900°C), and to buff in the temperature range from 1,652°F to 1,832°F (900°C to 1,000°C). According to Griffin and Beavis (1992), color changes can also be affected by the type of aggregate used in the concrete. The color change is more evident in concretes containing siliceous aggregate, compared to concrete with other types of aggregate. Griffin and Beavis (1992) also mentioned that a change in oxidation states of iron oxides present inside the aggregate may be responsible for reddish color of concrete.

2.2.4 Cracks and Spalling

Lee, Choi, and Hong (2010) stated that high temperature can also cause some visual changes, such as cracks, to concrete. When temperature is below 1,112°F (600°C), no crack or other changes are found. When temperature is higher than 1,292°F (700°C), cracks from 0.2 mm to 1.0 mm are observed. According to Griffin and Beavis (1992), expansion of concrete can be caused by increase in temperature, but the temperature increase can also lead to the shrinkage of the hardened concrete paste, which eventually can cause micro cracks during cooling process.

Griffin and Beavis (1992) mentioned that spalling can be caused by one-side heating on bridge deck, when temperature is increased rapidly on one side while the other side is still cool. Also, an increase in temperature can lead to conversion of entrapped water to steam and result in spalling.

2.3 Strands Exposed to High Temperature

2.3.1 Residual Strength

With heating the strand for a long period of time to various peak temperatures then cooling it down, residual ultimate strength of the strand decreases starting at when the maximum heating temperature exceeds 572°F (300°C). According to Moore (2008), the reduction of the residual strength starts increasing significantly when the temperature reaches to 752°F (400°C), and at 1,292°F (700°C), only 38% of ultimate tensile strength remains. The residual strength of the strands also depends on the time that strands were kept in the furnace. Strands kept at certain temperature for a shorter period were found to have higher residual strength. However, variation of cooling methods of strands did not have a significant influence on the results for the residual strength.

2.3.2 Relaxation

Similarly, stress relaxation occurs on the strands due to the heating, and the loss becomes irrecoverable after

the maximum temperature reaches to 752°F (400°C), according to MacLean (2007) and MacLean et al. (2008), The relaxation behavior is also affected by the maximum temperature applied to the strands. Higher temperature will produce much more stress relaxation losses. However, MacLean et al. (2008) also stated that relaxation is not affected by the time duration. As long as the temperature exceeds 752°F (400°C), even for a short period of exposure, the relaxation losses are still significant and irrecoverable.

2.4 Previous Experimental Research

2.4.1 Zheng and Hou (2008)

Zheng and Hou (2008) has conducted a series of fire experiments to study the mechanical behavior of pre-stressed concrete simply supported slabs subjected to fire. A furnace with dimensions 3 m by 4 m was used as heating equipment for the tests. The overview of the furnace used in Zheng's experiments is shown in Figure 2.3.

The results from Zheng and Hou (2008) is shown in Figure 2.4. From the figure, it is found that the tested temperature curve from thermocouples that were located near the exposed slab surfaces (short, dashed line) was slightly lower than ISO 834 (ISO, 2002) standard fire temperature (long dashed line), during the furnace test. These tested temperature measurements will be compared with the temperature measurements from this project tests in the future chapters.

2.4.2 Hou et al. (2014)

Hou et al. (2014) has also conducted a series of fire experiments using furnace as heating equipment. The heating chamber of the furnace with dimensions of 3 m by 4 m by 2.46 m was used as heating equipment, and eight oil burners are located inside the furnace in order to provide thermal energy. Thermocouples were distributed throughout the chamber to measure furnace temperature during the test. Figure 2.5 shows the comparison of temperature measurement from thermocouples attached at the furnace with ISO 834 standard fire curve. The temperature results from the furnace test verified that using furnace to simulate fire event can provide very similar air temperature compared to standard fire temperature curve. The surface temperature results from Hou (2014) will also be discussed and compared with the experimental results from this project in the future chapters.

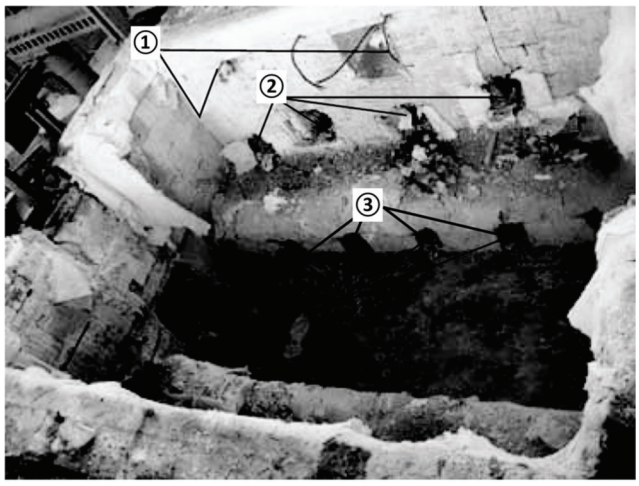

① fuel injection ② Thermocouples monitoring temperature of furnace ③ exhaust system

Figure 2.3 Overview of the furnace (Zheng & Hou, 2008).

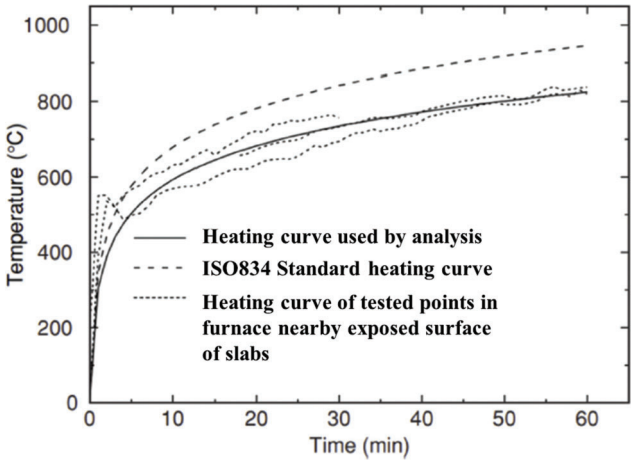

Figure 2.4 Surface temperature compared with ISO 834 standard curve (Zheng & Hou, 2008).

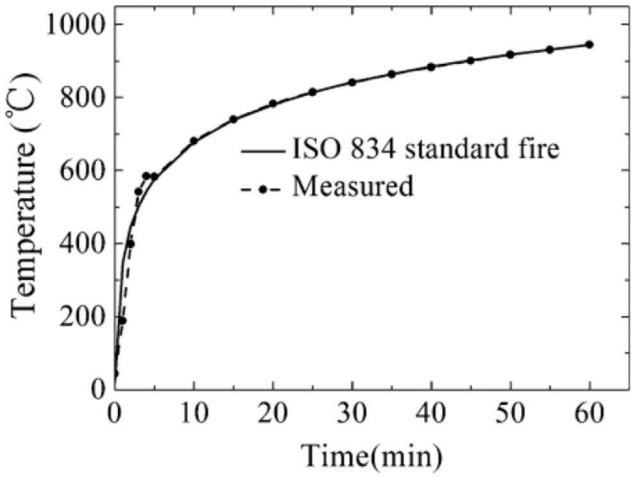

Figure 2.5 Measured temperature in the furnace during fire tests (Hou, 2014).

3. EXPERIMENTAL PROGRAM FOR CONCRETE DECK TESTS

3.1 Overview of Test Program

One-side heating tests were conducted using high-temperature ceramic heaters to evaluate the thermal and mechanical behavior of the specimen and measure

the temperature profiles through-depth. To evaluate concrete microstructure degradation, material tests were also conducted on samples taken from concrete cores from the specimen after heating.

Two concrete deck specimens were tested for 40 minutes and 80 minutes of heating following the ISO-834 (ISO, 2002) heating time-temperature curve. All deck specimens have the dimension of 48 in. by 48 in. with thickness of 8 in. The deck specimen was supported on rollers with 3-ft distance in between to allow free expansion in horizontal direction and provide supports in vertical direction. The rollers were 6 in. away from each end of the deck. The roller support system was placed on two 2-ft high concrete blocks to allow the instrumentation to be placed under the deck. The test setup is shown in Figure 3.1.

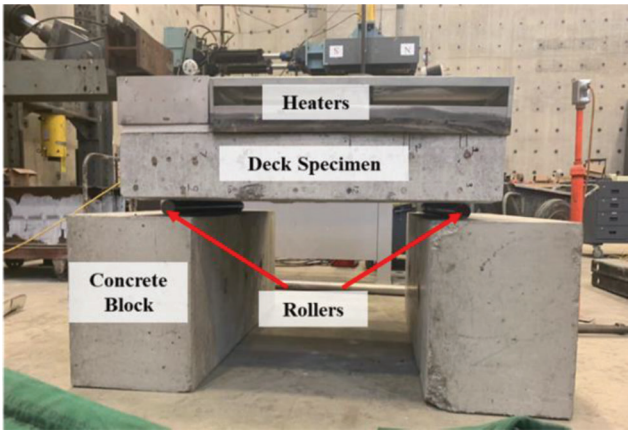

Figure 3.1 Test setup for heating experiment.

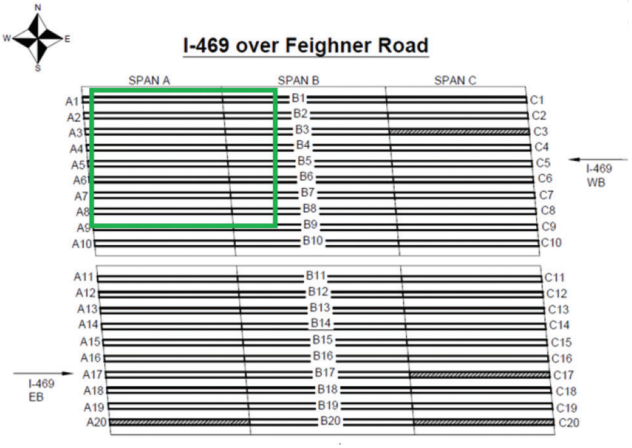

Figure 3.2 Plan view of I-469 over Feighner Road.

3.2 Test Details

3.2.1 Specimen Details

All test specimens were collected from I-469 bridge over Feighner Road. Deck sections were selected from the green area shown in Figure 3.2. The deck sections were cut and transported to Bowen Laboratory for testing. As shown in Figure 3.3, two pieces of deck sections with dimensions of 4 ft by 10 ft by 8 in. were originally cut from the bridge.

3.2.2 Preliminary Heating Test

A preliminary test was prepared and conducted in order to validate the installation method of thermocouple trees for the deck specimen and to verify that the testing method was representative to the standard fire test.

For the preliminary test, small beams with cross-section dimension of 6 in. by 6 in. and length of 22 in. were cast for testing. One thermocouple tree was installed before casting and another one was installed after casting in order to compare the temperature profiles between two sets of thermocouples. The thermocouple trees measured the temperature at 1 in., 1.5 in., and 2 in. from the exposed surface.

During the casting process, one set (Set A) of thermocouple trees was installed before casting. After the beam had been cured for a week, a 2-in. diameter hole was drilled to insert another set (Set B) of thermocouples. Once both sets of thermocouple trees were installed, packaged concrete mix was filled in the hole and cured for another week. The experiment was set up as shown in Figure 3.4. Insulation blocks were put on top of the small beam to avoid heater from coming into direct contact with concrete surface.

Figure 3.3 Original deck sections removed from I-469.

For the preliminary heating test, the small beam was heated for 100 minutes, and the surface temperature reached approximately 1,300°F (704°C).

3.3 Deck Heating Test Setup and Instrumentation

3.3.1 Heating System Setup

High-temperature ceramic-fiber radiant heaters were used to heat the deck specimens. Five ceramic heaters were placed above the deck, including three 36 in. by 16 in. heaters (Heater 1 to Heater 3) and two 24 in. by 12 in. heaters (Heater 4 and Heater 5), as shown in Figure 3.5.

Ceramic insulation cloth was placed in the gaps between heaters and at the edge of heaters. It can prevent heat loss during the test and avoid sensors from catching fire. Ceramic insulation blocks were also placed between the heater surface and the deck specimen so that heaters were not in contact with the specimen.

3.3.2 Thermocouples

Thermocouples were used to measure the temperature history at specific locations throughout the test. Type-K thermocouples were used, which are capable of measuring temperature up to 2,600°F (1,427°C).

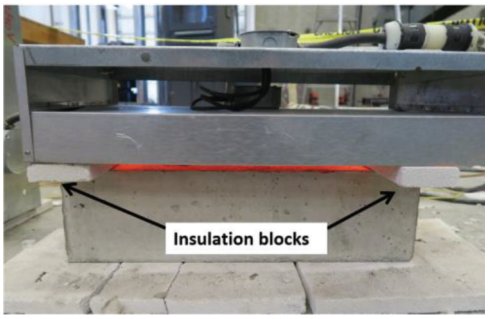

Figure 3.4 Preliminary test setup.

Thermocouples were placed at exposed surface of concrete to provide the temperature results at various locations during the test. One thermocouple tree was embedded at the center of the specimen to record the temperature through the depth of deck.

3.3.2.1 Surface thermocouples. In order to provide the temperature measurements throughout the surface area, thermocouples were placed at exposed surfaces of the deck at locations that are 1 ft away from the edge, at the center of the deck specimen, at the center of the heaters, and at the gaps between each heater, respectively, as shown in Figure 3.5. In total, 14 surface thermocouples were installed on each deck specimen, with one redundant thermocouple under each heater to make sure that the heater temperatures could be controlled and recorded.

3.3.2.2 Thermocouple tree. To provide the thermal profile through the depth of the deck specimen, a thermocouple tree was embedded at the center of the deck. As shown in Figure 3.6, the thermocouple tree contains 9 thermocouples welded along a steel rod at various depths: 0.25 in., 0.5 in., 0.75 in., 1 in., 1.25 in., 1.5 in., 2 in.

Each thermocouple was welded to the steel rod with its junction extending out from the rod; the thermocouples were also covered by the high temperature cement for insulating the thermocouples. A 2-in. diameter hole was drilled around the center of the deck specimen in order to place the thermocouple tree. After the thermocouple tree was positioned, the hole was filled with packaged concrete mix and cured for a week before the deck specimen was dried by a halogen lamp system.

3.3.3 Displacement Transducers

Displacement transducers (with 1-in. stroke) were used to measure the vertical displacement of the deck specimen. In total, five displacement transducers were

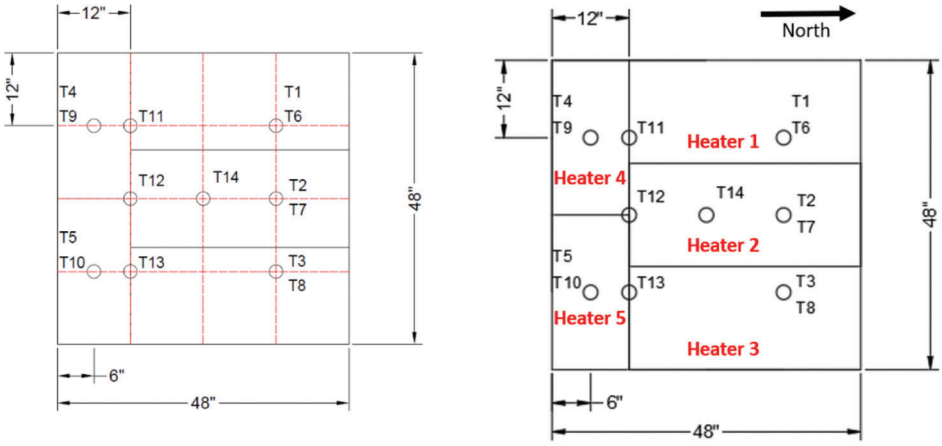

Figure 3.5 Layout of heating system and surface thermocouples.

placed under the bottom face of the deck specimen, four displacement transducers were located at quarter span, 12 in. from each edge, and one displacement transducer was at the center of the deck specimen.

3.4 Concrete Material Testing–Specimens Preparation and Evaluation Procedures

3.4.1 Location of Tested Cores

All test specimens used for material analysis were prepared from cores extracted from the deck specimens before and after heating events. The cored samples had the diameter of 2 in. and height of 8 in. As shown in Figure 3.7, the cores were removed from locations near the center of the specimen and close to the location thermocouple tree so that the results of material analysis results can be correlated with the through-depth temperature profiles of the concrete.

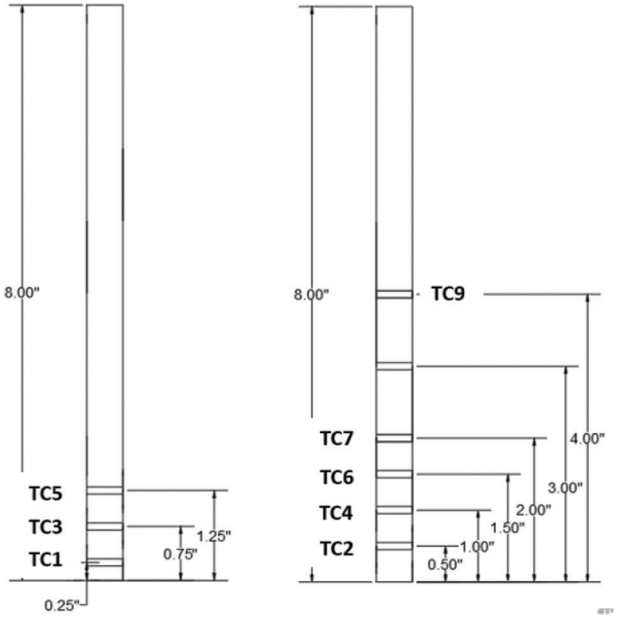

Figure 3.6 Thermocouple tree layout.

3.4.2 Preparation of the Scanning Electron Microscopy (SEM) Samples

The scanning electron microscopy (SEM) examination of the microstructure of concrete prior and after the exposure to the heating event can help to identify potential alterations of the microstructure, including estimation of the size and number of cracks, degree of debonding of aggregates, and qualitative assessment of changes in the type and the amount of phases.

The first step in preparation of the SEM specimens was removal of 2-in. thick slices from the top of the cores which were extracted from the deck specimens before or after heating tests. This disk was then vertically cut into two pieces (see Figure 3.7) with one of these pieces used for SEM analysis. The piece selected for SEM analysis was further cut into smaller specimens (about 1-in. thick) which were then epoxy impregnated and polished following the standard SEM samples preparation procedures. The specimens were mounted in the epoxy with the section of the vertical cut oriented horizontally to allow for examination of the changes in the microstructure with depth.

3.4.3 Preparation of Specimens for Differential Scanning Calorimetry (DSC) Analysis

Differential scanning calorimetry (DSC) is a method of material analysis that allows for quantification of the content of various phases (i.e., calcium hydroxide for the purpose of this research) based on the peak area associated with energy required for the decomposition of this particular phase.

To prepare the DSC samples, small pieces of concrete extracted from different depths were ground to

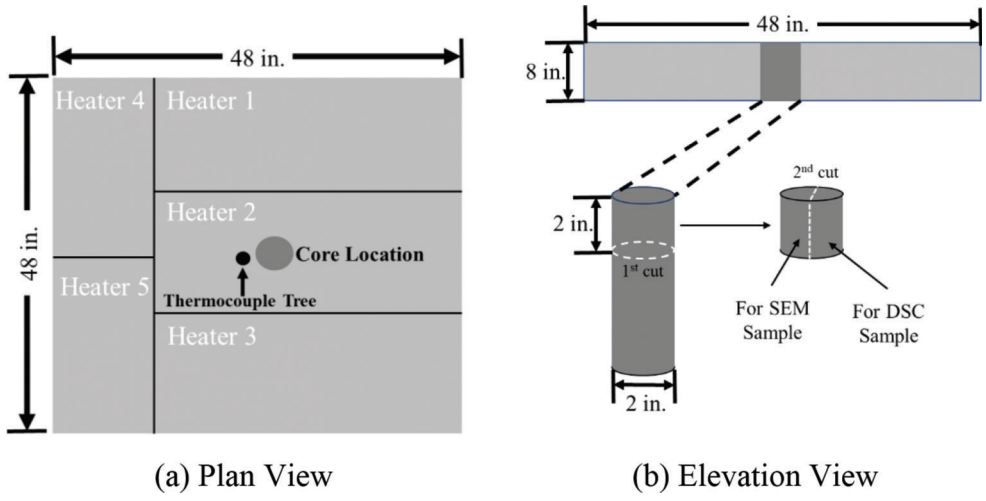

Figure 3.7 Location and preparation of material analysis samples from deck specimens.

obtain a powder that was then passed through a #200 (75 μm) sieve to ensure higher degree of homogeneity of the powder. About 10 mg to 18 mg sample was then removed from the previously prepared powder and transferred to an aluminum pan which served as a DSC sample holder. The pan was then placed in the DSC instrument and evaluated by heating the powder sample up to 600°C at the rate of 10°C/minute.

The quantification of the amount of calcium hydroxide (CH) present in the DSC sample required establishment of the calibration curve. The calibration curve was prepared by mixing various proportions of CH powder with fired kaolinite clay and determining the areas of the peaks in the DSC curves associated with the dehydration of this particular amount of CH. The amounts of CH used in the calibration process were as follows: 0%, 10%, 20%, 50%, and 100%. The calibration curve was produced by plotting these areas against the know amount of CH and determining the equation of the best-fitting line. The general equation of the resulting calibration line was as follows:

$$Content\ of\ CH\ (\%) = K\ x\ Peak\ Area\ (J/g)$$

where K is a constant that can be obtained from the best-fitting line.

4. EXPERIMENTAL RESULTS FOR CONCRETE DECK TESTS

4.1 Heating Test Results

Two 48 in. by 48 in. deck specimens with a thickness of 8 in. were heated using high-temperature ceramic fiber radiant heaters on one side. One specimen was heated for 40 minutes, and one specimen was heated for 80 minutes. The results were used to evaluate the through-thickness temperature profiles of concrete. Material tests conducted on core samples taken from the heated and unheated specimens were used to evaluate microstructure degradation and correlate it with through-thickness temperatures.

4.1.1 Preliminary Heating Test

A preliminary heating test was conducted to verify the testing method, heating approach, and the surface and thermocouple tree installation method used in the laboratory. The results were verified by comparing the measured temperature histories from the test with those reported in the literature from standard fire tests. One small beam with cross-sectional dimension equal to 6 in. by 6 in. and length equal to 22 in. was cast and tested. One thermocouple tree (Set A) was installed prior to casting, and another set (Set B) was installed after casting. The beam was over dried after installing the second set (B) of thermocouples. In this way, the temperature profiles measured and reported by the two sets of thermocouple trees (one placed before casting, and another installed after casting) could be compared.

Figure 4.1 shows the surface temperature-time curves measured during the preliminary heating test and compares them with (1) the ISO-834 (ISO, 2002) air temperature-time curve, and (2) the concrete surface temperature-time curves measured in standard furnace tests and reported in the literature. As shown in Figure 4.1, the surface temperature-time curves from the preliminary test were comparable to the concrete surface temperature-time curves from standard furnace tests reported in the literature by various researchers (Hou, 2014; Zheng & Hou, 2008). Thus, the high-temperature ceramic fiber radiant heaters used in the tests were able to simulate the heating associated with ISO-834 (ISO, 2002) standard fire tests.

Figure 4.2 shows the temperature histories measured by both sets (A and B) of thermocouple trees in the small beam specimen at corresponding depths. It is evident that the temperature histories for Set A and Set B are very similar and comparable. Thus, the through-depth temperatures can be measured accurately using thermocouple trees that were installed either before or after casting. Moreover, Figure 4.2 also compares the temperature-time histories from both sets of

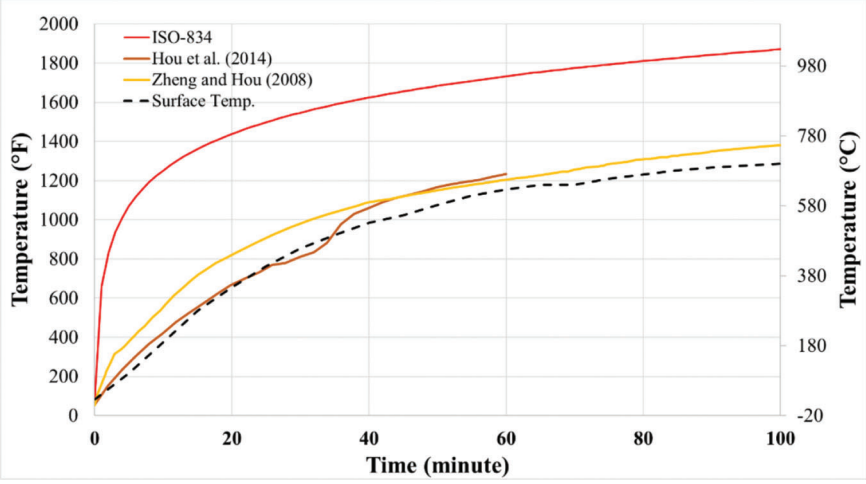

Figure 4.1 Surface temperature compared with standard fire tests.

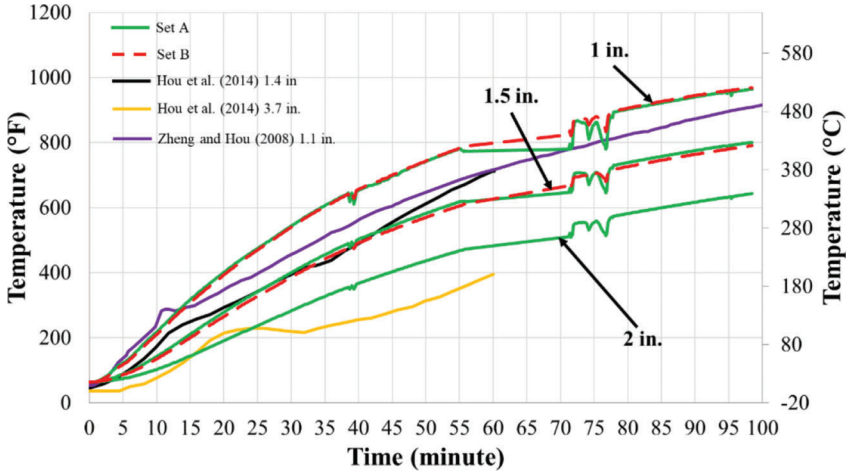

Figure 4.2 Through-depth temperature compared with previous research.

TABLE 4.1
Summary Table of Deck Specimen Names

Specimen Name	Duration of Heating
D-40-1100	40 Minutes
D-80-1600	80 Minutes

thermocouple trees with those reported by previous researchers. As shown, the temperature histories from the preliminary heating test compare reasonably with the temperature histories measured and reported within the concrete thickness by other researchers. This further verifies the heating approach and the temperatures measured by thermocouple trees installed before and after casting concrete.

4.1.2 Deck Specimen Heating Test

This section discusses the observations and results from the testing of concrete deck specimens (48 in. by 48 in. by 8 in.) from the I-469 bridge over Feighner Road. Each specimen is named as D—Test Duration in Minute—Maximum Surface Temperature in Fahrenheit. For example, D-40-1100 represents the deck specimen heated for 40 minutes to 1,100°F (593°F) at the exposed surface. A summary table of names of deck specimens is shown in Table 4.1.

4.1.2.1 40-minute heating test (D-40-1100). The first experiment involved heating the deck specimen on one side for 40 minutes. The heaters were placed on the exposed surface of the deck specimen. During the experiment, moisture was observed at 16 minutes, when the surface temperature was around 620°F (327°C) and kept coming out till the end of the test. Figure 4.3 shows the observation of moisture from deck specimen during the test. The locations with moisture were also observed to have cracks after the heating test.

After the test was finished, cracks on the exposed surface were observed and marked. It can be observed that cracks have developed due to thermal expansion. As shown in Figure 4.4, thin cracks (<0.005 in.) were observed. Most cracks were found along the locations of reinforcement bars, and some cracks extended into the side face of the specimen. No spalling was found at the surface of concrete. Concrete color at some areas at the exposed surface changed to darker grey after the heating test.

The test ended in 40 minutes. After 40 minutes of heating, the maximum surface temperature of concrete reached to 1,102°F (594°C), as shown in Figure 4.5. In addition, temperatures measured through the depth from 0.25 in. to 2 in. are also shown in Figure 4.5. Temperature at all depth increased constantly, with the same trend as surface temperature, till the end of test. Note that there is a plateau at around 200°F (93°C) due to the evaporation of free water from the concrete during heating.

The maximum temperatures for 40-minute heated specimen at 0.25 in., 0.5 in., 0.75 in., 1 in., 1.25 in., 1.5 in., and 2 in. are 897°F, 782°F, 667°F, 553°F, 495°F, 390°F, and 284°F (481°C, 417°C, 353°C, 289°C, 257°C, 199°C, and 140°C), respectively. As shown in Figure 4.5, temperature results for up to 0.25-in. depth from exposed surface is greater than the temperature to decompose calcium hydroxide (CH), for which the loss of CH can cause debonding cracks and increase in porosity in the microstructure of concrete and reduction in strength.

4.1.2.2 80-minute heating test (D-80-1600). The third experiment involved heating the deck specimen on one-side for 80 minutes. During the experiment, moisture was observed at 15 minutes, when the surface temperature was around 705°F (374°C) and kept coming out till the end of the test. Figure 4.6 shows the observation of moisture from deck specimen during test. The locations with moisture were also observed to have cracks after the heating test. At 69 minutes, duct tape on one of the heaters caught fire due to the extremely high temperature at the gap between heaters.

(a) At 16 Minutes–Surface Temperature: 620°F (b) At 36 Minutes–Surface Temperature: 1,041°F

Figure 4.3 Observation of moisture from D-40-1100 during test.

Figure 4.4 Map of cracks for D-40-1100.

All heaters were shut down for a safety check and turned back on. The whole process lasted for one minute and caused the decrease in temperature measurement.

After the test was finished, cracks on the exposed surface were recorded. As shown in Figure 4.7, wide cracks (about 0.005 in.) were observed. Most cracks were found along the locations of reinforcement bars, and some cracks extended into side face of the specimen. Spalling was easily found at the exposed surface. After the spalling part was cleaned, more aggregates were exposed. Concrete color at some areas at exposed surface changed to yellowish grey color after the heating test.

After 80 minutes of heating, the maximum surface temperature of concrete reached to 1,631°F (888°C), as shown in Figure 4.8. The temperature increased smoothly during the 80-minute test, except that the temperature slightly dropped for about 100°F (38°C) due to the shutdown of heaters at 70 minutes. Based on the surface temperature result from Figure 4.8, it can explain that spalling was caused not only by the thermal expansion but also by the decomposition of carbonates. When the temperature reaches to above 1,112°F (600°C), limestone starts to decompose and forms lime and gas, which causes the spalling on the heated surface.

The temperature from thermocouple tree was measured from 0.25 in. to 2 in. Through-depth temperature profile of D-80-1600 is shown as Figure 4.8. Temperature at all depth increased constantly till the end of test. The maximum temperatures at 0.25 in., 0.5 in., 0.75 in., 1 in., 1.25 in., 1.5 in., and 2 in. are 1,186°F, 1,080°F, 974°F, 880°F, 775°F, 692°F, and 553°F (641°C, 582°C, 523°C, 471°C, 413°C, 367°C, and 289°C), respectively. The shutdown of heaters at around 70 minutes caused the decrease in temperature till certain depth. As shown in Figure 4.8, temperature drop at 0.25-in. and 0.5-in. depth can be observed obviously. Also, temperature results for up to 1-in. depth from exposed surface is greater than the temperature to decompose calcium hydroxide (CH), for which the loss of CH can cause debonding cracks in the microstructure of concrete and reduction in strength.

4.1.3 Comparison Between 40-Minute and 80-Minute Heating Test Results

Figure 4.9 and Figure 4.10 show the comparisons of surface temperature and through thickness temperature between the 40-minute and 80-minute heating tests. The trends of measured temperature curves from 80 minutes of heating extend the trends of 40 minutes of heating. Finally, the maximum experienced temperatures at different depths of two deck specimens can be summarized as Table 4.2.

Figure 4.11 shows the comparisons of vertical deflection results at center between the 40-minute and 80-minute heating tests. As shown in Figure 4.11, deflections at centers of specimens increased with duration of heating and following the similar trends. The maximum deflections were 0.13 in. and 0.21 in. for two heating tests, respectively.

4.2 Microstructural Evaluation Results

4.2.1 Scanning Electron Microscope (SEM) Observations

The scanning electron microscope (SEM) equipped with the energy dispersive spectroscopy (EDS) x-ray detector was used to provide detailed information about the microstructure of concrete samples in terms of cracking, debonding of aggregates, and loss of phases by qualitative observations distribution of calcium hydroxide (CH) deposits.

The names and the exposure conditions of the SEM samples are summarized Table 4.3. In order to correlate

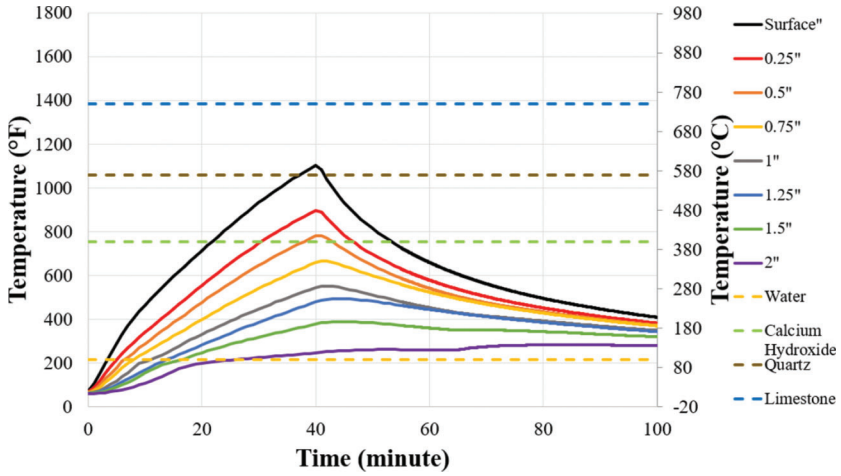

Figure 4.5 Through-depth temperature results of D-40-1100.

(a) At 15 Minutes–Surface Temperature: 705°F (b) At 76 Minutes–Surface Temperature: 1,597°F

Figure 4.6 Observation of moisture from D-80-1600 during test.

Figure 4.7 Map of cracks for D-80-1600.

to the temperature profiles to the microstructural changes the SEM observations were conducted at specified depths from the heated surface of the deck specimen (near the exposed surface, and at 0.25 in., 0.5 in., 0.75 in., 1 in., 1.5 in., and 2 in. from the exposed surface).

Figure 4.12 shows an example of SEM image which illustrates the main types of microstructural features that can be found in the micrograph of the typical hydrated cement paste. The full collection of images detailing various features of microstructure of specimens exposed to 40-minutes and 80-minutes heating tests is provided in Appendix B.

Figure B.1 and Figure B.2 show the SEM micrographs of the microstructure collected at various depths of, respectively, specimens heated for 40 minutes (Heated–40) and specimens heated for 80 minutes (Heated–80). In general, the microstructure of the paste in specimens extracted from shallower locations (i.e., those situated closer to the heated surface) appeared to be more damaged (i.e., it was more extensively cracked and contained larger voids) compared to the microstructure of specimens extracted from locations further away from the surface. When compared at the same depth from the surface, the porosity of the matrix increases with the increase in the temperature (e.g., compare images (a)–(d) of Figure B.1 with corresponding images of Figure B.2). Images collected from the microstructure of Heated–40 sample show extensive cracking to the depth of 0.5 in. form the heated surface whereas extensive cracking was observed to extend to the depth of 0.75 in. to 1.0 in. in Heated-80 specimen.

Figures B.3 to B.6 show locations of the CH (as identified by the EDS signal) within the microstructure of Heated–40 and Heated–80 specimens at different depths from the surface exposed to fire. In a normal mature concrete, the CH deposits are commonly found in the interfacial zone between the paste and the aggregate and appear as a thin, "whitish" layers ("ribbons") around the perimeter of the aggregate particles. These can be easily identified by a characteristic

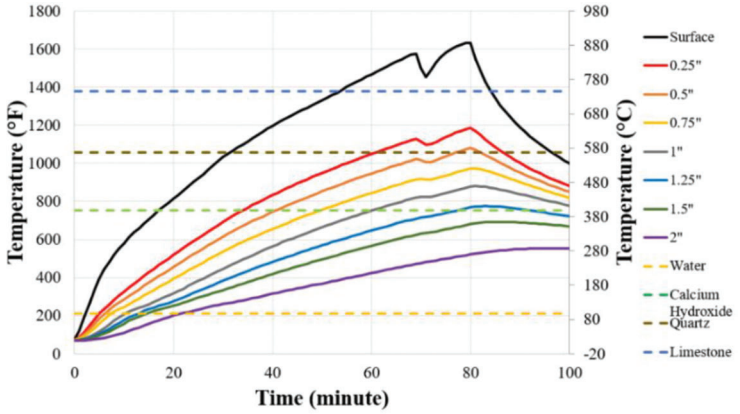

Figure 4.8 Through-depth temperature results of D-80-1600.

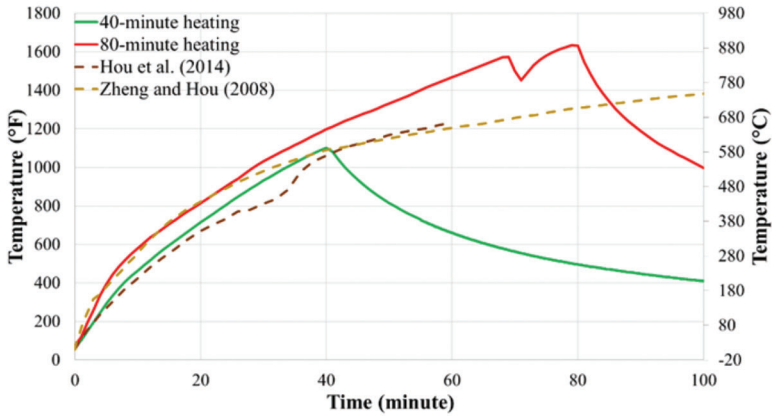

Figure 4.9 Comparison of surface temperature between 40- and 80-minute tests.

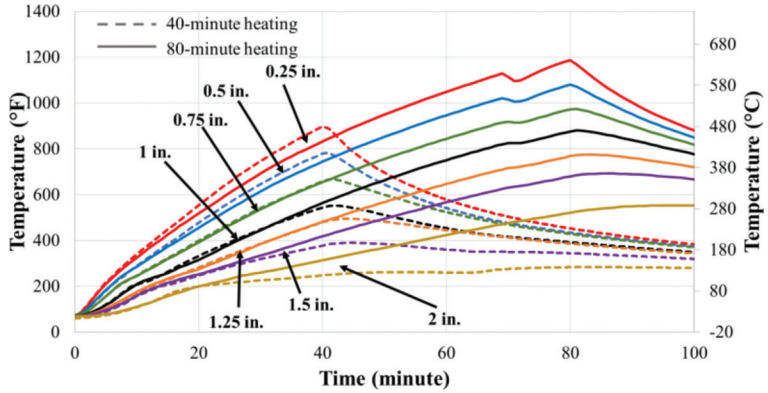

Figure 4.10 Comparison of temperature profiles between 40- and 80-minute tests.

calcium (Ca) peak in the EDS spectrum. If the temperature at the given location within the specimen increases to above 752°F (400°C), the CH starts losing water and decomposes. As such, the presence (or absence) of CH at a given location can serve as an indicator of the level of temperature that existed at a certain depth of concrete. CH deposits have been difficult to find in the microstructure in places where the temperature reaches the level of about 752°F to 932°F (400°C to 500°C) and lasted for more than 20 minutes.

To summarize, it is easier to find deposits of CH at locations more removed from the heated surface than it is to find them at locations closer to the heated surface. Specifically, in the case of Heated–40 specimen hardly any CH can be found around the pores or in the

TABLE 4.2
Maximum Temperatures at Through-Depth

Location	40-Minute Heating		80-Minute Heating	
	Maximum Temperature (°F[°C])	Time at Max. Temperature (min.)	Maximum Temperature (°F[°C])	Time at Max. Temperature (min.)
Surface	1,102 [594]	40	1,631 [888]	80
0.25 in.	897 [481]	40	1,186 [641]	80
0.5 in.	782 [417]	41	1,080 [582]	80
0.75 in.	667 [353]	41	974 [523]	81
1 in.	553 [289]	42	880 [471]	81
1.25 in.	495 [257]	44	775 [413]	83
1.5 in.	390 [199]	44	692 [367]	85
2 in.	284 [140]	79	553 [289]	94

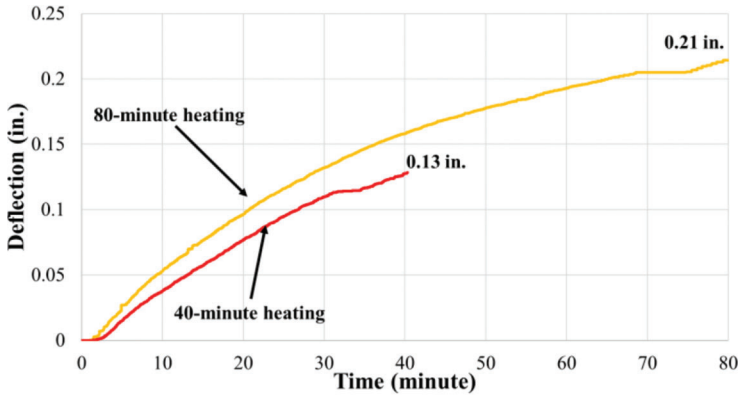

Figure 4.11 Comparison of vertical deflections at center between 40- and 80-minute tests.

TABLE 4.3
Summary of Names and Exposure Conditions for the SEM Specimens

Sample Name	Duration of Heating
Heated–40	40 Minutes
Heated–80	80 Minutes

interfacial transition zone (ITZ) at locations within the first 0.5 in. from the surface. In this specimen, the CH becomes more visible at depths greater than 0.75 in. from the heated surface. Similarly, only occasional deposits of CH (typically located along the cracks), can be found in the first 1.0 in. of the Heated–80 specimen. These findings corroborate the previously mentioned effects of high temperature on the microstructure.

4.2.2 Results of CH Content Determination from the DSC Analysis

Differential Scanning Calorimetry (DSC) is a material analysis method which can be used to quantify the content of various phases (i.e., CH in this case) and thus to indicate the impact of fire on the characteristics of the hydrated cement paste. Using this method, the content of a specific phase is calculated based on the area of the peak associated with the energy (heat flow) required to decompose this particular phase. Thus, DSC can provide quantitative estimation of the percent of CH present in the microstructure of concrete collected from a particular depth of the deck specimen.

The quantification process of any phase requires preparation of the calibration curve for this particular phase. In the current study, the calibration curve was developed by analyzing the DSC signal (heat flow) obtained by heating a mixture of known quantities of kaolinite and calcium hydroxide powders. The individual mixtures of powders contained the following percentages of these two materials: 0% CH (100% fired kaolinite), 10% CH, 20% CH, 50% CH, and 100% CH.

The decomposition of CH generates a peak in the DSC signal in the temperature range from 752°F to 932°F (400°C to 500°C) and the area of the peak is directly proportional to the amount of CH present in the sample being analyzed. These two paraments were plotted in the graph shown in in Figure 4.13 yielding linear relationship shown below:

$$CH\ Content\,(\%) = 0.0917\,x\,Peak\ Area\ (J/g)$$

Figures 4.14, 4.15, and 4.16 show the DSC curves for, respectively, the concrete powder collected from various depths of the unheated specimen and two of the

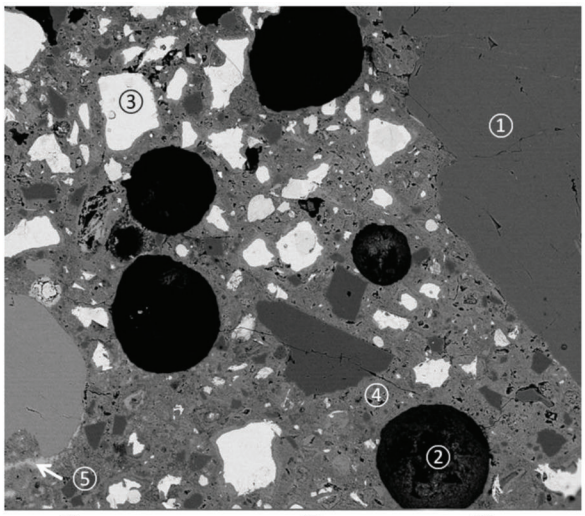

Note: ①: Aggregate ②: Pore ③: Unhydrated Cement ④: Paste Matrix ⑤: CH at Interfacial Transition Zone

Figure 4.12 Main microstructural features observed in SEM images.

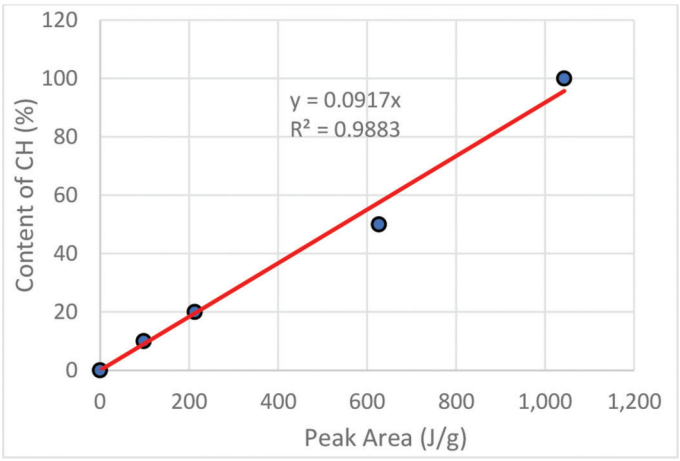

Figure 4.13 Calibration curve used for determination of the CH content.

heated specimens. In each case, the DSC signals contain two main groups of peaks. The first group of peaks can be found at the temperature of about 212°F (100°C) while the second group can be found in the temperature range from 754°F to 932°F (400°C to 500°C). The first group of peaks represents the change of energy associated with removal of the evaporable water, a process which does not lead to a reduction of strength. However, the changes in the relative intensities and associated areas of these peaks give a good indication of the duration and the level of the elevated temperature event happening at this particular location. The peaks in the temperature range from 754°F to 932°F (400°C to 500°C are associated with the decomposition of calcium hydroxide (CH). The smaller the peak, the higher the amount of CH lost from the microstructure. Substantial losses (more than 40%–50%) of the CH will make the matrix more porous and reduce its strength and durability.

Figure 4.14 shows the results of the DSC analysis for the unheated specimen. As can be seen, the CH peak obtained from the material located within the first 0.25 in. from the surface is smaller than the peaks obtained from powders collected from greater depths. This reduced content of CH is the result of the carbonation of the near-surface concrete, a process that converts CH into calcium carbonate. The sizes of the peaks at depths greater than 0.5 in. from the surface are similar, indicating that at these locations the effects of carbonation were insignificant.

Figure 4.15 shows the DSC results obtained from the Heated–40 sample. As can be seen, the CH peak for material located within the first 0.25 in. is significantly smaller than the peaks associated with materials from greater depths. It is also smaller than the CH peak obtained for the same region of the unheated sample, indicating severe effects of the elevated temperature in this part of the specimen. Figure 4.16 shows the results

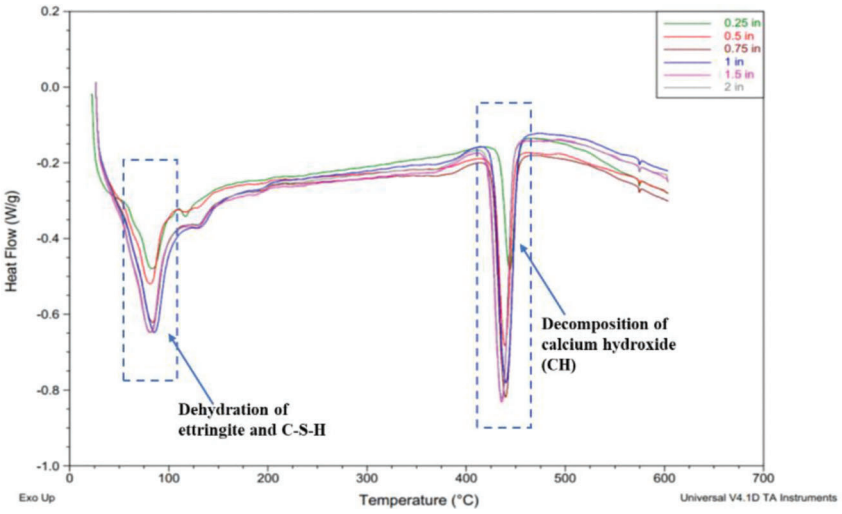

Figure 4.14 DSC curves for analysis of powders collected from different depths of unheated specimen.

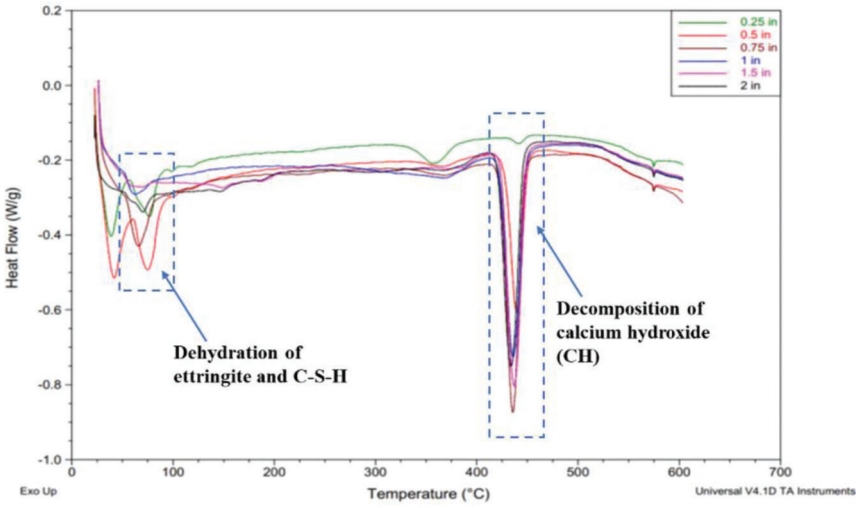

Figure 4.15 DSC curves for analysis of powders collected from different depths of specimen heated–40.

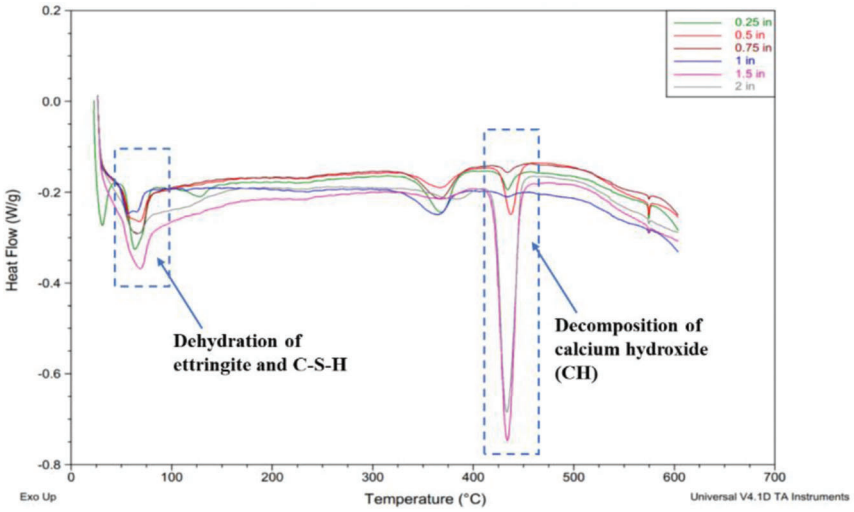

Figure 4.16 DSC curves for analysis of powders collected from different depths of specimen heated–80.

TABLE 4.4
Estimated CH Content of All DSC Specimens

	Unheated		Heated–40			Heated–80		
Depth (in)	Peak Area (J/g)	CH (%)	Peak Area (J/g)	CH (%)	% Change in CH (%)	Peak Area (J/g)	CH (%)	% Change in CH (%)
0.25	24.13	2.21	1.24	0.11	94.9	2.84	0.26	88.2
0.5	39.18	3.59	34.86	3.20	11.0	8.65	0.79	77.9
0.75	57.30	5.25	55.65	5.10	2.9	1.22	0.11	97.9
1	60.53	5.55	52.02	4.77	14.1	0.84	0.08	98.6
1.5	61.00	5.59	56.73	5.20	7.0	53.56	4.91	12.2
2	58.94	5.40	53.57	4.91	9.1	47.75	4.38	19.0

Note:
Where $\%\ Change\ in\ CH = (CH_{Unheated} - CH_{Heated})/CH_{Unheated}\ x\ 100\%$.

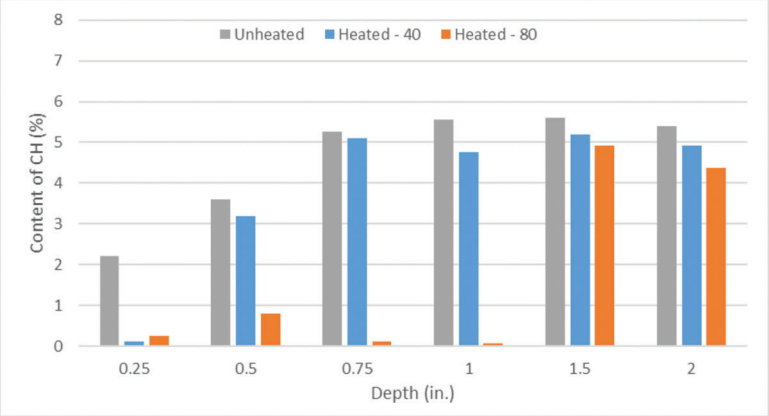

Figure 4.17 Comparison of CH content for all DSC samples.

of the DSC analysis from the Heated–80 sample. In this case, the reduced sizes of the CH peaks are observed all the way to a depth of about 1.0 in. from the surface, indicating the severity of the 80 minutes heating cycle.

The calculated quantities of the CH obtained from the DSC measurements are summarized in Table 4.4 and shown graphically in Figure 4.17. These quantitative results also indicate that while the 40-minutes heating cycle may be affecting only the first 0.25 in. of the specimens (i.e., the zone located closest to the heat source), the increase of the heating duration to 80 minutes impacts the microstructure to the depth of about 1.0 in. from the heated surface.

5. EXPERIMENTAL PROGRAM FOR PRESTRESSED CONCRETE PRISMATIC SPECIMENS

5.1 Overview of Test Program

Eight-foot-long prestressed concrete members with a cross-sectional dimension of 8 in. by 8 in. were cast in the laboratory to simulate the bottom flanges of INDOT Bulb-Tee girders (Figure 5.1). The test specimens consist of three groups with different magnitudes of prestressing force, heating durations, and heating conditions. The specimens were first tested in the laboratory with radiation-based ceramic heaters. For the specimens tested in the laboratory, they were supported on rollers with 80-in. distance in between

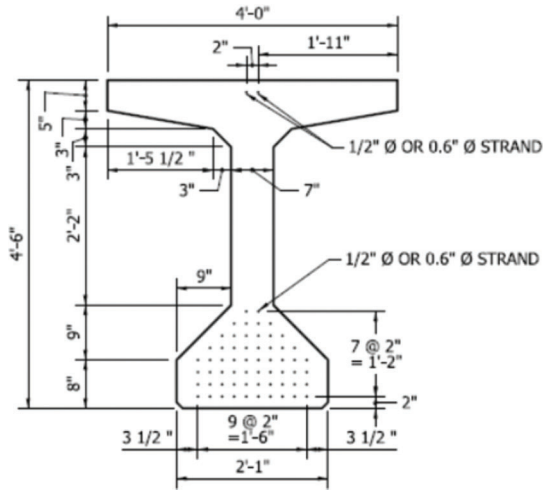

Figure 5.1 Typical INDOT bulb-tee section (INDOT, 2013).

to allow the specimen to expand and rotate freely in longitudinal and transverse directions. The rollers were 8 in. away from each end of the concrete member. The roller support system was placed on two 2-ft high concrete blocks to allow the radiation-based heaters to be set on two sides or four sides to the specimen. The test setup is shown in Figure 5.2.

After conducting the heating tests in the laboratory, two prestressed concrete specimens were transported to Beck Agricultural Center to perform a pool fire (Figure 5.3). About 132 gallons of kerosene was used, and the specimens were burned for about 48 minutes. Once the specimens were cooled sown, samples were cored from the heated specimens. Material tests were carried out on the cored samples to determine the degree of degradation of the concrete microstructure.

5.2 Test Details

5.2.1 Specimen Details

Considering the INDOT design output for the typical prestressed concrete bridge girders; prismatic specimens with two different layouts of prestressing strands were designed and constructed; the first one consists of two strands with initial prestressing stress of 185 ksi which simulates stress conditions for the midspan; the other one is the case that consists of six strands initially stressed to 203 ksi that simulates stress conditions for the ends of a bridge girder.

Figure 5.2 Test setup for heating experiment with radiation-based heaters.

Figure 5.3 Completed test setup for pool fire test observed from south.

To achieve the target initial prestress levels and reproduce the INDOT practical designs, seven-wire low relaxation strands with an ultimate breaking strength of 284 ksi and a diameter of 0.52 in. were stressed to provide decent compression to the sections. It should be noted that the locations of prestressing strands and rebars were designed following 2 in. by 2 in. grids, and the strands were located at 2 in. from the concrete surfaces, which follows the design layout of the typical prestressed bridge girders. Finally, stirrups were also placed along the span to provide adequate confinement in the transverse direction. The design details for prismatic specimens are illustrated in Figure 5.4.

Concrete used for fabricating the specimens was designed to follow the INDOT design practice and met the requirements in INDOT standard specifications (INDOT, 2016). Type III cement was used to achieve adequate early-age compressive strength while cutting the stressed strands for stresses transferring. There are two batches for different series of specimens, first one (Batch 1) is for specimens consist of two prestressed strands and the other one (Batch 2) is for specimens with six strands. The mix proportions in each cubic yard of concrete are shown in Table 5.1.

Table 5.2 shows the concrete compressive strengths at different ages which are obtained from the concrete cylinder tests. To introduce the designed prestressing force to the specimens, strands were released once the concrete compressive strength reached 6,000 psi. From the test results, the strands were released at 11 days and 14 days from casting for two series of specimens, respectively.

5.3 Setup and Instrumentation for Heating Test with Ceramic Heaters

5.3.1 Test Matrix and Heating System Setup

Table 5.3 tabulates the test matrix of the prismatic specimens, the first two prismatic specimens with two prestressing strands (PS1 and PS2) were heated on two sides for different heating durations (40 minutes and 80 minutes) using radiation-based heaters. The heating system setup consisted of six ceramic-fiber radiant heaters. On each side, three heaters (two with 36 in. by 8 in. and one with 24 in. by 8 in.) were connected together by steel angles and placed on the supports to cover whole specimen, as shown in Figure 5.5(a).

After the first two specimens were tested, according to the measured temperature profiles, only the specimen heated for 80 minutes had experienced the temperature that was high enough to decompose of CH in concrete. Therefore, the two-sided heating test on the specimen with six strands was conducted only for 80 minutes heating duration (PS3) following the identical testing setup and procedure.

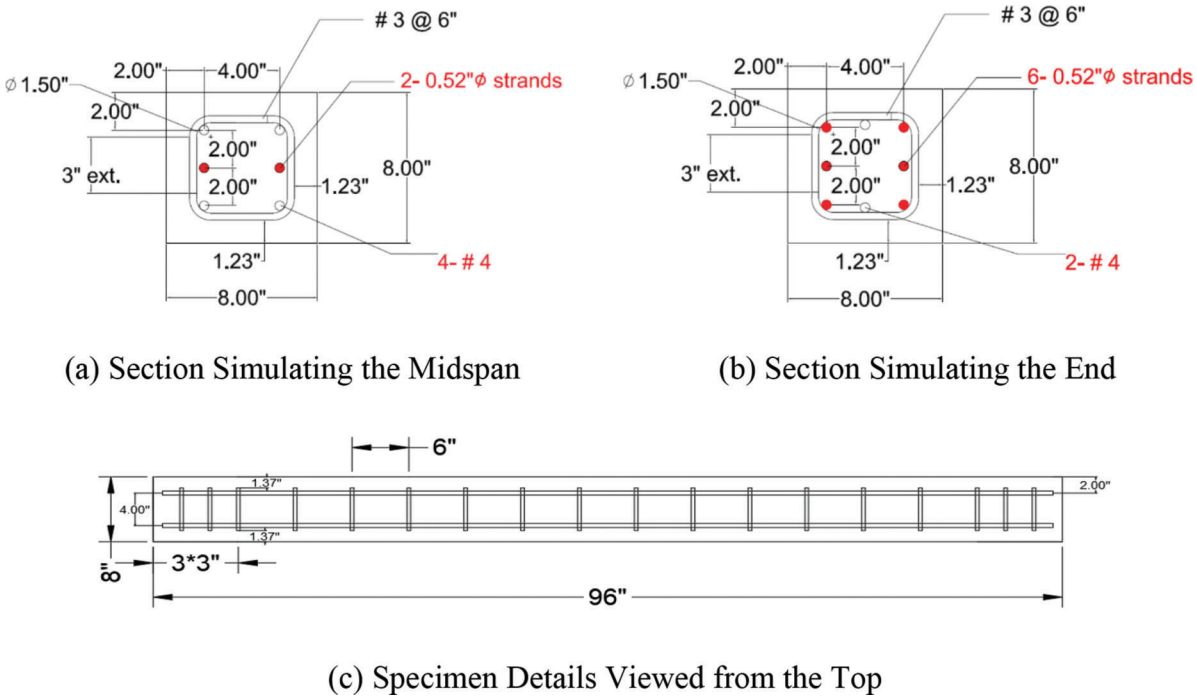

Figure 5.4 Design details for prismatic specimens.

TABLE 5.1
Batch Proportions of Concrete Mixes

Description (per cubic yard)	Batch 1 (01/2019)	Batch 2 (07/2019)
Cement (Type III), lb.	730	732
#11 Coarse aggregate, lb.	1,700	1,716
#23 Fine aggregate, lb.	1,240	1,192
Water, lb.	267	270
W/C Ratio	0.366	0.369

TABLE 5.2
Concrete Compressive Strengths History

Batch 1 (01/2019)		Batch 2 (07/2019)	
Age	Compressive Strength (psi)	Age	Compressive Strength (psi)
1 Day	3,450	2 Days	5,250
4 Days	4,690	5 Days	5,550
7 Days	4,790	9 Days	5,860
11 Days	6,090	14 Days	6,130

TABLE 5.3
Test Matrix of Prismatic Specimens

Test Specimens	No. Heating Faces	Heating Time (min)	No. Strand	fpi (ksi)	fpe (ksi)	Avg. Concrete Stress (ksi)	Test Day Compressive Strength (psi)
PS1	2	40	2	185	163	0.77	5,540
PS2	2	80	2	185	163	0.77	5,740
PS3	2	80	6	203	163	2.26	6,170
PS4	4	30	6	203	163	2.26	6,350
PS5	Pool Fire	48	6	203	163	2.26	6,380
PS6	Pool Fire	48	6	203	163	2.26	6,380

The heating condition for the last group of tests is the four-sided heating case; the radiation-based heaters were placed surrounding the specimens with six strands to simulate the extreme scenario (PS4). Two 36 in. by 8 in. heaters and one 24 in. by 8 in. heater were placed on the top, moreover, two 24 in. by 8 in. heaters were supported by wood blocks to heat the bottom of the specimen. As demonstrated in Figure 5.5(b), including six heaters laid in two sides, there were a total of eleven heaters to heat the specimen. The specimens were expected to be heated for 80 minutes. However, at 30 minutes from the beginning of the four-sided heating test, severe spalling was observed at a corner of the specimen, and the test was terminated for safety concerns. Lastly, a pool fire test was performed on two of the specimens with six strands (PS5 and PS6) to investigate the performance of the specimens in real hydrocarbon fire scenario.

5.3.2 Thermocouples

To obtain the internal temperature profile through the depth of the prismatic specimen. Three thermocouple trees including two different layouts were installed in each specimen. The first layout (layout A) contains 10 thermocouples welded along a steel rod within the length of 8 in. at different locations: 0.5 in., 1 in., 1.5 in., 2 in., 3 in. from both side surfaces. The second layout (layout B) consists of 7 thermocouples: 0.25 in., 0.75 in., 1.25 in. located from both side surfaces and one thermocouple was weld in the midpoint.

Moreover, several thermocouples were also installed in strands and reinforcing bars for measuring the temperature-time history at the metal components. The thermocouple was welded to the strands or reinforcing bars first, afterwards, the high temperature cement was applied on the thermocouple to provide the insulation.

5.3.3 Strain Gauges

The variation of prestressing forces can be estimated by the measured strains in the reinforcing bars and strands. To monitor strains of the specimens, several strain gauges were attached to the specimens. For directly measuring the prestressing force variation, strain gauges were also applied on the strands. The procedure of the installation is like that for the rebars; however, the strand consisted of seven steel wires so the strain gauge can only be placed at one of the wires.

Figure 5.6 and Figure 5.7 present the instrumentation layouts for the prismatic specimens. To summarize,

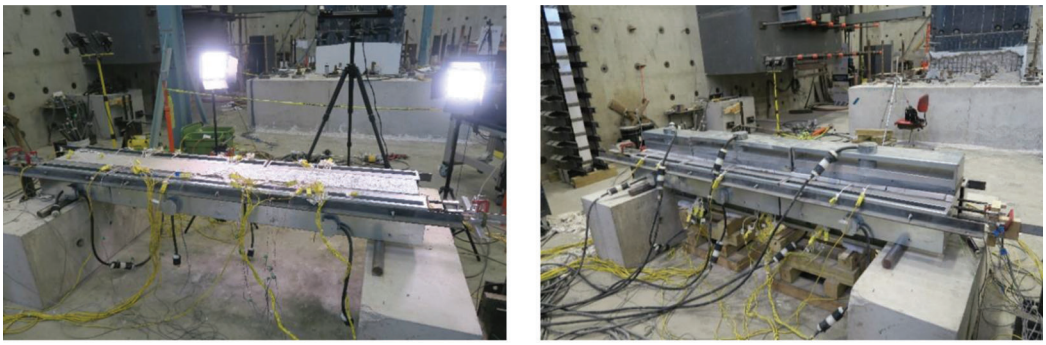

(a) Two-Sided Heating Test (b) Four-Sided Heating Test

Figure 5.5 Setup for controlled heating tests.

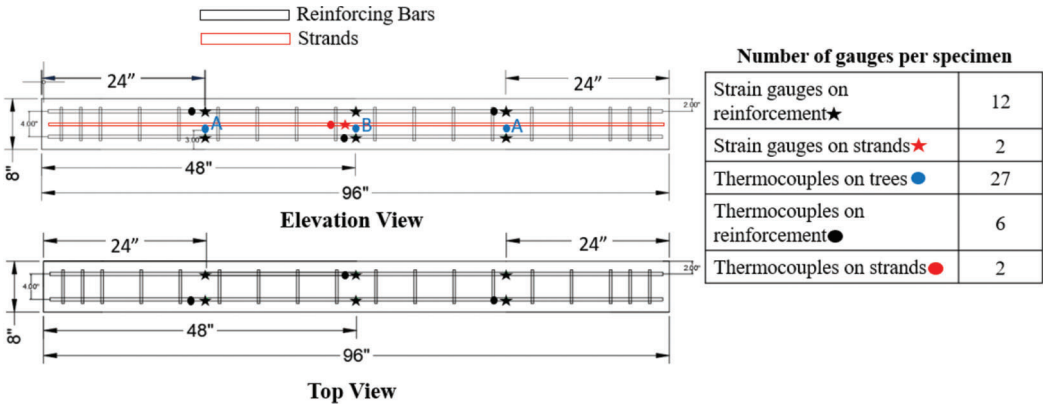

Number of gauges per specimen

Strain gauges on reinforcement★	12
Strain gauges on strands★	2
Thermocouples on trees●	27
Thermocouples on reinforcement●	6
Thermocouples on strands●	2

Figure 5.6 Instrumentation layout for specimens PS1 to PS2.

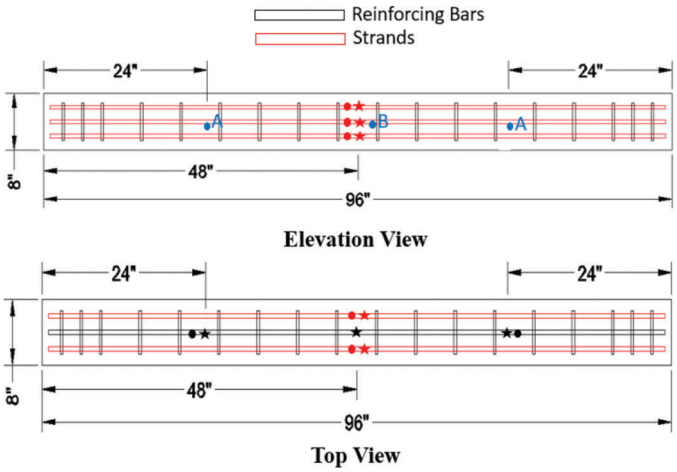

Number of gauges per specimen

Strain gauges on reinforcement ★	6
Strain gauges on strands ★	6
Thermocouples on trees ●	27
Thermocouples on reinforcement ●	4
Thermocouples on strands ●	6

Figure 5.7 Instrumentation layout for specimens PS3 to PS6.

there are 35 thermocouples and 14 strain gauges for the specimens consisting of two strands (PS1 to PS2). Moreover, there are 37 thermocouples and 12 strain gauges for the specimens consisting of six strands (PS3 to PS6). It should be noted that the layouts of the thermocouple trees are identical for these two series of specimens.

5.3.4 Displacement Transducers

For the specimens PS1 and PS2, four displacement transducers were used to measure the deformation of the strands and two displacement transducers were used to measure the displacement of the concrete in two ends. Considering the specimens PS3 and PS4, twelve displacement transducers were used to measure the deformation of the strands and two displacement transducers were used to measure the displacement of concrete. To stabilize the sensor setup, displacement transducers were clamped to the aluminum angles and the angles were connected to a steel stand sitting on the floor.

5.4 Setup and Instrumentation for Pool Fire Test

5.4.1 Design and Test Setup for The Pool Fire Test

A pool fire test was conducted on two of the prismatic specimens containing six strands (PS5 and PS6) in the Beck Agricultural Center of Purdue University in March 2020. A 4 ft by 8 ft by 11 in. pool was used to contain kerosene as the fuel to burn the specimens. The amount of the kerosene was estimated according to the equations provided by the *SFPE Handbook of Fire Protection Engineering* (Hurley et al., 2016) based on the selected type of fuel and pool size. After calculation, about 132 gallons of the kerosene is needed to sustain a 1-hour burning duration and it would cause a flame with the height in 16.8 ft.

To trap the flame during the test, twelve 2 ft by 4 ft by 2 ft concrete blocks were used to build the barriers surrounding the specimen to restrain the fire. Moreover, two 48 in by 70 in by 1 ft decommissioned deck sections obtained from I-65 over Wabash River were placed on the top of two prismatic specimens for concentrating the fire.

5.4.2 Thermocouples

Figure 5.8 shows the layout of the thermocouples in the pool fire test. Two internal thermocouples located at 0.5 in. and 1 in. from bottom of each specimen were used and connected to the data acquisition system (DAQ). Moreover, 22 thermocouples installed on the bottom surfaces and side surfaces of two prismatic specimens. Moreover, there were also two thermocouples located at the center of each overlaying deck section to measure the temperature-time history of the deck bottoms. Lastly, four thermocouples were fixed on a rebar which was inserted into the ground. These four thermocouples were located at 1 ft, 2 ft, 3 ft, and 4 ft from the surface pool bottom for measuring the fire temperatures at various locations during the test.

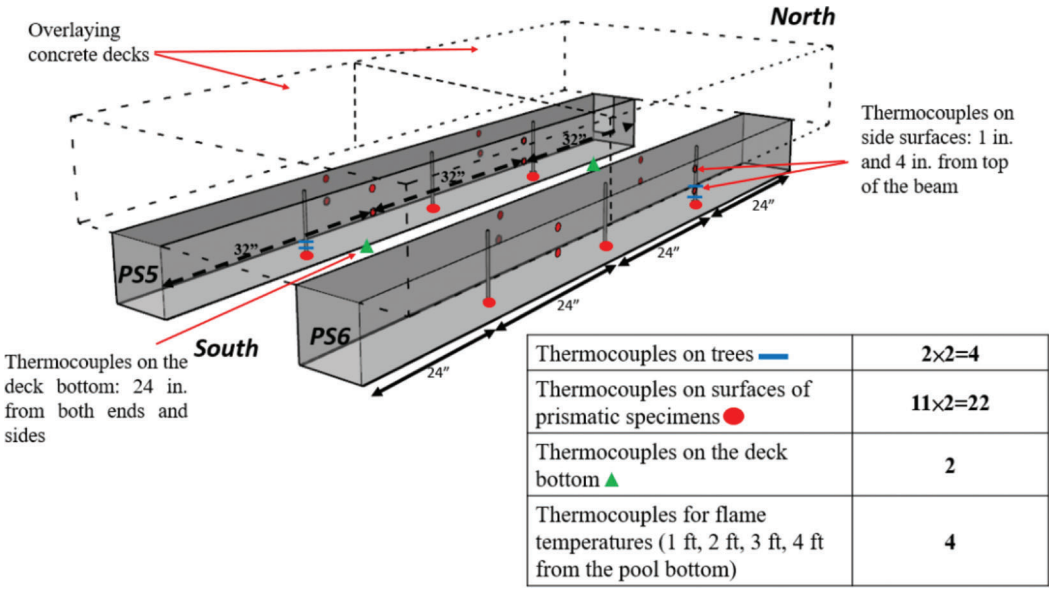

Thermocouples on trees	2×2=4
Thermocouples on surfaces of prismatic specimens	11×2=22
Thermocouples on the deck bottom	2
Thermocouples for flame temperatures (1 ft, 2 ft, 3 ft, 4 ft from the pool bottom)	4

Figure 5.8 Instrumentation layout of pool fire test.

6. EXPERIMENTAL RESULTS FOR PRISMATIC SPECIMENS TESTS

6.1 Test Results for Prismatic Specimens Heated by Ceramic Heaters

Four 8 in. by 8 in. prismatic prestressed concrete specimens with a span of 8 ft were heated using ceramic radiation-based heaters. Two specimens consist of two strands were heated from two sides for 40 and 80 minutes, and one specimen with six strands was heated from two sides for 80 minutes. Lastly, a specimen consists of six strands was heated by the surrounded heaters, the test was terminated at 30 minutes due to the severe spalling.

6.1.1 Heating Test Results

The tested specimens discussed in this section including: (1) PS1 (specimen with 2 strands heated for 40 minutes from two sides); (2) PS2 (specimen with 2 strands heated for 80 minutes from two sides); (3) PS3 (specimen with 6 strands heated for 80 minutes from two sides); and (4) PS4 (specimen with 6 strands heated for 30 minutes from four sides).

6.1.1.1 40-minute two-sided heating test for specimen with two strands (PS1). During the experiment, moisture was observed along with a crack on the top at 23 minutes, when the average exposed surface temperature reached 875°F (468°C). The moisture kept seeping out and spreading during the heating test until heaters were turned off. Figure 6.1 shows the moisture observed on top of the specimen during the test at different stages.

After the test finished and the specimen cooled down to the room temperature, cracks on the exposed surface were observed and marked. As presented in Figure 6.2, relatively narrow cracks (widths $<$ 0.005 in.) were observed. Most cracks were found along the locations of stirrups on both sides of the specimen, and some cracks extended into top of the specimen. No spalling was found at the surface of concrete. Concrete color at some areas at exposed surface changed to darker grey after the heating test.

The test was terminated at 40 minutes. After 40 minutes of heating, the maximum surface temperature of concrete reached to 1,121°F (605°C). Temperature profile of PS1 is demonstrated in Figure 6.4. Maximum temperatures at different depths is summarized in Table 6.1. Based on the experience gained from the deck tests, concrete from the exposed surface to 0.25 in. depth is greater than the temperature to decompose calcium hydroxide (CH). Therefore, the loss of CH in this region might be observed in test results from the material analysis conducted on this specimen.

The temperatures in the reinforcing bar and the strand during the test are shown as Figure 6.5. Since the rebars and strands were located at 2 in. from the exposed surface, the concrete temperature profile in this depth is also presented in this figure for comparison. It can be observed that, the trends and values for these three curves are similar, showing the fact that the temperatures in steel components and the surrounded concrete at the same distance from exposed surface would be close. Thus, the concrete temperature measurement in a specific location can represent the temperature of steel embedded in the same location.

The relative displacement can be calculated by subtracting the average strand displacement from the concrete displacement, as presented in Figure 6.6. Relative displacement between concrete and strands was increasing during the heating and remaining at the same level after turning off the heaters at 40 minutes. The residual relative displacement of specimen PS1 is 0.227 in., which might be resulted

from the bond lose and the temperature gradient distribution of the section during the heating, however it needs to be investigated further to confirm the real effects causing this phenomenon.

6.1.1.2 80-minute two-sided heating test for specimen with two strands (PS2). The second experiment involved heating the prismatic specimen with two strands on both sides for 80 minutes. During the experiment, escaped moisture was observed at 27 minutes, when the surface temperature was around 887°F (475°C). Figure 6.7 shows the observation of moisture for specimen PS2 during test at different testing durations.

After 80 minutes of heating, the test was stopped and the maximum surface temperature of concrete reached 1,323°F (717°C), as shown in Figure 6.3. Spalling could

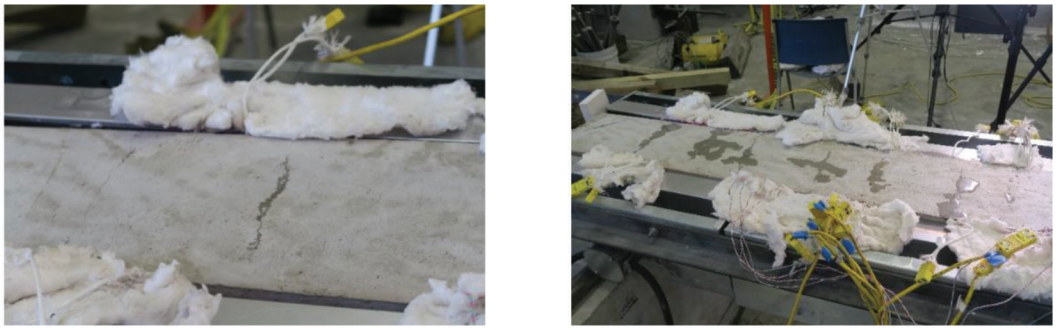

(a) At 23 Minutes–Surface Temperature: 875°F

(b) At 40 Minutes–Surface Temperature: 1,121°F

Figure 6.1 Observation of moisture from specimen PS1 during test.

(a) Cracks on the East Surface

(b) Cracks on the West Surface

Figure 6.2 Map of cracks for PS1.

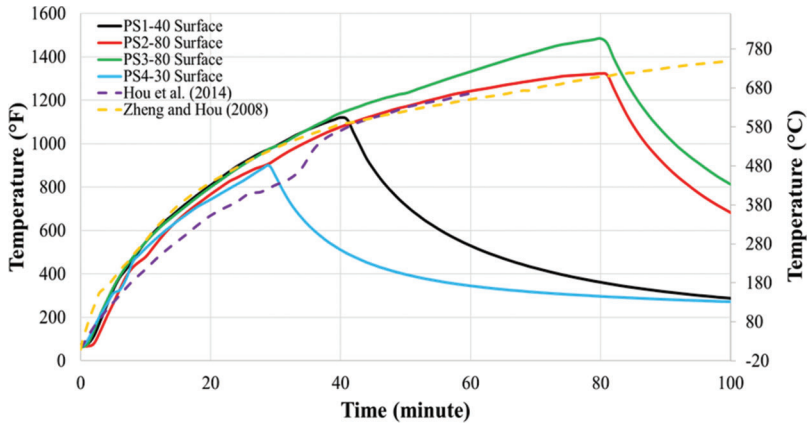

Figure 6.3 Comparison of surface temperature between PS1 and PS4 tests.

be found at some areas under heaters and the aggregates were exposed, as shown Figure 6.8. The temperature profile of PS2 is shown in Figure 6.4. It can be noticed that concrete temperature at all depth increased constantly till the end of test. Maximum temperatures at different is shown in Table 6.1. According to the results from the deck tests, the CH decomposition would possible be seen in the material analysis conducted on the concrete sample located from the surface to 0.5 in. depth.

Figure 6.6 displays the measured displacements of the specimen PS2. Similar to the specimen PS1, there was a significant relative displacement existing between the concrete and prestressing strands. After the specimen

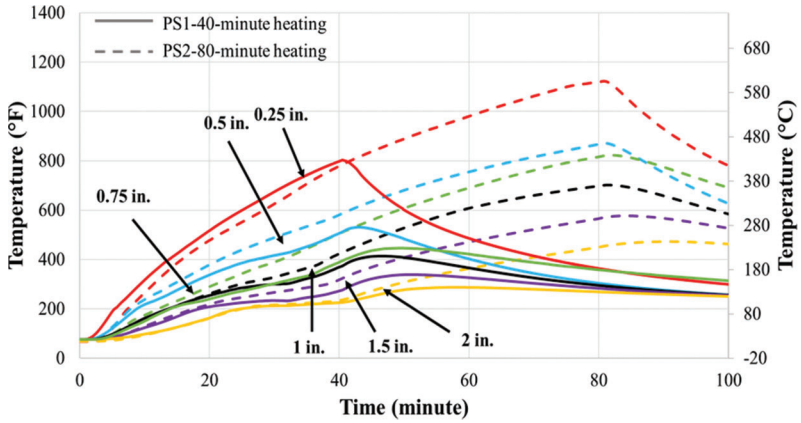

Figure 6.4 Comparison of temperature profiles between PS1 and PS2 tests.

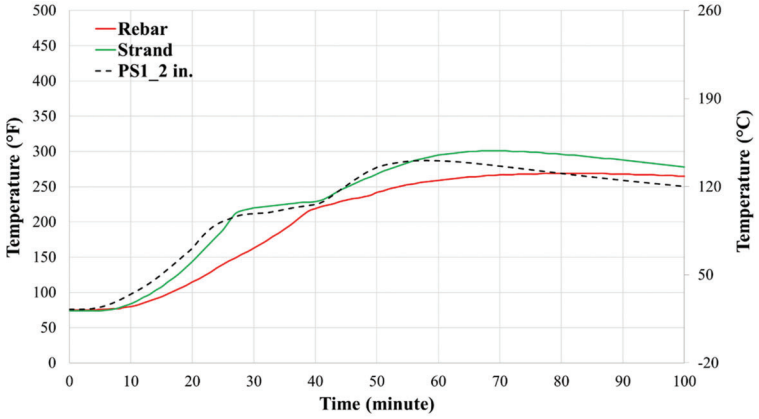

Figure 6.5 Temperature in rebar and strand of PS1.

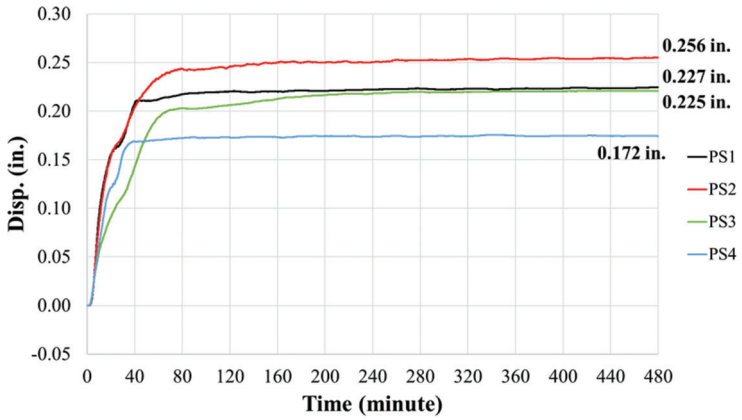

Figure 6.6 Comparison of relative displacements between concretes and strands.

(a) At 27 Minutes–Surface Temperature: 887°F

(b) At 38 Minutes–Surface Temperature: 1,054°F

Figure 6.7 Observation of moisture from Specimen PS2 during test.

Figure 6.8 Spalling at exposed surface for PS2.

TABLE 6.1
Maximum Through-Depth Temperatures for PS1 and PS2 Specimens

	PS1-40-Minute Heating		PS2-80-Minute Heating	
Location	Maximum Temperature (°F[°C])	Time at Max. Temperature (min.)	Maximum Temperature (°F[°C])	Time at Max. Temperature (min.)
Surface	1,121 [605]	40	1,323 [717]	80
0.25 in.	803 [428]	41	1,123 [606]	81
0.5 in.	531 [277]	43	871 [466]	81
0.75 in.	446 [230]	49	823 [439]	82
1 in.	414 [212]	47	702 [372]	82
1.5 in.	339 [171]	51	577 [303]	84
2 in.	287 [142]	58	473 [245]	90

completely cooled down to the room temperature, the measured residual relative displacement was 0.256 in.

6.1.1.3 80-Minute two-sided heating test for specimen with six strands (PS3). The third experiment introduced a heating test performed on the prismatic specimen with six strands on both sides for 80 minutes. During the experiment, escaped moisture initially appeared at 19 minutes, when the surface temperature reached 779°F (415°C). The observation of moisture for specimen PS3 during test at different heating durations are presented in Figure 6.9. As this figure shows, there was a significant increasing of the seeped moisture in the top surface when the specimen was heated for 44 minutes and the surface temperature arrived to 1,185°F (641°C).

Similar to the PS2 specimen, spalling at the heated surfaces can be observed after the 80-minute heating test, as presented in Figure 6.10. The temperature measurement shows that, the maximum surface temperature of concrete reached to 1,485°F (807°C) after 80 minutes heating, and the internal temperature profile of PS3 during the heating test is demonstrated in Figure 6.11. Maximum temperatures measured at various locations is tabulated in Table 6.2. Based on the experience obtained from deck tests, the CH decomposition could probably be observed at the region between the exposed surface to 0.5 in. depth.

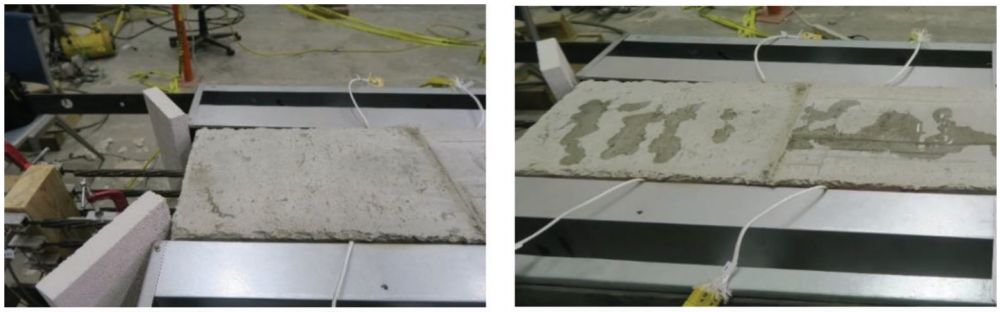

Figure 6.9 Observation of moisture from Specimen PS3 during test.

Figure 6.10 Spalling at exposed surface for PS3.

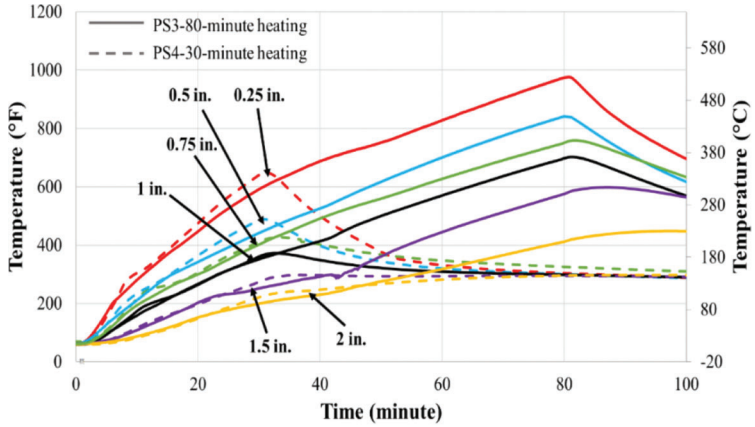

Figure 6.11 Comparison of temperature profiles between PS3 and PS4 tests.

TABLE 6.2
Maximum Through-Depth Temperatures for PS3 and PS4 Specimens

	PS3-80-Minute Heating		PS4-30-Minute Heating	
Location	**Maximum Temperature (°F[°C])**	**Time at Max. Temperature (min.)**	**Maximum Temperature (°F[°C])**	**Time at Max. Temperature (min.)**
Surface	1,485 [807]	80	899 [482]	29
0.25 in.	976 [524]	80	647 [342]	31
0.5 in.	842 [450]	80	489 [254]	31
0.75 in.	759 [404]	82	427 [219]	33
1 in.	703 [373]	82	372 [189]	33
1.5 in.	598 [314]	87	298 [148]	36
2 in.	449 [232]	98	297 [147]	95

Figure 6.6 shows the Relative displacement in specimen PS3, the raise of the relative displacement became unobvious after the heaters were turned off at 80 minutes. The residual relative displacement was measured as 0.225 in. after the concrete temperature reduced back to the room temperature.

6.1.1.4 30-minute four-sided heating test for specimen with six strands (PS4). The last experiment conducted on the prismatic specimen in the laboratory was a heating test performed on the prismatic specimen with six strands on four sides. Since the specimen was surrounded by heaters, the escaped moisture was hardly observed during the experiment. Nevertheless, the moisture could still be seen in the end of specimen, as presented in Figure 6.12, the moisture seeped out from where strands located at 16 minutes from the beginning of test while the surface temperature was 668°F (353°C).

The test was initially planned to be performed for 80 minutes duration. However, when the specimen was heated for 20 minutes, a severe spalling unexpectedly happened at one corner of the specimen. Therefore, the test was terminated at 30 minutes concerning the safety issue. After the specimen cooled down entirely, the top heaters were removed, the spalling of the specimen is shown in Figure 6.13. As it can be seen, part of the concrete at corner was broke apart, caused a significant section loss for the specimen. The broken concrete pieces were then cleaned for taking measurement, as displayed in Figure 6.14. The length of the spalling is 32 in., moreover, the maximum width as well as height are 3.5 in. and 2 in. respectively. A possible explanation for the incident happened in this test is that the setup of the four-sided heating may trap moisture in the concrete, and along with the internal stress caused by prestressing, causing significant pore-water pressure leading to spalling.

Figure 6.3 presents the surface temperature-time history for the specimen PS4, since the severe spalling happened during the test, the heaters were shut down at 29 minutes from the start of test. The maximum surface temperature of concrete reached 899°F (482°C) when the heating test was stopped. The through-depth concrete temperature profile of PS4 during the heating test is illustrated as Figure 6.11. As showed in the figure, the measured maximum temperatures can be summarized in Table 6.2. It can be expected that CH decomposition should be insignificant for this specimen since all internal measured temperatures are lower than the required temperature to decompose the CH in concrete.

Figure 6.12 Escaped moisture in the end of Specimen PS4.

Figure 6.13 Spalling during the test at Specimen PS4.

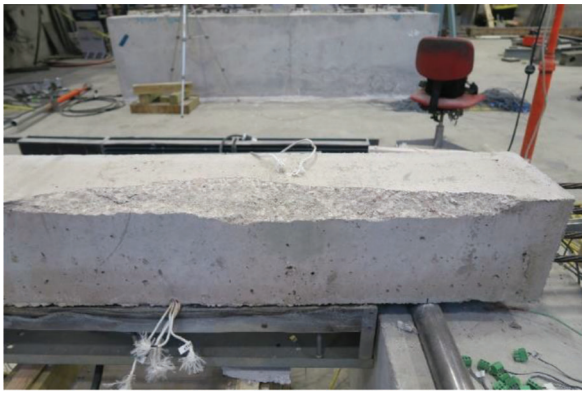

Figure 6.14 Damaged section of Specimen PS4.

Figure 6.6 shows the measured displacements during the heating test for the specimen PS4. Similar to the previous cases, the relative displacement between concrete and strands kept raising until the heaters were shut down. The residual relative displacement of the specimen was 0.172 in. The comparison of the test results will be described in the following sections.

6.1.2 Comparison Between Test Results from PS1 to PS4

Figure 6.3 presents the comparison of surface temperature-time history curves for PS1 to PS4 heating tests and the concrete surface temperature curves reported by different researchers. From the recorded testing data, it can be observed that the trends of measured surface temperatures and reported temperatures for the specimens tested in furnaces following ISO-834 (ISO, 2002) standard fire curve are comparable. Which suggests the rationality for the test methods employed in this experimental program. Moreover, Figure 6.4 and Figure 6.11 illustrate the

comparison of measured temperature profiles for specimens with two strands (PS1 and PS2) and specimens consist of six strands (PS3 and PS4). As the figures show, the trend of internal temperature curves from longer duration of heating extend the trend of shorter duration of heating.

6.2 Test Results for Prismatic Specimens Exposed to Pool Fire

6.2.1 Heating Test Results

The concrete of the specimens was aged 8 months at the test day. The test was conducted on March 16, 2020, at 10:20 AM, the average recorded wind speed was 5 mph from southeast to northwest (NOAA, 2020). Flame accompany with heavy smoke engulfed the specimens immediately at the beginning of the test, as shown in Figure 6.15. During the test, the presented wind on the site influenced the flame significantly, the flame was blown from south to north and caused an uneven fire distribution to the specimens. After 15 minutes of heating, concrete of the overlaying decks and the surrounded blocks began to spall on the surfaces with continuous popping sound. The spalling kept occurring till the end of test, and the concrete pieces even be seen on the top of specimens, as shown in Figure 6.16.

The pool fire test ended at 48 minutes from the beginning of test due to the depletion of the fuel. It should be noted that, although the estimated burning duration was 1 hour, the real burning time might be affected by many factors of the actual environment on site, which would lead to a different burning duration. After the test, there are lots of spalling and cracks can be observed in the specimens, and the maximum depth of the spalling in deck sections was about 5 in., as shown in Figure 6.17.

The specimens were placed on the site and cooled for 1 day, after that they were transported back to the laboratory for coring the material samples and measuring the deflections. It could be observed that there were two major longitudinal cracks existing for both beams. The first crack was on the inner surface in midspan with

Figure 6.15 Observation of the pool fire test.

Figure 6.16 Observation of spalling during test.

Figure 6.17 Observation of spalling after test.

the length of 18 in., and the other crack was observed on the bottom surface in midspan with the same length, as presented in Figure 6.18(a) and Figure 6.18(b). After the specimen was turned upside down for coring material samples, severe appalling could be seen on the bottom surface of the prismatic specimen. Moreover, a transverse crack could be noticed in the midspan, which connected two longitudinal cracks mentioned together, as shown in Figure 6.18(c). By the inspection at the cored locations, the longitudinal cracks existing on the inner and the bottom surfaces did not extend through the depth, instead of that, they were prone to developed inclinedly toward each other, as shown in Figure 6.18(d).

The fire temperatures at different heights were measured and presented in Figure 6.19. It can be noticed that the temperatures were fluctuating due to the inconsistency of the presented fire, the reason for that should be the disturbance caused by the wind. The thermocouples for measuring the flame temperature were install in the south end of specimens, however, it was observed that the flame was blown to the north of specimens during the fire test, causing the fluctuation in the temperature readings. Nevertheless, the maximum temperatures of the flame could still be captured under this circumstance, which was 2,056°F (1,124°C) at 3 ft from the bottom of pool. Moreover, this figure also compares the measurements with ISO-834 (ISO, 2002) standard fire curve and Eurocode hydrocarbon fire curve (BSI, 2002). It can be observed that the measured

Figure 6.18 Observation of prismatic specimens after pool fire test.

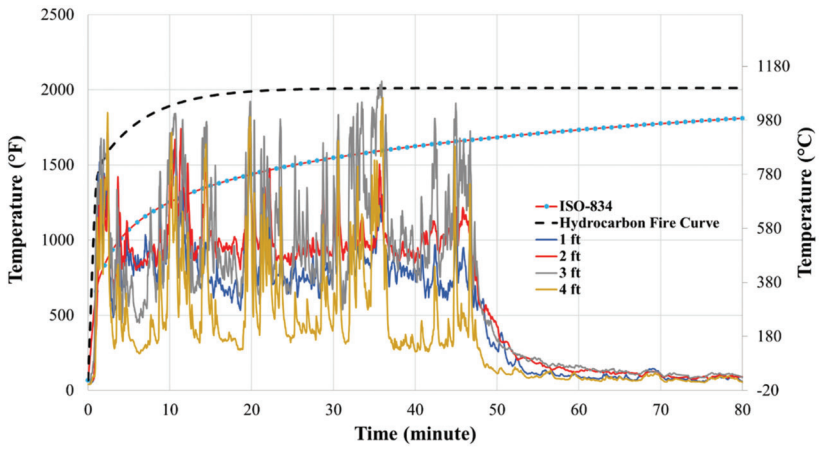

Figure 6.19 Flame temperature for pool fire test.

fire temperature during the pool fire test was obviously above the ISO standard fire curve, however, it generally following the trend of the standard hydrocarbon fire curve.

The temperature measurement at the bottom surfaces for PS5 and PS6 specimens are shown in Figure 6.20 and Figure 6.21. It can be observed that the measured temperatures are higher in the north for both specimens, which should be resulted from the presence of the wind during test, as discussed previously. The maximum bottom surface temperatures for PS5 from south to north were 1,305°F (707°C), 1,552°F (844°C), and 1,643°F (895°C), respectively. On the other hand, the maximum bottom surface temperatures for PS6 reached 1,427°F (775°C), 1,514°F (823°C), and 1,716°F (936°C) from south to north. The measurements indicate the effects of the presented wind obviously, which were consistently existing on both two specimens.

Lastly, four through-thickness thermocouples were installed in two prismatic specimens, however only the thermocouples located at the depths of 0.5 in. and 1 in. in specimen PS5 provided reasonable records as shown in Figure 6.22. The maximum experienced

temperatures of PS5 were 486°F (252°C) and 408°F (209°C) for 0.5 in. and 1 in. from the bottom surface, respectively.

6.2.2 Comparison Between Controlled Heating Test and Pool Fire Test

Figure 6.20 and Figure 6.21 present the comparison of measured surface temperature between specimens heated by the ceramic radiation-based heaters (PS1 and PS2) and that burned by the pool fire (PS5 and PS6). It can be seen from the figures, the exposed surface temperatures measured in the pool fire test increased faster and could arrived higher temperatures than controlled heating test conducted in the laboratory. For the specimens heated by the heaters, the surface temperature after 80-minute heating was at the same level, or even lower than the that of the specimens heated in hydrocarbon fire. According to these data, it can be inferred that the concrete in real fire instance may experience more severe impacts on the surface comparing to specimen that heated in the laboratory following the standard fire curve proposed by the specification.

Figure 6.22 shows the comparison of concrete internal temperatures for different testing condition at 0.5 in. and 1 in. from the exposed surface. The temperatures measured from the specimens heated by the real fire for 48 minutes are comparable with the measurements obtained from specimens tested in the laboratory for 40 minutes. The findings illustrate that, even the concrete surface temperatures are in different levels of magnitude, the experienced temperatures inside the concrete are still comparable for the specimens in different heating conditions.

6.3 Microstructural Evaluation Results

Microstructural evaluation of concrete from the prismatic specimens was conducted using the same experimental techniques (i.e., scanning electron microscopy (SEM), energy dispersive spectroscopy (EDS), and differential scanning calorimetry (DSC)) as those used to evaluate the microstructure of specimens from the bride deck (see Section 4.2). The overall objective of these investigations was also the same as previously, i.e., to correlate the alteration of the microstructure with the measured temperatures through the depth of the specimens.

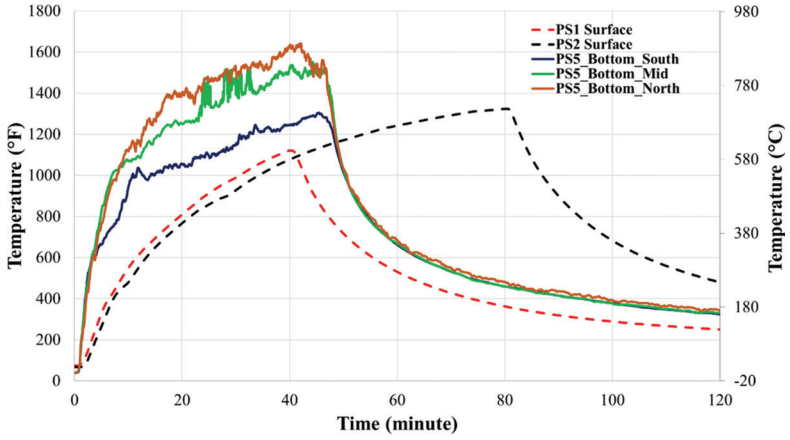

Figure 6.20 Comparison of surface temperature between PS1, PS2, and PS5.

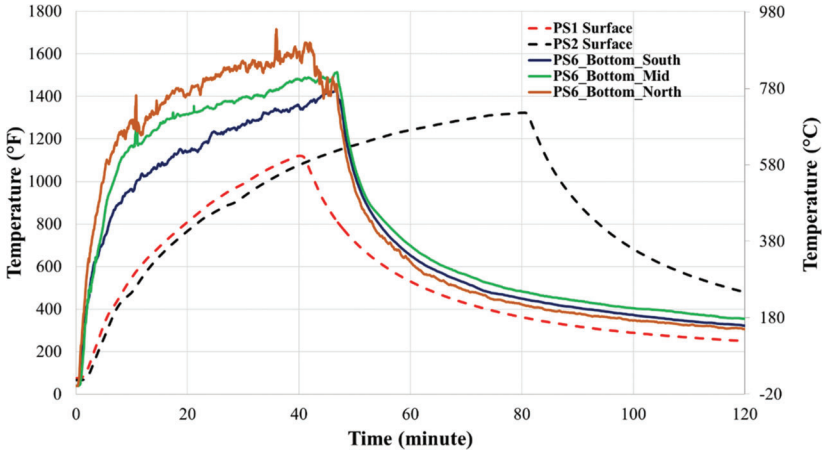

Figure 6.21 Comparison of surface temperature between PS1, PS2, and PS6.

6.3.1 SEM/EDS Observations of Heated Prismatic Specimens

Table 6.3 summarizes the names and the heating conditions of specimens used in microstructural analysis. Similar to what was done in the case of the deck specimens, the evaluation was performed at various depths from the heated surface.

The full collection of images containing the detailed features of microstructure of specimens is provided in Appendix C. The overall appearance of the microstructure of specimens at various depths is shown in the SEM micrographs presented in Figure C.1 to C.6. The main findings resulting from the analysis of these micrographs can be summarized as follows:

1. For the prismatic specimen that was only heated for 30 minutes (i.e., PS4-30), the substantial alteration of the microstructure was only apparent within the first 0.25 in. from the heated surface (compare Figure C.1(d) with Figures C.2 to C.6(d)). These alterations involved the development of numerous cracks in the matrix and partial debonding of aggregates. The hydrated cement matrix seems to be relatively intact at locations further away from the heated surface. It should also be pointed out that, due to relatively short (i.e., 30 minutes) period of heating, the internal temperatures of concrete within this region were relatively modest, varying from 860°F to 628°F (460°C to 331°C).
2. A network of slightly wider cracks that those previously discussed in connection with specimen PS4-30 was observed in the top 0.25 in. of prismatic specimen heated for 40 minutes (PS1-40)—see Figure C.1(a). Furthermore, unlike in the case of PS4-30 specimen, the next layer of the microstructure of PS1-40 specimen (i.e., a zone located 0.25 in. to 0.50 in. from the heated surface) also contained a network of cracks, albeit not as wide as those in the layer directly above (see Figure C.2(a)). The cracks become progressively thinner and less numerous with further increase in the distance from the heated surface (see Figures C.3(a) and C.4(a) and all but disappeared at depths greater than about 1.0 in. from the heated surface (see Figures C.5(a) and C.6(a)).
3. In specimens exposed to more intense heating scenarios (i.e., 80 minutes under the heater for specimens PS2-80, PS3-80) and the pool fire (specimen PS5-48) the extensive cracking of the paste is visible within the first 0.75 in. from the heated surface (see images (b), (c), and (e) of Figure C.1 to C.3). For this set of specimens, the region below 0.75 in. from the surface (all the way to the depth of 2.0 in.) becomes progressive less altered, with no indication of damage past the depth of 1.5 in. (see corresponding images in Figures C.4 to C.6).
4. The extent of microstructural damage in another prismatic specimen exposed to the pool fire (PS6-48) was slightly more extensive than that observed in specimen PS5-48, with significant cracking present to the depth of 1.0 in. from the heated surface (see images (f) in Figures C.1 to C.4. Past the depth of 1.0 in. from the heated surface, the microstructure of concrete appears to be relatively unaffected (see images (f) in Figures C.5 and C.6).

Figures C.7 to C.11 show images of the distribution of the deposits of calcium hydroxide (CH) within the concrete matrix as identified by the energy

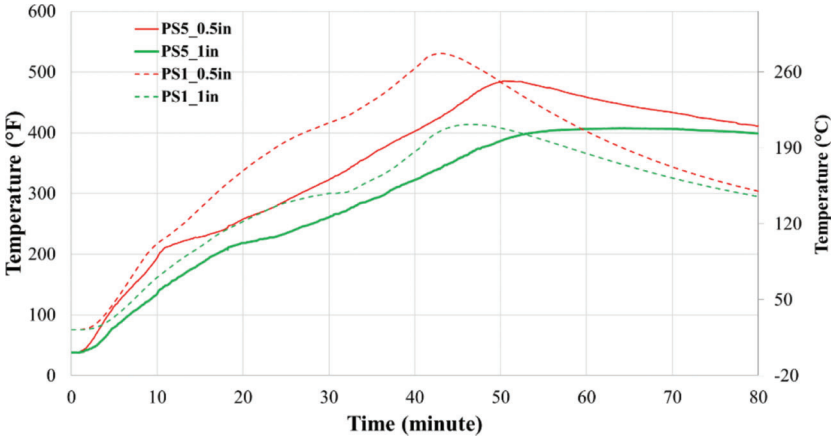

Figure 6.22 Comparison of temperature profiles between PS1 and PS5 tests.

TABLE 6.3
Summary of All Specimens Used in Microstructural Testing

Specimen Name	Heating Duration	Heating Conditions
PS1–40	40 Minutes	Heater–2 Sides
PS2–80	80 Minutes	Heater–2 Sides
PS3–80	80 Minutes	Heater–2 Sides
PS4–30	30 Minutes	Heater–4 Sides
PS5–48	48 Minutes	Pool Fire
PS6–48	48 Minutes	Pool Fire

dispersive spectroscopy (EDS) x-ray method. In mature concrete, such CH deposits are commonly found in the interfacial zone between the paste and the aggregate and appear as a thin, "whitish" layers ("ribbons") around the perimeter of the aggregate particles and show a chemical signature (peak) for calcium (Ca) in the EDS spectrum.

For all specimens examined in this part of the study, there was a noticeable scarcity of CH deposits in the microstructure of concrete located within the first 0.25 in. from the source of the heat. The CH deposits become more prevalent in the deeper parts of the specimens, the relative amounts being function of the length of high temperature exposure (and thus the magnitude of the internal temperature). As an example, only limited CH deposits can be observed within the 0.25 in. of the microstructure located closest to the source of heat for specimens PS1-40 and PS4-30 (images (a) and (d) in Figure C.7). However, such deposits are easily spotted at depths farther away from the heated surface (see images (a) and (c) in Figures C.8 to C.11). Similarly, the CH deposits are nearly absent from the first 0.75 in. of the microstructure of specimens PS2-80, PS3-80, PS5-48 and PS6-48 (see images (b), (c), (e) and (f) of Figures C.7 to C.9, respectively). However, more frequent deposits of CH can be observed in the region of the specimen located between 0.75 in. and 2 in. from the heated surface, especially in the interfacial regions near the aggregates and in the pores (see images (b), (c), (e) and (f) of Figures C.10 and C.11, respectively).

6.3.2 DSC Analysis of Heated Prismatic Specimens

As discussed in Section 3.4.3, the differential scanning calorimetry (DSC) method was used to quantify the amount of CH present in the matrix of various specimens. The DSC analysis was performed on both, unheated and heated samples in order to identify the depth of the zone affected by elevated temperatures as indicated by the reduction of the amount of CH. To correlate the results of CH content determination with the measured temperature profile of the specimens, the DSC samples were collected from the depths of 0.25 in., 0.5 in., 0.75 in, 1 in., 1.5 in., and 2 in. from the heated surface of the prismatic beams.

As an example, Figure 6.23 shows the DSC results for the PS6-48 prismatic specimen exposed to pool fire. The results are presented in the form of the heat flow curves for material collected from different depths plotted as the function of the temperature the test specimen was exposed to during the DSC experiment. The downward facing peaks of these curves identify the amount of energy required to dehydrate specific phases present in the hydrated cement paste. The larger the area under the peak, the higher the amount of energy required, which means that this particular phase is present in larger quantities.

It can be seen that the first series of peaks appears in the temperature range from about 77°F (25°C) to about 248°F (120°C). These peaks are associated with removal of the evaporable water from the calcium silica hydrate (C-S-H) gel and other products of hydration, such as ettringite. While removal of water from these phases does not have negative effects on strength of concrete, the magnitude of the peak itself serves as a good indicator of the temperature experienced by the particular region of the sample, with smaller peaks corresponding to higher temperatures. Analysis of data presented in Figure 6.23 indicates that for this particular specimen the effects of exposure to elevated temperature are confined to the zone located between the heated surface and about 1.0 in. into the specimen.

The second main peak shown in Figure 6.23, located between 754°F to 932°F (400°C to 500°C), indicates decomposition of calcium hydroxide (CH) into lime (CaO) and water. The changes in the magnitude of this peak are particularly relevant to the present study as it will be discussed later. The areas under the CH peak can be converted to the percent of CH actually present in the

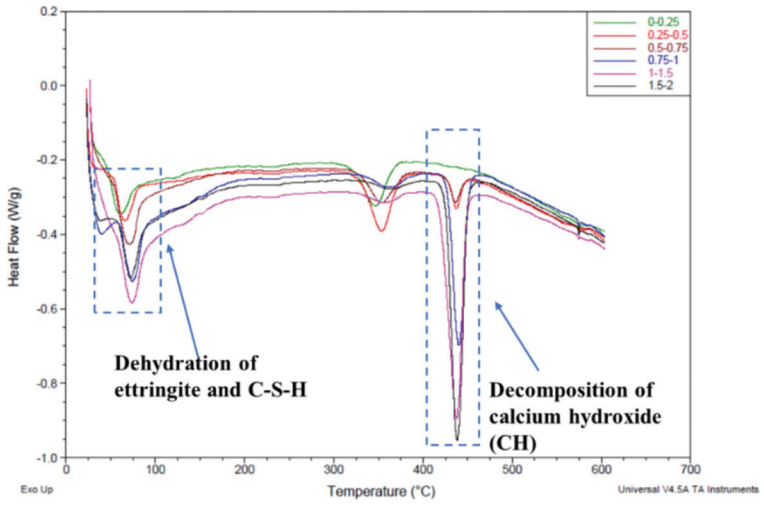

Figure 6.23 Results of DSC analysis of PS6-48 Specimen.

sample using the calibration scheme described in Section 3.4.3 and the calibration curve shown in Figure 4.13. This approach has been used to calculate the CH content at various depths from the surface for both, the unheated specimens (to obtain the base-line values) and the specimens exposed to various heating scenarios.

Table 6.4 presents the amounts of CH at different depths of the unheated sample. It can be seen that, with the exception of the top 0.25 in., the content of CH at greater depths stays relatively constant, oscillating between 4.6% to 5.7%, with the average value of about 5.3%. The reduced level of CH (~2.3%) in the very top layer of the specimen is the result of combined effects of leaching and carbonation. The content of CH in the heated samples is given Tables 6.5 to 6.7. For the ease of comparison, the data from Tables 6.4 to 6.7 are also presented in a graphical form in Figures 6.24 to 6.26.

Looking at the data presented in Tables 6.4 to 6.7 and in Figures 6.24, 6.25 and 6.26, it can be concluded that the content of CH was drastically depleted in the first 0.25 in. from the exposed surface. The degree of depletion varied as a function of exposure, and was almost complete (i.e., 100%) for PS1-40, PS2-80, PS3-80, PS5-48 and PS6-48 specimens. The reduction of CH in the unheated specimen and the specimen heated for 30 minutes (PS4-30) was about 60%. The amount of CH lost from layers located at greater depths also varied with the duration and the intensity of heating, with the percentage lost decreasing with the increase in the depth from the heated surface. As an example, in specimens exposed to 80 minutes of two-sided heating (PS2-80 and

TABLE 6.4
Quantitative Estimation of CH Content for Unheated Specimens

	Unheated	
Depth (in)	**Peak Area (J/g)**	**CH (%)**
0.25	25.56	2.34
0.5	62.16	5.70
0.75	61	5.59
1	62.32	5.71
1.5	53.57	4.91
2	50.52	4.63

TABLE 6.5
Quantitative Estimation of CH Content for PS1 and PS2 Specimens

	PS1-40			PS2-80		
Depth (in)	**Peak Area (J/g)**	**CH (%)**	**Measured Temperature Range (°F) [°C]**	**Peak Area (J/g)**	**CH (%)**	**Measured Temperature Range (°F) [°C]**
Surface	N/A	N/A	1,121 [605]	N/A	N/A	1,323 [717]
0.25	2.357	0.22	1,121–803 [605–428]	1.129	0.10	1,323–1123 [717–606]
0.5	35.92	3.29	803–531 [428–277]	5.635	0.52	1,123–871 [606–466]
0.75	77.82	7.14	531–446 [277–230]	34.13	3.13	871–823 [466–439]
1	73.06	6.70	531–414 [230–212]	59.94	5.50	823–702 [439–372]
1.5	60.92	5.59	414–339 [212–171]	81.77	7.50	702–577 [372–303]
2	54.54	5.00	339–287 [171–142]	69.95	6.41	577–473 [303–245]

TABLE 6.6
Quantitative Estimations of CH Content for PS3 and PS4 Specimens

	PS3-80			PS4-30		
Depth (in)	**Peak Area (J/g)**	**CH (%)**	**Measured Temperature Range, (°F) [°C]**	**Peak Area, J/g**	**CH (%)**	**Measured Temperature Range, (°F) [°C]**
Surface	N/A	N/A	1,485 [807]	N/A	N/A	899 [482]
0.25	0.23	0.02	1,485–976 [807–524]	24.06	2.21	899–647 [482–342]
0.5	11.55	1.06	976–842 [524–450]	62.97	5.77	647–489 [342–254]
0.75	37.75	3.46	842–759 [450–404]	53.37	4.89	489–427 [254–219]
1	59.29	5.44	759–703 [404–373]	49.26	4.52	427–372 [219–189]
1.5	59.34	5.44	703–598 [373–314]	68.97	6.32	372–298 [189–148]
2	46.51	4.26	598–449 [314–232]	67.60	6.20	298–297 [148–147]

TABLE 6.7
Quantitative Estimations of CH Content for PS5 and PS6 Specimens

Depth (in)	PS5			PS6		
	Peak Area (J/g)	CH (%)	Measured Temperature Range (°F) [°C]	Peak Area (J/g)	CH (%)	Measured Temperature Range (°F) [°C]
Surface	N/A	N/A	1,305 [707]	N/A	N/A	1,427 [775]
0.25	0.00	0.00	N/A	0.00	0.00	N/A
0.5	15.01	1.38	486 [252] at 0.5 in.	5.63	0.52	N/A
0.75	39.50	3.62	N/A	5.48	0.50	N/A
1	65.45	6.00	405 [209] at 1 in.	40.59	3.72	N/A
1.5	67.69	6.21	N/A	63.03	5.78	N/A
2	71.94	6.60	N/A	61.81	5.67	N/A

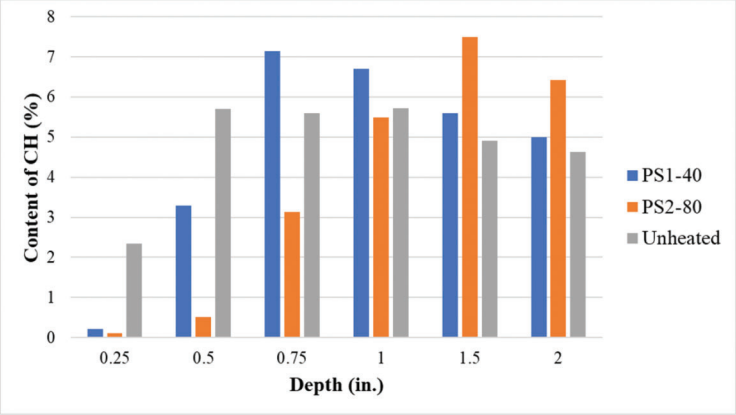

Figure 6.24 Comparison of CH contents for PS1, PS2, and unheated specimens.

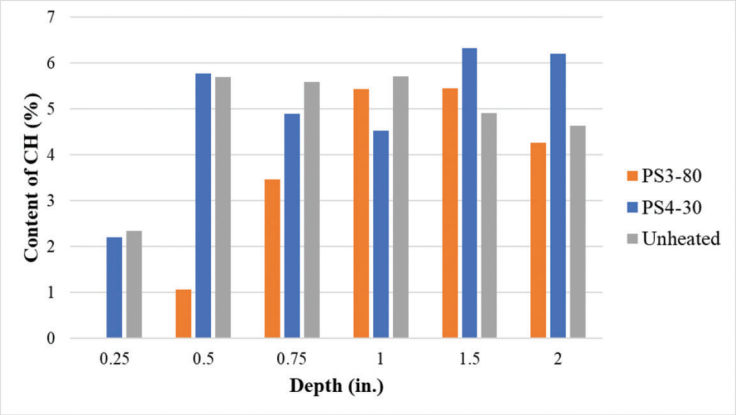

Figure 6.25 Comparison of CH contents for PS3, PS4, and unheated specimens.

PS3-80), there was about 80%–90% CH loss from the depths up to 0.5 in. from the surface and about 30%–50% loss from the depths up to 0.75 in. from the surface. In contrast, there was practically 0% CH lost from the depth between 0.25 in. and 0.50 in. for the specimen exposed to 30 minutes of four-sided heating (PS4-30).

When it comes to specimens exposed to the 48 minutes pool fire test, the amount of CH lost in specimen PS5-48 was about 90% for the region between 0.25 in. and 0.50 in. from the heated surface, and about 40% for the region between 0.50 in. and 0.75 in. from the heated surface. On the other hand, for specimen PS6-48 about 90% of CH loss was observed in the region from 0.25 in. to 0.75 in. from the surface and about 30% loss was observed for the region from 0.75 in. to 1.0 in. from the surface.

In general, the levels of the CH decomposition observed in the PS5-48 and PS6-48 specimens were comparable to those observed in the specimens heated in the laboratory for 80 minutes (see Figures 6.24, 6.25 and 6.26).

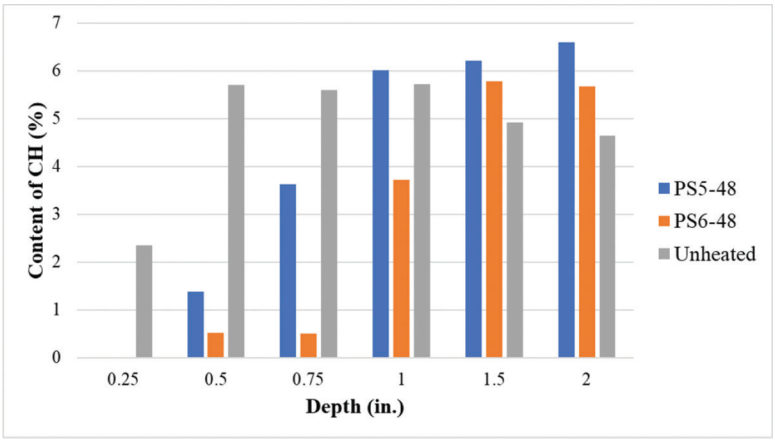

Figure 6.26 Comparison of CH contents for PS5, PS6, and unheated samples.

7. EXPERIMENTAL PROGRAM FOR FULL-SCALE AASHTO TYPE I GIRDERS

7.1 Overview of Test Program

This chapter introduces the experimental tests performed on decommissioned AASHTO Type I girders (INDOT, 2013). The prestressed concrete girders were obtained from the bridge carrying I-469 (westbound) over Feighner Road in Fort Wayne, Indiana, as indicated by the hatched girders in Figure 7.1. The girders had a total length of 38.5 ft. To evaluate the residual loading-carrying capacities of prestressed concrete girders after being subjected to fire, load tests were conducted on the girders under both ambient and post-fire conditions. Two tests were conducted for each condition, one shear-controlled test and one flexure-controlled test. The details of the specimens and the tests conducted on the AASHTO Type I girders are provided in the following sections.

7.2 Specimen Details

Based on the results of a visual inspection to identify suitable girders for the test program, Beams C2, C5, and C7 from the I-469 bridge over Feighner Road (see Figure 7.1) were selected for the experimental program described herein. The girders were removed from the bridge and transported to Bowen Laboratory at Purdue University. The girders were extracted from the bridge by cutting the through the deck, leaving approximately 2 in. of deck overhand on each side of the top flange of the beams. Therefore, the deck section remaining on the girders was approximately 16-in. wide and had a nominal thickness of 8 in. According to the original bridge plans (Indiana Department of Highways, 1987), the bottom surface of the deck was located a minimum of 1/2 in. from the top surface of the precast girders. The specific compressive strength of the concrete, f'_c, according to the original bridge plans

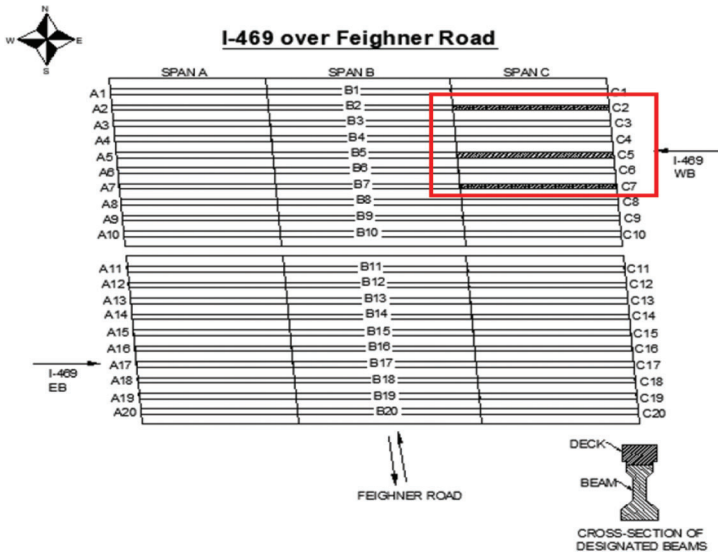

Figure 7.1 Plan view of selected specimens.

(Indiana Department of Highways, 1987) is 5,000 psi. The average strength obtained from tests on cored samples taken from five girders from the same bridge indicate that the actual compressive strength is approximately 8,170 psi. For these five girders, the strengths ranged from 7,270 psi to 9,240 psi. The girders were prestressed with eight 1/2-in. diameter strands with an initial jacking stress of 189 ksi according to the original bridge plans (Indiana Department of Highways, 1987). The details of the girders are provided in Figure 7.2. Four of the strands were straight and four were harped as indicated in the figure.

7.3 Setup and Instrumentation for Load Tests Conducted on AASHTO Type I Girders

7.3.1 Test Matrix and Experimental Setup

Two tests were conducted on a single girder (Beam C2) to evaluate the strength of the bridge members under ambient conditions (that is, the strength of the members not exposed to fire). Because the layout of the transverse reinforcement was unsymmetrical about the centerline of the member (that is, the stirrup spacing near the two ends of the girder was different), a flexure-controlled test could be conducted near one end of the girder where stirrups were had a wider spacing, and a shear-controlled test could be conducted near the other end where a tighter stirrup spacing was provided. Here, the terms flexure-controlled and shear-controlled are based on the governing limit state (flexure or shear) using the corresponding strength equations in the AASHTO LRFD specifications (AASHTO, 2017). For the flexure-controlled test, the specimen was placed on two roller supports to create a span of 312 in., as shown in Figure 7.3. The overhangs of the specimen beyond the supports were 48 in. on the south side and 102 in. on the north side. The specimen was loaded 54 in. from the south support as shown. The spacing of the stirrups at the loading point was 6 in. The specimen in position for the flexure-controlled load test is

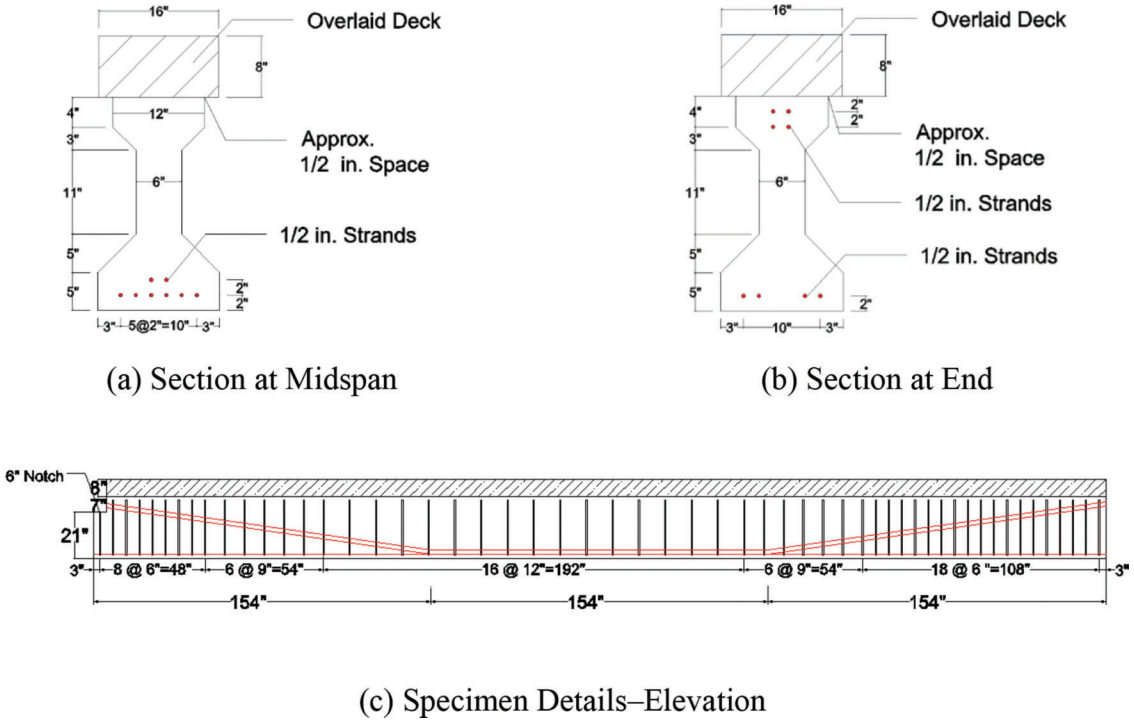

Figure 7.2 Details of prestressed concrete girders.

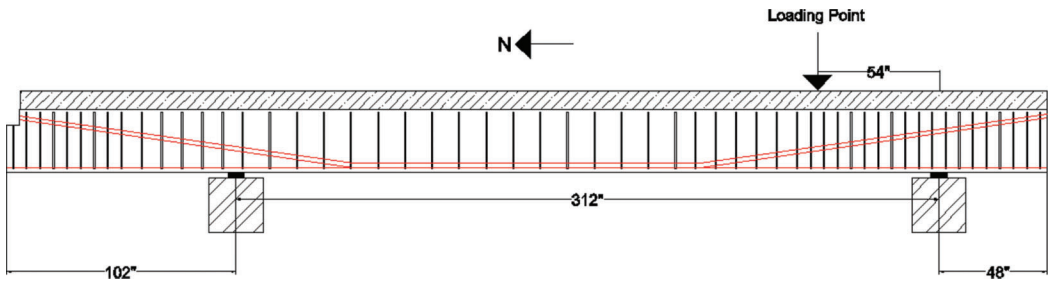

Figure 7.3 Setup for flexure-controlled load tests.

pictured in Figure 7.4. After the first test, the specimen was supported as shown in Figure 7.5 for the shear-controlled load test. For this setup, the span between the supports was 276 in., and the stirrup spacing within the shear test region was 9 in. To avoid influence from the damage from the first test, the overhang farthest from the loading point was increased by 36 in. compared to the first test, as pictured in Figure 7.6. It should be noted that the length of the test region for the load tests, equal to 54 in., resulted in a shear span to effective depth ratio, *a*/*d*, of approximately 1.59. Here, the effective depth, *d*, is measured to the centroid of the strands at the centerline of the member. Because the *a*/*d* ratio is less than 2.0, the 54-in. shear span can be said to be dominated by D-region behavior.

Beams C5 and C7 were selected to be exposed to fire and later tested in the laboratory. After the pool fire test was performed as described in Section 7.4, the girders were transported to the laboratory and loaded using the same two test setups as were used for the ambient load tests. Beam C7 was tested in the flexure-controlled setup as shown in Figure 7.3, whereas Beam C5 was loaded in the shear-controlled setup presented in Figure 7.5. The portion of the girders within the test region (that is, the design stirrup spacing within the test regions) corresponded to the portion of the girder within the test region for the ambient load tests. Thus, the structural capacities of the reference specimen (that is, the ambient specimen) and the burned specimens at both ends can be directly compared. The test matrix for the load tests is presented in Table 7.1.

7.3.2 Instrumentation

For the load tests, linear string potentiometers were used to measure the deflection of the bottom surface of the specimens at the loading point and at midspan. At both locations, two potentiometers were used, one near each corner of the bottom flange. The string potentiometers had strokes of 5 in. or 20 in. Furthermore, to measure the displacement at the ends of the member and at the supports, eight linear potentiometers with 1-in. strokes were used, two at each location near each corner of the bottom flange. At each location, the readings from the two sensors were averaged to obtain the deflection of the member. To supplement the displacement readings, an automated visual tracking system was also used to provide deflection data in the event that the potentiometers failed.

The load applied to the member was obtained through the use of a calibrated pressure transducer located in-line with the hydraulic cylinder located at the loading point.

7.4 Setup and Instrumentation for the Pool Fire Test Conducted on AASHTO Type I Girders

7.4.1 Design and Setup for the Pool Fire Test

A pool fire test was performed on two of the decommissioned prestressed girders (Beams C5 and C7) at the same site where the pool fire test discussed in Section 5.4 was conducted. The same 4 ft by 8 ft by

Figure 7.4 Setup for the flexure-controlled ambient load test.

Figure 7.6 Overhang (length of 138 in.) of specimen during shear-controlled ambient load test.

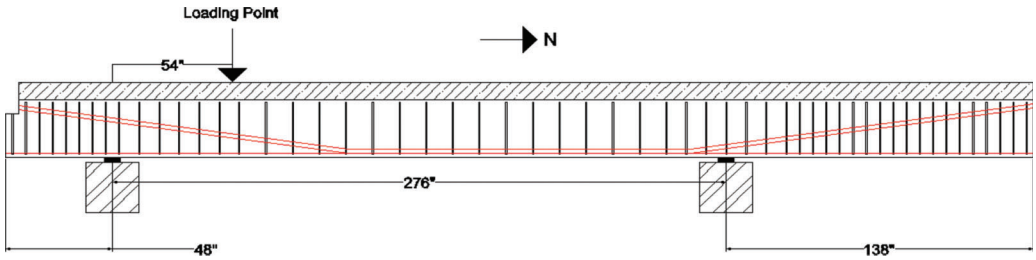

Figure 7.5 Setup for shear-controlled load tests.

TABLE 7.1
Test Matrix for AASHTO Type I Girders

Test Specimens	North Overhang (in.)	South Overhang (in.)	Shear Span to Depth Ratio	Stirrup Spacing at Loading Point (in.)	Specimen Condition	Expected Failure Mode
C2-Flexure	102	48	1.59	6	Unburned	Flexural
C2-Shear	138	48	1.59	9	Unburned	Shear
C7	102	48	1.59	6	Burned	Flexural
C5	138	48	1.59	9	Burned	Shear

Figure 7.7 Girders on concrete blocks in preparation of pool fire test.

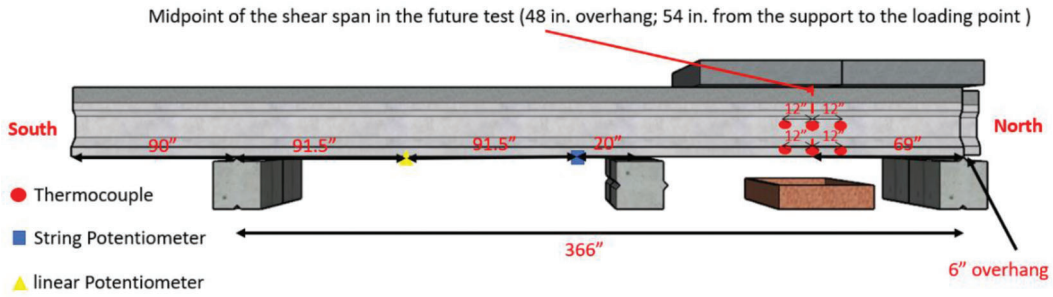

Figure 7.8 Pool fire test setup for Girder C5.

11 in. steel pan was used and the amount of kerosene was also the same as that used for the previous test (approximately 132 gallons).

To facilitate correlation of results to those of the ambient load tests, Beam C5 (to be tested in the shear-controlled setup) was positioned such that the steel pan was centered under the 54-in. shear span to later be tested in the laboratory. Therefore, the center of the pool was located 75 in. from the end of the specimen. For Beam C7 (to be tested in the flexure-controlled test setup), the steel pan was centered under the point where load was to be applied during the future load test. Thus, the center of the pool was located 102 in. from the end of the girder. The two prestressed concrete girders were each supported by two concrete blocks with height of 2 ft, as shown in Figure 7.7. The girders were placed side-by-side with a spacing of 4 ft measured center-to-center of the girder cross sections. The placement of Beam C5 and Beam C7, including the location of the pool relative to the specimens, are illustrated in Figure 7.8 and Figure 7.9, respectively.

The final setup for the pool fire test on the prestressed concrete girders is illustrated in Figure 7.10, and a photograph of the setup is shown in Figure 7.11. To trap the flame during the test, two segments of a decommissioned bridge deck, each with dimensions of 70 in. by 120 in. by 12 in., were placed on top of the girders, as shown in Figure 7.12. Furthermore, to contain the flame within the immediate vicinity of the girders, two barriers consisting of stacked concrete blocks were constructed and surrounded the test region. Lastly, to prevent the specimens from falling into the pool in the event of a catastrophic failure of the members during the fire test, two concrete blocks were placed under the specimens near the midspan of the members.

After the fire test was completed, the specimens were allowed to cool for over 24 hours prior to being

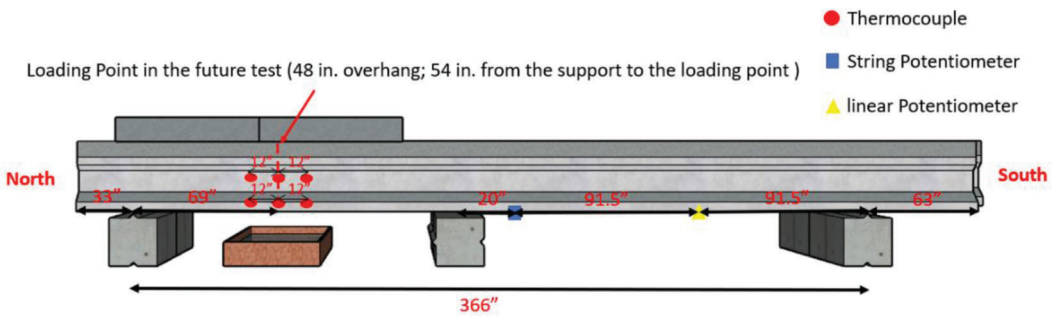

Figure 7.9 Pool fire test setup for Girder C7.

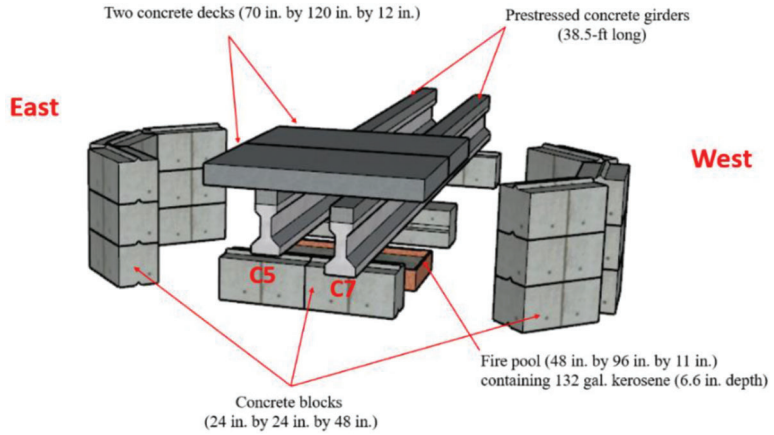

Figure 7.10 Final setup for the pool fire test.

Figure 7.11 Completed test setup with surrounding barriers.

Figure 7.12 Overlaying concrete deck sections.

transported to the laboratory for load testing. After the post-fire loading tests, large concrete pieces that had detached from the specimens were collected to perform material evaluation.

7.4.2 Thermocouples

To obtain the temperature information of the specimens during the pool fire test, thermocouples were installed on the concrete surfaces at various locations. The layout of the thermocouples is presented in Figures 7.8, 7.9, and 7.13. A total of 30 thermocouples were installed on the bottom and side surfaces of the two prestressed girders. For each girder, three thermocouples were placed on the bottom surface, three were placed on each of the side surfaces of the bottom flange, and three were placed on each of the web surfaces. Furthermore, two thermocouples were installed on the bottom surface of the slab panels. Lastly, to measure the flame temperature, thermocouples were positioned at the four corners of the pool. At each of these four locations, thermocouples were installed on a steel bar and located 2 ft and 4 ft from the pool bottom in order to obtain the temperature data at two different elevations. In total, 40 thermocouples were used during the pool fire test, as indicated in Figure 7.13.

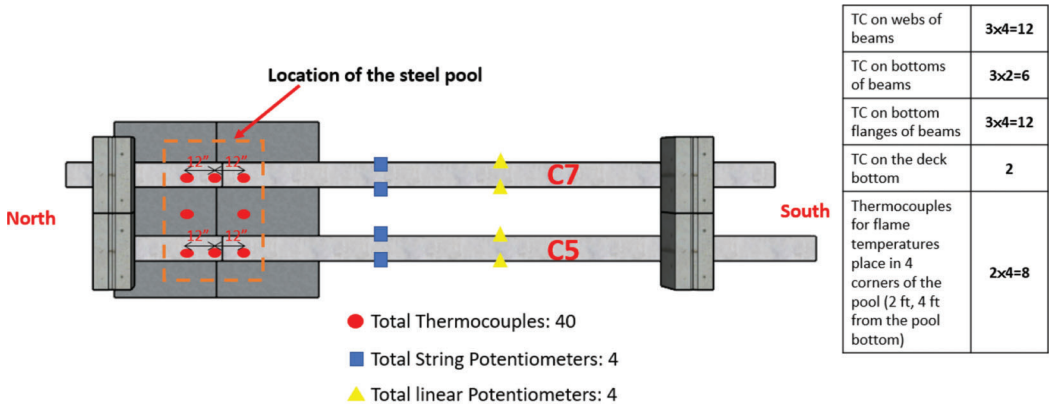

TC on webs of beams	3x4=12
TC on bottoms of beams	3x2=6
TC on bottom flanges of beams	3x4=12
TC on the deck bottom	2
Thermocouples for flame temperatures place in 4 corners of the pool (2 ft, 4 ft from the pool bottom)	2x4=8

Figure 7.13 Bottom elevation view of instrumentation layout.

7.4.3 Displacement Sensors

Displacement sensor were also installed on the girder specimens to monitor the deflections of the members during the fire test. The layout of the displacement sensors is shown in Figure 7.13. Because the sensors cannot sustain extreme temperatures, they could not be installed at locations near the pool. Therefore, a linear string potentiometer was installed at midspan on each side of the bottom flange of each of the two girders. Moreover, a linear potentiometer was installed on each side of the bottom flange of the members at three-quarters of the span length as shown in Figure 7.13.

8. EXPERIMENTAL RESULTS FOR FULL-SCALE AASHTO TYPE I GIRDERS

8.1 Test Results for Prestressed Girders Exposed to Pool Fire

8.1.1 Fire Test Observations

The pool fire test was performed on August 07, 2020, at 10:30 AM. Based on the weather record (NOAA, 2020), the average wind speed on the test day was 3 mph with a wind direction that was primarily northwest to southeast. The kerosene was ignited using a propane torch to begin the test. Smoke appeared immediately and engulfed the specimens. A photograph of the girders near the beginning of the test is shown in Figure 8.1(a). The presence of the light wind during the test obviously affected the distribution of the flames. During most of the test, the flame was general blown from west to east, which caused more combustion products to deposit on the outside surface (west side) of Beam C7 relative to the other side surfaces of the specimens.

After 10 minutes from the start of the test, the fire propagated along the top of the test girders, as shown in Figure 8.1(b) due to the combustible thin epoxy overlay on the composite deck. Consequently, the fire advanced toward the south and even reached the midspan of the girders, interrupting measurements from the string potentiometers installed at that location.

After 28 minutes of heating, severe concrete spalling could be observed at the corners of the top and bottom flanges, as presented in Figure 8.1(c). Moreover, the two deck segments placed on top of the girders as well as the surrounding concrete blocks also experienced spalling during the test.

The test was concluded after 43 minutes when the fuel was exhausted. After the test, the specimens were kept within the setup and allowed to cool until the concrete temperature decreased to the ambient temperature.

The damage experienced by the test girders was inspected after the setup cooled down. For Beam C5, it was observed that the inside and outside (west and east) corners of the top and bottom flanges were damaged severely and that notable spalling and cracking occurred within most of the burned region, as shown in Figure 8.2(a) and (b). Furthermore, the concrete surfaces above the pool became yellowish gray and extensive microcracking was observed.

The condition of the inside (east) surfaces of Beam C7 is shown in Figure 8.2(c). The prestressed girder sustained serious damage to the flanges above the pool. Like Beam C5, the flanges engulfed by the flame spalled and cracked, and the concrete surface within the corresponding region turned to yellowish gray. The damage to the outside (west) surfaces of the specimen, however, was less significant, as shown in Figure 8.2(d). Although some spalling and cracking could still be observed at the corner of the top flange, most of the concrete above the pool was relatively intact. The influence of the light wind on the flames caused the development of different damaged conditions on the two sides of Beam C7.

Finally, due to the unanticipated propagation of the fire along the girders, spalled concrete pieces were distributed extensively around the test setup. Because of their high temperature, some of the concrete pieces burned the wires of the displacement sensors. As a result, all signals from the displacement sensors were lost after 15 minutes from the beginning of the test.

(a) Smoke and Flame Distribution During the Test

(b) Propagation of Fire During the Test

(c) Cracking and Spalling of Concrete

Figure 8.1 Observations during the pool fire test.

(a) Inside of Girder C5 (West Side)

(b) Outside of Girder C5 (East Side)

(c) Inside of Girder C7 (East Side)

(d) Outside of Girder C7 (West Side)

Figure 8.2 Cracking and spalling of burned girders.

8.1.2 Fire Test Results

As described in Section 7.4.2, to measure the flame temperature at different locations, eight thermocouples were installed at different elevations surrounding the pool. Although several thermocouples failed during the fire test, most of the sensors were still recording temperatures properly after the test, as shown in Figure 8.3. It can be observed that the measurements were affected by the movement of the flame; all measured temperatures fluctuated dramatically during the test period. Nevertheless, the trends of the fire temperatures could still be obtained. Based on observations during the test, the flames were generally blown from west to east due to the wind direction. Therefore, the fire temperatures measured at the west side (SW-2 ft and SW-4 ft) were less than those for the other locations. Furthermore, it can be noted that the trends of the measured fire temperatures followed the Eurocode hydrocarbon fire curve (British Standards Institute, 2002). The fire temperature, however, generally exceeded the ISO-834 standard fire curve (ISO, 2002). Overall, the maximum fire temperature measured during the test was 2,066°F (1,130°C).

The measured concrete surface temperatures at different locations on Beam C5 are displayed in Figure 8.4. The corresponding maximum surface temperatures

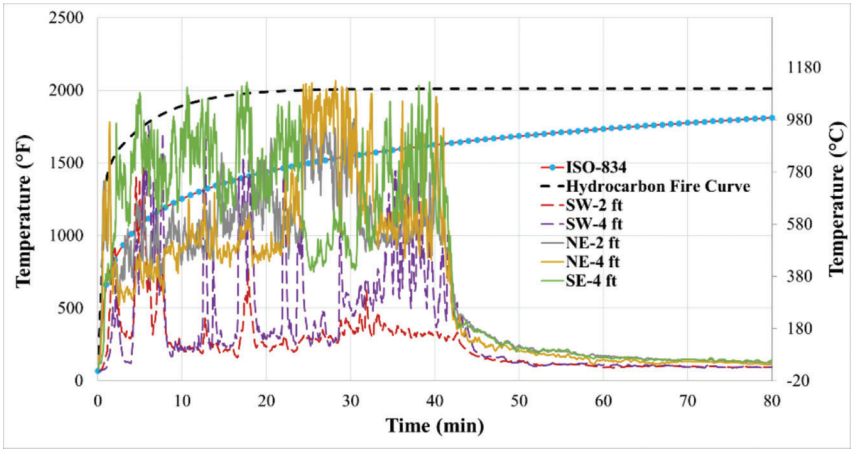

Figure 8.3 Flame temperatures for pool fire test.

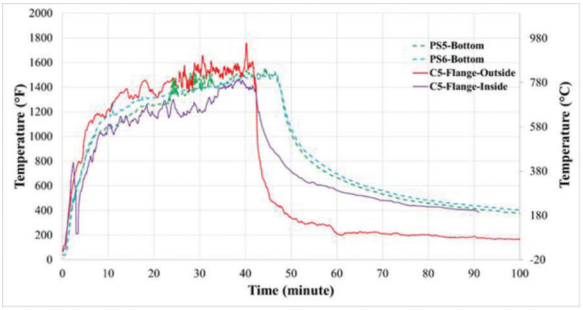

(a) Flange Surface Temperatures

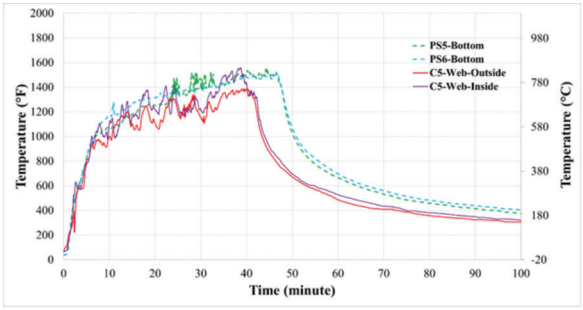

(b) Web Surface Temperatures

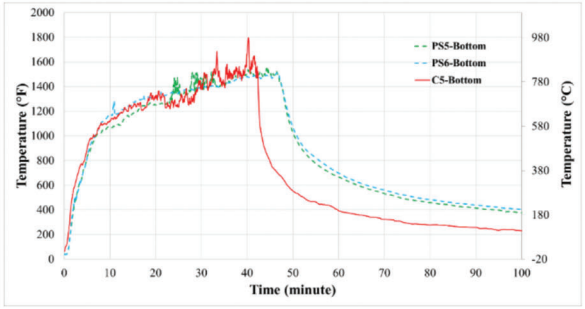

(c) Bottom Surface Temperatures

Figure 8.4 Temperature measurements for Beam C5.

measured during the test are summarized in Table 8.1. In Figure 8.4(a), temperature histories for both the inside and outside vertical surfaces of the bottom flange of the specimen are shown. These two curves follow a similar trend overall. The maximum measured temperatures at these locations on the bottom flange were 1,759°F (959°C) on the outside surface and 1,462°F (794°C) on the inside surface. Moreover, the temperature measurements obtained from the previous pool fire test (discussed in Section 6.2) are also plotted on the same figure to provide a comparison. It can be observed that, although the burning durations were slightly different for the two different pool fire tests (48 minutes for Specimens PS5 and PS6; 43 minutes for Beams C5 and C7), the surface temperature-time curves are quite comparable.

Figure 8.4(b) and (c) present the temperature measurements at the web and the bottom surface of Beam C5. It can be observed that the temperature-time curves for the inside and outside surfaces of the web are similar. Moreover, the surface temperatures of the web and the bottom surface were also comparable to the data obtained from Specimens PS5 and PS6, which illustrates the repeatability of the pool fire tests performed for the research program.

The temperature data for Beam C7 are plotted in Figure 8.5, and the maximum experienced surface temperatures are listed in Table 8.1. For Beam C7, the temperatures experienced by the inside surfaces of the member were significantly greater than those experienced by the outside surfaces. This observation is especially true for the temperature measured on the surfaces of the web. The observed trend is attributed to the uneven fire distribution due to the presence of wind during the pool fire test. Finally, the temperature histories for both the bottom surface and the inside surfaces follow the same trend as the surface time-temperature curves for the prismatic Specimens PS5 and PS6, indicating the similarities of the testing conditions for these two pool fire tests.

TABLE 8.1
Maximum Temperatures at Different Locations for Beams C5 and C7

	Beam C5	Beam C7
Location	**Maximum Temperature (°F) [°C]**	**Maximum Temperature (°F) [°C]**
Bottom Surface	1,796 [980]	1,536 [836]
Inside Bottom Flange	1,462 [794]	1,488 [809]
Inside Web	1,560 [849]	1,488 [809]
Outside Bottom Flange	1,759 [959]	1,094 [590]
Outside Web	1,389 [754]	852 [456]

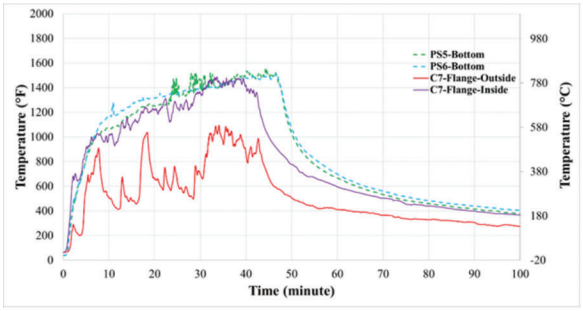

(a) Flange Surface Temperatures

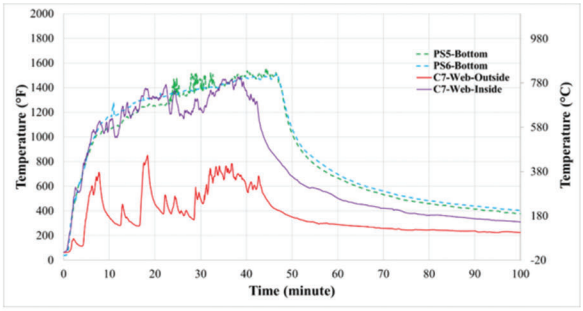

(b) Web Surface Temperatures

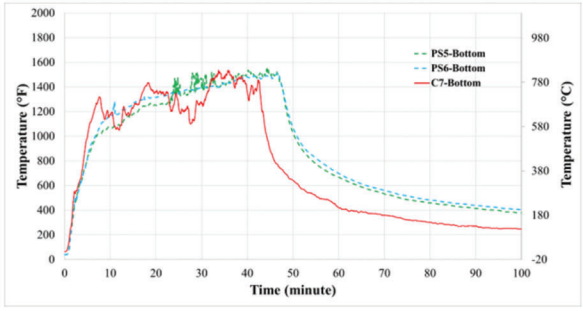

(c) Bottom Surface Temperatures

Figure 8.5 Temperature measurements for Beam C7.

8.2 Test Results for Ambient Load Tests on Prestressed Girders

As described in Section 7.3.1, Beam C2 was tested in its natural condition to provide a comparison to the specimens exposed to fire. The spacing of the stirrups facilitated two unique tests on the girder. The flexure-controlled test was conducted first, followed by the shear-controlled test.

8.2.1 Flexure-Controlled Load Test (C2-Flexure)

The flexure-controlled ambient load test (C2-Flexure) used the test setup presented in Figure 7.3. During the test, cracking was first observed at an applied load of 140 kips; vertical flexural cracks were noted near the loading point. Upon further loading, flexural cracks continued to develop and propagate, and shear cracking (both web-shear and flexural-shear cracks) also developed. Cracking at an applied load of 200 kips is shown in Figure 8.6.

The load-deflection curve for the test is presented in Figure 8.7. During the test, the maximum applied load resisted by the specimen, P_{test}, was 269 kips. The bending moment at the location of the loading point, M_{test}, corresponding to this maximum applied load is 1,016 kip-ft. The specimen experienced a flexural failure, resulting in a sudden loss in load carrying capacity at a deflection of 2.12 in. measured at the location of the loading point. Figure 8.8 shows the failure region of the specimen. Failure was characterized by concrete crushing in compression within the composite deck and the opening of a flexural crack located approximately 1 ft from the loading point, as shown in Figure 8.8. The occurrence of concrete crushing and opening of the crack took place simultaneously. Moreover, rupture of strands (both bottom strands and harped strands) could be observed after removing the concrete at the damaged region. The load-deflection plot in Figure 8.7 includes a load plateau, indicating ductile behavior prior to the occurrence of the flexural failure.

8.2.2 Shear-Controlled Load Test (C2-Shear)

The shear-controlled ambient load test (C2-Shear) used the test setup presented in Figure 7.5. Similar to the flexure-controlled test, flexural cracking during the test was initially observed at an applied load of 140 kips. When the applied force reached 160 kips, the first diagonal crack, a web-shear crack, was observed. Cracks continued to develop and propagate upon further loading. The cracking at an applied load of 240 kips is shown in Figure 8.9. Significant shear

(a) North Side of the Loading Point (b) South Side of the Loading Point

Figure 8.6 Cracking for C2-Flexure at an applied load of 200 kips.

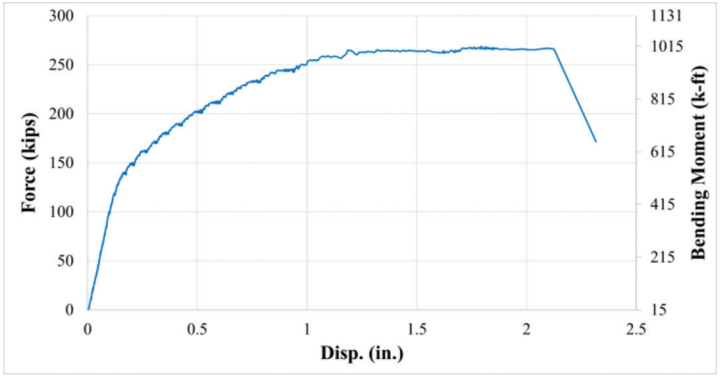

Figure 8.7 Load-deflection curve for C2-Flexure.

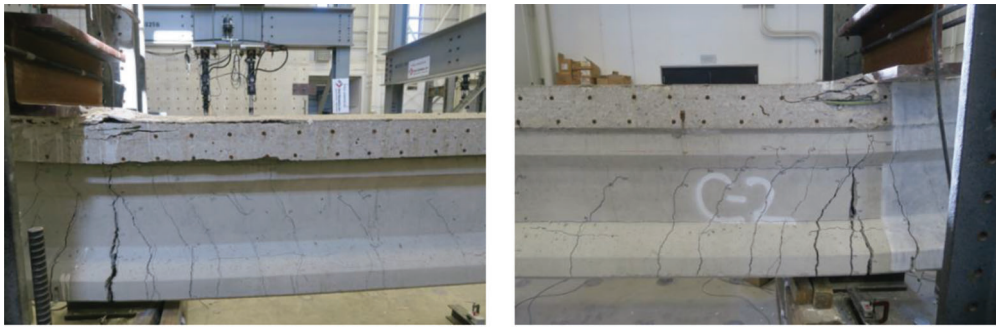

(a) East Side of the Specimen (b) West Side of the Specimen

Figure 8.8 Failure condition for C2-Flexure.

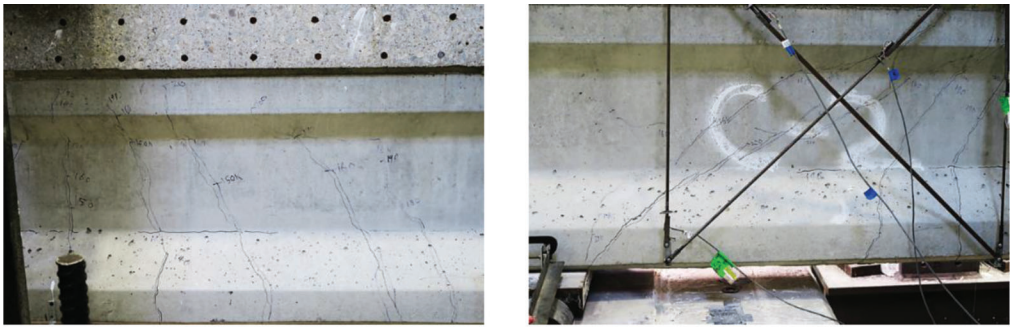

(a) North Side of the Loading Point (b) South Side of the Loading Point

Figure 8.9 Cracking for C2-Shear at an applied load of 240 kips.

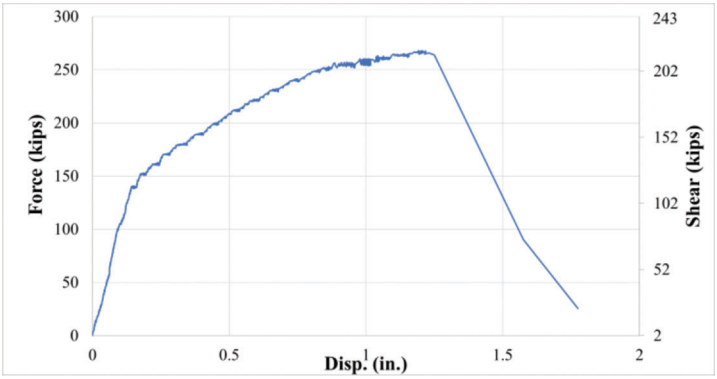

Figure 8.10 Load-deflection curve for C2-Shear.

cracking is noted within the 54-in. shear span of the girder (Figure 8.9(b)).

The load-deflection curve for the test is presented in Figure 8.10. The maximum applied load resisted by the specimen, P_{test}, was 268 kips, which corresponds to a shear force, V_{test}, of 217 kips within the 54-in. shear span. A sudden shear failure along with a sudden loss in load-carrying capacity occurred at a deflection of 1.25 in. measured at the location of the loading point. The shear failure was characterized by slip along the primary diagonal crack and can be classified as being dominated by D-region shear. The specimen after failure is shown in Figure 8.11. Because of the shear-dominated behavior of the girder during the test, a clear load plateau is not observed in the load-deflection curve in Figure 8.10.

The maximum applied loads resisted during the tests C2-Flexure and C2-Shear were very similar (269 kips and 268 kips, respectively). However, the difference in stirrup spacing resulted in different failure behaviors. The reader should also keep in the mind the slight difference in the setups between the two tests

(a) East Side of the Specimen (b) West Side of the Specimen

Figure 8.11 Failure condition for C2-Shear.

(a) East Side of the Specimen (b) West Side of the Specimen

Figure 8.12 Damaged condition of Beam C7 near loading point prior to load test.

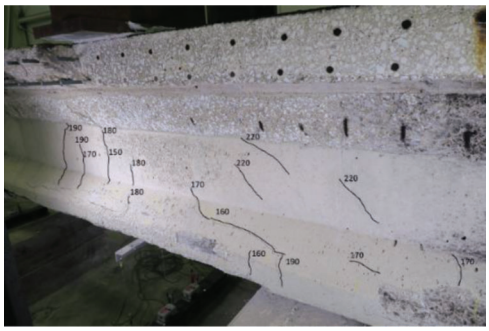

Figure 8.13 Cracking of Beam C7 at an applied load of 220 kips.

(see Figures 7.3 and 7.5) when considering the relationship between the applied load and both the bending moment and the shear force.

8.3 Test Results for Post-Fire Load Tests on Prestressed Girders

After being exposed to fire during the 43-minute-long pool fire test, Beams C5 and C7 were transported to the laboratory to conduct post-fire load tests. To allow direct comparison with the results from the ambient load tests, the test setups for Beams C5 and C7 were identical to those used for the ambient tests (C2-Shear and C2-Flexure).

8.3.1 Flexure-Controlled Load Test (C7)

The setup for flexure-controlled load tests was used for the test on Beam C7. The damaged state of Beam C7 prior to the load test is shown in Figure 8.12. Due to the distribution of the flames during the pool fire test, the intensity of the temperatures experienced by the specimen was different for the two sides of the member, as described in Section 8.1. On the west side of the specimen (Figure 8.12(b)), severe spalling of both the top and bottom flanges is noted. A large portion of the top flange of the precast girder was lost. Additionally, the flaking of the concrete surface of the web of the specimen can be seen in the figure. On the east side of the specimen (Figure 8.12(a)), however, the damage was less severe due to the lower temperatures that were experienced. Although some spalling is noted, the flanges were mostly intact for this side of the specimen.

The cracking for Beam C7 under an applied load of 220 kips is shown in Figure 8.13. New crack development observed during the load test is indicated with black lines. As with the previous tests on Beam C2 at a similar loading stage, both flexure and shear cracks were observed within the test region.

The load-deflection curve for Beam C7 is presented in Figure 8.14. The specimen resisted a maximum applied load, P_{test}, of 265 kips, corresponding to a bending moment, M_{test}, of 1,001-kip-ft and a shear force, V_{test}, of 222 kips. The ultimate failure of the specimen and a sudden loss in load-carrying capacity occurred at a deflection of 2.22 in. measured at the location of the loading point. The specimen experienced failure within the region north of the loading point (that is, the longer shear span), as shown in Figure 8.15. The failure behavior seemed to be influenced by a combination of flexure and shear. Sudden slip along the primary failure crack in the web of the girder was accompanied by crushing of concrete in the composite deck (Figure 8.15(c)) and buckling of the compression bars. It can be observed that the primary failure crack propagated horizontally into the bottom flange north side of the loading point for a distance of approximately 12 ft, splitting the bottom flange. It should be noted that the load-deflection curve in Figure 8.14 includes a load plateau similar to the response curve for the C2-Flexure test that resulted in a flexural failure of Beam C2.

8.3.2 Shear-Controlled Load Test (C5)

The setup for shear-controlled load tests was used for the test on Beam C5. The damaged condition of the member prior to the load test is shown in Figure 8.16. The damage caused by the hydrocarbon fire was significant for both sides of the specimen. In the test region, the top flange had experienced severe spalling. Furthermore, cracking and spalling impacted the bottom flange on both its side surfaces and bottom surface. The spalling caused a reduction in the cross section of the member.

The first notable crack that developed during the load test was observed at an applied load of 100 kips near the support reaction. The cracking of Beam C5 at an applied load of 170 kips is shown in Figure 8.17. It should be noted that the cracking of the girder was not closely inspected when the applied load exceeded 180 kips due to safety concerns.

The load-deflection curve for Beam C5 is provided in Figure 8.18. The maximum load applied to the specimen, P_{test}, was 246 kips, corresponding to a bending moment, M_{test}, of 900-kip-ft and a shear force, V_{test}, of 200 kips. The ultimate failure of the specimen occurred at a deflection of 1.19 in. measured at the location of the loading point. Failure occurred within the 54-in. shear, as shown in Figure 8.19. The primary failure crack extended from the loading point to the support reaction, indicating failure along the strut extending between the load and the support. As shown in Figure 8.19, a horizontal crack propagated along the bottom flange and extended beyond the loading point (Figure 8.19(c)). The lack of a load plateau along the load-deflection curve in Figure 8.18 resembles the response curve for the C2-Shear test on Beam C2.

8.4 Comparison Between Ambient and Post-Fire Load Tests

The load-deflection curves for the flexure-controlled (C2-Flexure and C7) and shear-controlled (C2-Shear and C5) load tests are compared in Figures 8.20 and 8.21, respectively. The maximum applied force, initial stiffness, and the corresponding shear force and bending moment are summarized in Table 8.2 for the four tests. Furthermore, the ratios for the values for the fire-damaged girders to those for the ambient tests are shown in parentheses.

For the flexure-controlled load tests, the maximum applied load for Beam C7 was 265 kips, which is equal to 98.5% of the maximum load resisted by Beam C2 not damaged by fire. However, the initial stiffness of the fire-damaged specimen was significantly less than that observed for the ambient test. In this case, a 34.6% reduction in initial stiffness occurred. The load-deflection plots in Figure 8.20, however, reveal that there is essentially no difference in the load plateau demonstrated by the behaviors of both specimens, and the maximum displacements achieved are very similar.

For the shear-controlled load tests, the maximum applied load for the post-fire test (C5) was 246 kips. This value is equal to 91.8% of the maximum applied load for the shear-controlled test on Beam C2. Again, a significant reduction in initial stiffness due to the fire damage is observed. Specifically, the reduction on the

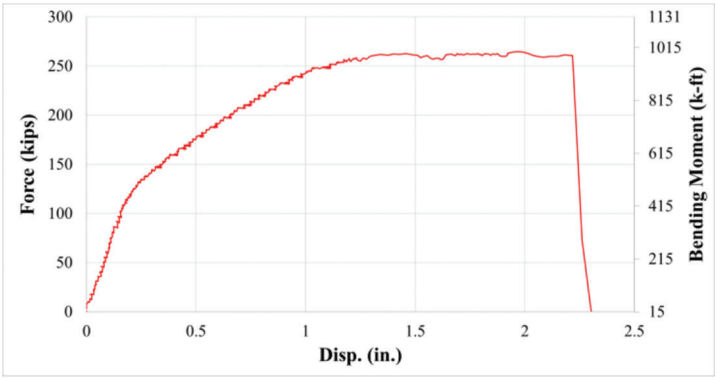

Figure 8.14 Load-deflection curve for Beam C7.

(a) East Side of the Specimen

(b) West Side of the Specimen

(c) Crushed Concrete Near the Loading Point

Figure 8.15 Failure condition of Beam C7.

(a) East Side of the Specimen

(b) West Side of the Specimen

Figure 8.16 Damaged condition of Beam C5 near loading point prior to load test.

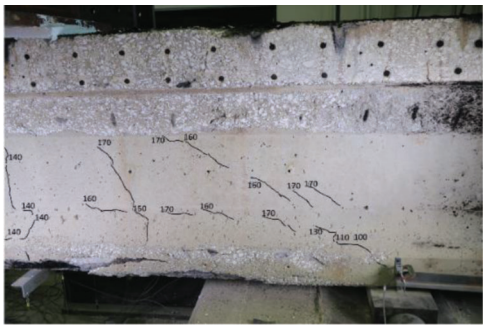

Figure 8.17 Cracking of Beam C5 at an applied load of 170 kips.

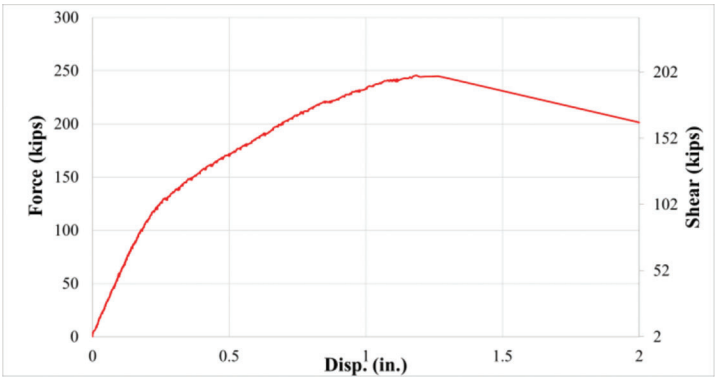

Figure 8.18 Load-deflection curve for Beam C5.

(a) East Side of the Specimen

(b) West Side of the Specimen

(c) Cracking Extending Along Beam C5

Figure 8.19 Failure condition of Beam C5.

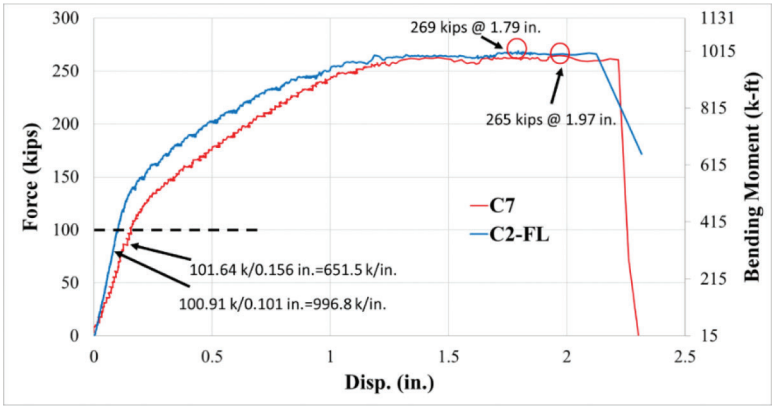

Figure 8.20 Comparison of load-deflection curves for flexure-controlled load tests.

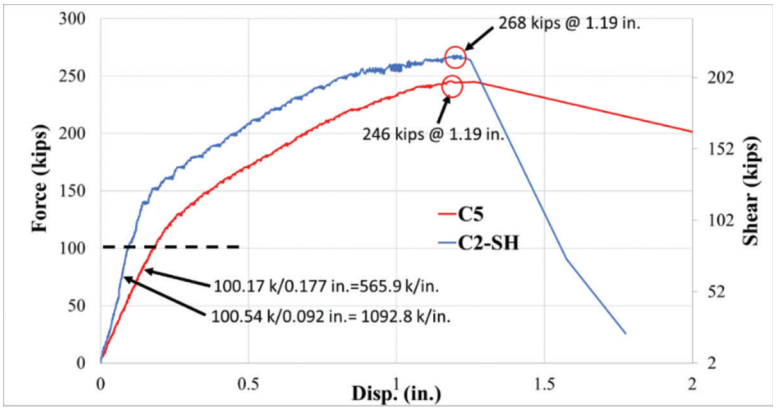

Figure 8.21 Comparison of load-deflection curves for shear-controlled load tests.

TABLE 8.2
Comparison of Test Results for Ambient and Post-Fire Load Tests

Specimen	Max. Applied Load, P_{test} (kips)	Max. Shear Force, V_{test} (kips)	Max. Bending Moment, M_{test} (k-ft)	Initial Stiffnes (kips/in.)
C2-Flexure	269	226	1,016	996.8
C2-Shear	268	217	979	1,092.8
C7	265 (98.5%)	222 (98.2%)	1,001 (98.5%)	651.5 (65.4%)
C5	246 (91.8%)	200 (92.2%)	900 (91.9%)	565.9 (51.8%)

initial stiffness for the damaged girder was 48.2% compared to the specimen not exposed to fire. Despite this difference in behavior between the specimens, the overall behaviors demonstrated by the load-deflection plots in Figure 8.21 are similar.

Furthermore, consideration of the development length of the straight prestressing strands in the bottom flange can provide observations related to the bond between strands and concrete. For design, the calculated development length represents the length over which the stress in the strands can increase from zero at the member end to the stress corresponding to the nominal flexural strength, f_{ps}. For the specimens tested in flexure, the distance from the beam end to the point of maximum moment was 102 in., and the development length of the strands was 129 in. as calculated in accordance with Equation 5.9.4.3.2-1 of the AASHTO LRFD specifications (AASHTO, 2017). The calculated value of f_{ps} is equal to 265 ksi (assuming the strands are low-relaxation strands and f_{pu} is equal to 283 ksi obtained from strand tests), and f_{pe} considering all losses is calculated as 156 ksi for the test girders. Therefore, the maximum moment occurred within the calculated development length measured from the end of the girder. Because the maximum applied loads for the flexural tests on Beam C2 (C2-Flexure) and Beam C7 were very similar, it can be inferred that the stress in the strands achieved by the fire-damaged specimen was similar to the stress achieved by the strands of the undamaged specimen. Although the calculated development length is typically conservative (Article C5.9.4.3.2 of AASHTO LRFD (AASHTO, 2017)), it is significant to note that no indication of bond degradation within the calculated development length of the strands is observed. It should also be noted, however, that only a portion of the girder along the development length of strands experienced extreme temperatures caused by the fire. In this region, the strands were still encased in concrete. Effects on strand bond in the immediate vicinity of the fire are difficult to assess, and an extreme fire at the end of the member or that causes severe spalling of the concrete cover along the strands may have resulted in different effects on the development length.

Lastly, during flexural load tests on concrete members, a change in the slope of the load-deflection response typically occurs when the member cracks in flexure. For simply supported prestressed beams, cracking occurs when the effect of prestress is overcome at the bottom of the member and the tensile stress reaches the modulus of rupture, f_r, of the concrete. Therefore, the prestress losses in the prestressing strands caused by fire can be considered by comparing the calculated cracking loads (i.e., the load at which a slope change is expected) and the loads corresponding to the change in slope of the experimental load-deflection plots. The values corresponding to this comparison are presented in Table 8.3. It should be noted that for the fire-damaged girder (Beam C7), the load is calculated assuming that there were no fire-induced prestress losses (f_{pe} taken as 156 ksi) and that the specimen was pre-cracked in flexure after the pool fire test (f_r is taken as 0). For the ambient test, the modulus of rupture was assumed to equal $7.5\sqrt{fc}$. It should also be noted that any loss in the effective cross section of the damaged specimen is not considered for this comparison. Comparing the calculated and experimental load values corresponding

TABLE 8.3
Comparison of Loads Corresponding with Cracking/Change in Slope

Specimen	Calculated Load (kips)	Measured Load Corresponding to Slope Change (kips)
C2-Flexure	149	138
C7	103	116

to a change in slope of the load-deflection plot as presented in Table 8.3, no effect on the prestress force in the strands is indicated if the assumption that the damaged girder was effectively pre-cracked in flexure is indeed correct (see Section 8.1.1).

In summary, although the strengths of the damaged and undamaged girders were relatively similar, the reduction in initial stiffness due to damage caused by the hydrocarbon fire is apparent. However, based on the discussion above, the fire event does not seem to have a significant influence on the bond of prestressing strands and on the prestress losses.

8.5 Results of the Evaluation of Microstructure of Concrete

The evaluation of changes in the microstructure of concrete exposed to the hydrocarbon fire was conducted by examining polished specimens obtained from the fire-damaged part of the prestressed bridge girder under the scanning electron microscope (SEM) equipped with the energy dispersive spectroscopy (EDS) x-ray detector. Based on the material analysis conducted on the deck specimens and prismatic specimens (see Sections 4.2 and 6.3, respectively), it was assumed that the concrete microstructure degradation could be severe within the first 1-in. depth from the exposed surface and may not be significant at depths beyond 1 in., even for extreme conditions of the hydrocarbon fire the girder was exposed to. Based on these assumptions, the SEM specimens were prepared by sectioning (with the water-cooled saw) several concrete pieces with thicknesses greater than 2 in. that had spalled from the test region during the load test. Because the condition of the fire damaged concrete was similar for both the two prestressed girders (with the exception of one side of Beam C7), samples from Beam C5 were selected for performing the representative material analyses.

The results of the SEM observations of the microstructure of concrete from Beam C5 are shown in Figure D.1 (in Appendix D). The examination of the microstructure of the specimen located within the first 0.75 in. from the surface of the girder exposed to fire (Figure D.1 (a–c)) reveals severe alterations of the microstructure. These alterations involve the development of multiple, relatively wide cracks and debonding of aggregate from the matrix. In some cases (Figure D.1(c)) cracks from the matrix extend into the aggregate particles. The extensive network of cracks observed in this region suggests that concrete microstructure was severely damaged by high temperatures experienced by the girder. Although some cracks can still be seen in the microstructure of specimen located at the depth between 0.75 in. and 1 in. from the fire-exposed surface (Figure D.1(d)), these cracks are less numerous and finer than those observed in the section closer to the surface. The overall appearance of the paste appears to be less altered compared to the appearance of the paste from locations closer to the exposed surface. Lastly, at depths beyond 1 in. from the exposed surface (Figure D.1 (e and f)), only a limited number of minor cracks can be observed, and the cement matrix appears to be nearly intact. These observations suggest a negligible effect of fire on the microstructure of concrete located within this region.

Figure D.2 shows locations of calcium hydroxide (CH) deposits in the microstructure of concrete at various depths from the surface exposed to fire. These deposits were identified using energy dispersive spectroscopy (EDS) x-ray detector that allows for characterization of elemental chemical composition of the analyzed area. Since the CH decomposes in the temperature range from about 752°F–932°F (400°C–500°C) see Sections 4.2 and 6.3 for more detailed analysis, the relative changes in the frequency of these deposits provide an indirect indication of the range of temperatures that part of the beam was exposed to.

The locations of the CH deposits (as identified by the EDS x-ray signal) within the microstructure of concrete from the fire-damaged Beam C5 at various depths from the surface directly exposed to the hydrocarbon fire are shown in Figure D.2. In mature concrete, such CH deposits are commonly found in the interfacial zone between the paste and the aggregate. As seen from Figure D.2, there is a notable scarcity of CH deposits in the interfacial zone of concrete located within the first 0.75 in. from the surface exposed to fire. In fact, in many cases the continuity of the interfacial zone has been compromised by development of debonding cracks devoid of CH. These observations indicate that the maximum temperature within this region likely exceeded 752°F (400°C).

In contrast, the microstructure of concrete located at depths between 0.75 in. and 2 in. contains numerous deposits of CH in the interfacial zones. These can be easily identified by the presence of somewhat "whitish in appearance" thin, continuous "ribbons" of material located at the boundary between the paste and the aggregate particle with a "chemical signature" of calcium (Ca), see Figure D.2(d–e). The presence of the CH deposits indicates that the maximum temperature within this region was likely below 752°F (400°C). Furthermore, only a few small cracks were observed in this region, indicating that the fire-induced damage at these depths was relatively insignificant.

In summary, the microstructure concrete from Beam C5 was quite similar to the microstructure of concrete in the prismatic specimens heated using a pool fire (see discussion of data for specimens PS6 in Section 6.3), indicating that while the first 0.75 in. of concrete was severely damaged, the material located at greater depths was relatively unaffected by the hydrocarbon fire. Additionally, the damaged conditions are also comparable to the results from the prismatic specimens heated for 80 minutes using the radiation-based heaters, suggesting that the 80-minute controlled heating tests conducted in the laboratory can properly simulate the damage conditions resulting from a pool fire.

9. POST-FIRE INSPECTION GUIDELINES

9.1 Overview

This chapter provides guidelines for engineers or first responders to inspect and assess prestressed concrete bridge girders after fire events. These recommendations are developed based on the findings of the research project and provided for the following purposes:

1. Identifying regions with critical fire damage.
2. Taking samples/cores.
3. Conducting non-destructive and microstructure evaluations.
4. Estimating the maximum temperature and duration of heating.
5. Estimating structural degradation using (a)–(d).
6. Proposing potential plans for short-term repair/rehabilitation.

A checklist for inspectors and engineers has been developed and shown in Table 9.1. The following sections summarize details about the provided recommendations.

9.2 Color Change Inspection

As discussed in Section 2.2.3, the exposed concrete surface changes color after sustaining exposure to elevated temperatures. Figure 9.1 presents the color change of heated concrete surfaces (with and without exposed aggregates) for various temperature ranges. Shortly after the fire event, engineers shall inspect the color of the heated concrete surfaces and use the provided figure to estimate the maximum surface temperatures at different locations of concrete bridge components. A contour map of the observed color changes and estimated maximum temperature should be developed for different regions of the bridge and its components.

9.3 Concrete Hardness Testing

An impact rebound hammer (Schmidt Hammer) shall be used to test the concrete surface hardness for different regions of the bridge and its components. The impact rebound hammer shall be used to obtain (1) reference readings in regions away from fire exposure, and (2) readings in regions with fire exposure and damage but no spalling. A contour map of the concrete surface hardness should be developed for the fire damaged regions of the bridge and its components. The contour maps of (1) concrete color, (2) estimated maximum temperature, and (3) surface hardness can be overlaid for comparison.

9.4 Concrete Coring and Material Testing

Concrete samples or cores shall be obtained from regions with the anticipated maximum surface temperature and damage. These concrete samples should be collected and their microstructure should be evaluated as soon as possible (preferably within 1–2 days after the

TABLE 9.1
Checklist for Recommended Practices

Step	Title	Content
1	Visual Inspection	Inspect and record concrete color change at different locations. Record the distribution of concrete cracking and spalling. Develop a concrete color/surface temperature contour map for the damaged girder. If available, record the method used to extinguish the fire.
2	Non-Destructive Testing	Use Schmidt Hammer to test concrete hardness. Establish a concrete hardness contour map for the damaged girder. Compare the concrete hardness and color contour maps.
3	Concrete Sample Coring (Optional)	Take concrete samples using coring equipment for material analysis. The diameter of the core should not be greater than 2 in. The core depth need not be greater than 1 in. unless the fire duration was >1 hour.
4	Material Analysis (Optional)	Conduct material evaluation on cored samples. These can include one or more of the following: scanning electron microscopy (SEM), energy dispersive spectroscopy (EDS), and differential scanning calorimetry (DSC).
5	Damaged Concrete Removal	Remove loose and damaged concrete using manual procedures or appropriate equipment/tools as needed.
6	Mesh Protection	Use protective mesh to cover the damaged regions and protect vehicles and personnel from concrete debris.
7	Short-Term Repair Plans	Develop short-term repair plans for prestressed girders. These can consist of removing and replacing fire damaged concrete (up to depth of 1 in.) with fresh concrete or mortar.

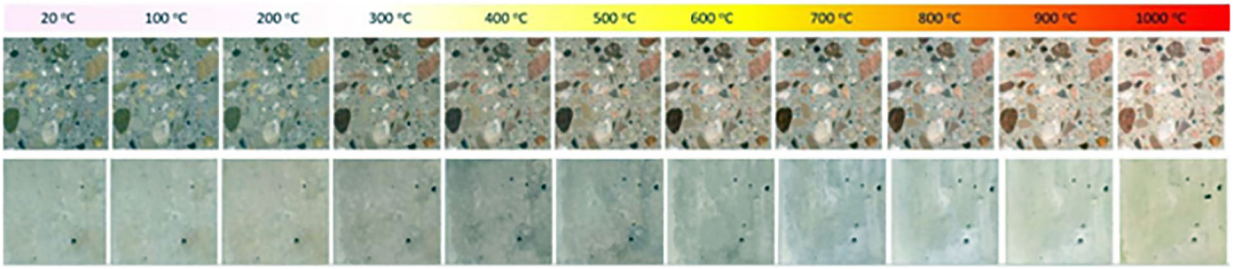

Figure 9.1 Color variation of heated concrete (Hager, 2013).

TABLE 9.2
Fire Type and Duration vs. Concrete Temperature and Damage Depth

Fire Type	Duration (min.)	Air/Fire Temperature	Concrete Surface Max. Temperature	Depth of Concrete Damage (in.)
Standard	40 min.	1,600°F	1,100°F	0.25
Standard	80 min.	1,800°F	1,600°F	0.75
Hydrocarbon	50 min.	2,000°F	1,600°F	1.0

fire event) to avoid potential microstructural alteration. The sample/core depth need not be greater than 1.5 in. from the surface. For situations with fire duration of 60 minutes or less, the core depth need not be greater than 1.0 in. from the surface. In some cases, the concrete may spall off from the region with maximum temperature and damage, and coring may not be required to collect samples. Microstructural evaluation of concrete from the heated concrete bridges may be performed using scanning electron microscopy (SEM), energy dispersive spectroscopy (EDS), differential scanning calorimetry (DSC) or thermogravimetric analysis (TGA). These microstructural evaluations are optional but may be useful to establish or confirm the extent/depth of concrete microstructure cracking and damage as well as decomposition of calcium hydroxide if needed for specific evaluation/assessment.

9.5 Assessment

The extent of concrete material damage on the surface and through the depth of the component shall be assessed using: (1) the information available about fire type and approximate duration, (2) the information collected about concrete surface color and hardness, (3) the information about the method used to extinguish the fire, and (4) the information obtained from microstructure evaluation (optional). The fire temperature can be much higher than the concrete surface temperature, which lags behind because of the thermal mass and properties of the concrete. Experimental results are summarized as Table 9.2 for reference. In most cases, even an intense hydrocarbon fire with a duration of about 50 minutes does not cause the depth of the concrete damage to exceed 1.0 in., while the maximum concrete surface temperature reaches 1,600°F and the maximum fire/air temperature reaches 2,000°F.

Experimental investigations conducted on prestressed concrete bridge girders (decommissioned from an existing bridge in service for approximately 30 years) indicate that even the intense hydrocarbon fire (described above in Table 9.1) does not cause significant (less than 10%) degradation in the flexural strength and shear strength after the fire event. Concrete material damage is superficial and remains constrained to depths of up to 1 in. from the fire exposed surface. The initial stiffness of the prestressed girders will likely be reduced.

9.6 Short-Term Repair/Rehabilitation

The first step is to remove the loose and damaged concrete using manual procedures or hydro-blast methods if appropriate. The second step is to use a metal mesh to surround and constrain the damaged concrete to prevent debris breaking loose or falling. The short-term repair of prestressed concrete bridge girders can consist of removing fire damaged concrete up to depth of 1 in. and replacing with fresh concrete or mortar. Moreover, externally bonded fiber reinforced polymer (FRP) sheets can be added to confine the repaired area. The long-term durability of such fire damaged, repaired prestressed concrete girders has not yet been investigated.

9.7 Checklist

A checklist for inspectors and engineers has been developed and shown in Table 9.2.

9.8 Potential Long-Term Repair Strategies

Long-term repair methods for fire damaged prestressed concrete bridge girders have not been researched in the past. Some repair methods have been discussed previously in the literature (Stoddard, 2004); however, there is much more research on the repair of prestressed concrete bridge girder subjected to impactive damage (Harries, 2012). An appropriate repair method should restore the load-carrying capacity, long-term serviceability, and durability of the bridge. Additionally, the construction economy and feasibility of the repair method needs to be assessed.

The typical long-term repair methods for fire-damaged prestressed concrete bridge components combine concrete replacement with pre-compression restoration if needed. For example, the first step is to remove the loose, spalling concrete either manually or by hydro-blast methods. If damage has extended to the prestressing strands, which is rare, then the prestressing force can be reintroduced by applying vertical preload or installing new prestressing strands. Subsequently, new cementitious material is cast to replace the removed concrete. A bonding agent can be placed between the new material and old concrete to provide adhesive bond as needed. Finally, the preload or prestress can be released to compress the new concrete. Furthermore, fiber-reinforced polymer (FRP) materials can also be used with appropriate structural adhesives (Harries, 2012) to cover and wrap the replaced concrete material. If needed, the FRP wrap can be used to provide additional stiffness or strength to the repaired concrete girders.

These are just examples, and the actual repair methods should be designed for the specific damage situation and construction/repair activity constraints. This is part of the recommended future work as discussed in Chapter 11.

10. CONCLUSIONS

Based on the experimental investigations conducted as part of this project, including fire (heating) tests, material tests, and structural loading tests, the following conclusions are drawn:

1. The duration of heating determines the temperature profile through the thickness of concrete. If the fire lasts for a longer duration, the temperature through the depth of the concrete increases.
2. If the concrete surface temperature history is known, then the temperature profile through the concrete depth can be estimated using 1D heat conduction analysis.
3. The extent or portion of the concrete subjected to temperatures higher than 752°F (400°C) can be determined from the temperature profile through the depth of concrete.
4. The portion of concrete subjected to temperatures higher than 752°F (400°C) loses significant amounts of calcium hydroxide (CH), which decomposes by losing water and converting to calcium oxide (lime). The decomposition of CH increases porosity of the affected area. In addition, the portion of the concrete affected by CH decomposition also developed significant cracking, which further reduces the strength and increases permeability.
5. Since it is well known that the increased porosity and extensive cracking will reduce strength and increase permeability of the paste matrix, it is highly recommended that the portion of concrete exposed to temperatures higher than 752°F (400°C) be considered fully damaged and repaired or replaced with new material.
6. When concrete components are heated following the ISO-834 standard fire curve, 0.25 in. of concrete from the exposed surface is compromised after approximately 40 minutes due to loss of CH and extensive cracking.
7. After about 80 minutes of ISO-834 standard fire heating, 0.75 in. of concrete from the exposed surface is compromised by the loss of CH and extensive cracking.
8. After about 50 minutes of an intense hydrocarbon fire, 0.75–1.0 in. of concrete from the exposed surface is compromised by the loss of CH and extensive cracking.
9. Prestressed concrete girders exposed to about 50 minutes of intense hydrocarbon fire undergo superficial concrete material damage with loss of CH and extensive cracking and spalling extending to the depth of 0.75–1.0 in. from the exposed surface.
10. However, these prestressed concrete girders exposed to about 50 minutes of intense hydrocarbon fire do not undergo a significant (less than 10%) reduction in flexural strength or shear strength in spite of the superficial concrete material damage, cracking, and spalling. The reduction in the initial stiffness of the specimens may be notable due to concrete damage and loss of cross-sectional area.
11. Based on the development of stresses within the calculated development length of the strands, degradation of bond between the strands and the concrete in the fire-damaged girder tested in flexure was not observed. Furthermore, considering the expected loads at which a change in slope of the experimental load-deflection plots is expected as explained in Section 8.4, prestress losses were not indicated.

Based on these conclusions, bridge inspectors can infer the extent of damage to prestressed concrete bridge girders in the event of a fire and develop a post-fire assessment plan cognizant of the findings. In most cases, no more than 1.0 in. of the concrete from the exposed surface undergoes material damage/deterioration due to loss of CH, cracking, and spalling. The impact on the strength of prestressed concrete girders is relatively minor based on experimental results. Their initial stiffness, however, will likely be notably reduced.

10.1 Expected Benefits from Deliverables, Implementation, and Cost Savings

This project contributed to the INDOT strategic plan with particular focus on key areas, including safety, asset sustainability, and economic competitiveness. The project deliverables and their contributions to these key areas are described below:

1. *Safety:* Experimental investigations conducted as part of this project indicate that prestressed concrete bridge girders sustain only superficial concrete material damage (less than 1 in. from the exposed surface) even after

extreme hydrocarbon fire exposure. The degradation in structural capacity is not significant. This finding can help INDOT engineers/inspectors develop appropriate safety plans immediately after a fire event.

2. *Asset Sustainability:* The magnitude of fire damage for prestressed concrete bridges can be inspected and assessed using the recommended guidelines and checklist provided in this report. This assessment will be beneficial for evaluating the sustainability of bridges exposed to fire. Moreover, subsequent rehabilitation and maintenance activities can also be planned based on the collected information.
3. *Economic Competitiveness:* Results of this project indicate that even intense fire events (e.g., 50-minute hydrocarbon fire, or 80-minute standard fire) do not have a significant influence on the strength of prestressed concrete bridge girders. In many cases, these bridge girders can be repaired and put safely back into service instead of replacing them. Depending on the particular situation, replacement with new girders can be expensive, time consuming, requiring traffic redirection and management, and also impact the environment with additional construction operations.

11. RECOMMENDATIONS FOR FUTURE WORK

The research results presented in this report focused on the effects of fire on (1) concrete material degradation in bridge decks, and (2) concrete material and structural strength degradation in prestressed concrete girders. These research results can be used to conduct post-fire inspection and assessment of prestressed concrete bridge girders and decks. They can also be used to develop plans for short-term repair of fire damaged prestressed bridges. However, additional research is needed to address the following items:

1. The long-term durability of fire exposed bridge girders and decks has not been investigated. In the event of a short fire (less than 20 minutes), there may not be significant concrete cracking, spalling, or structural degradation,
   and repairs may not be needed, but the long-term durability of the fire exposed bridge girders and decks due to the superficial concrete cracking of the exposed surface (up to a depth of 0.25 in.) needs to be evaluated.
2. In the event of a significant fire (approximately 50–60 minutes), there will be concrete material degradation, cracking and spalling in the exposed region. There may not be much degradation in the structural strength, but the damaged concrete material needs to be replaced. Repair procedures for replacing the damaged concrete material (up to 1-in. depth) in the exposed area need to be developed with focus on in-situ implementation. Additionally, the long-term durability of the fire damaged and then repaired bridge girders and decks need to be evaluated.
3. In the event of an extremely significant fire (>60 minutes) accompanied with impactive or impulsive (blast pressure) loading, structural damage of the prestressed concrete girders may also occur. Detailed repair procedures may need to be developed for rehabilitating damaged girders. The construction feasibility, structural performance, and long-term durability of different repair strategies needs to be evaluated.

In summary, future research should focus on: (1) investigating the long-term durability of fire damaged prestressed concrete bridge girders that do not need extensive repair, and (2) developing repair methods for prestressed concrete bridge girders with extensive fire damage, and with focus on the construction feasibility of the repair procedures, structural performance, and long-term durability of the damaged-repaired girders.

LIST OF REFERENCES

AASHTO. (2017). *AASHTO LRFD bridge design specifications* (8th ed.). American Association of State Highway and Transportation Officials.

ACI Committee 318. (2014). *Building code requirements for structural concrete (ACI 318-14): Commentary on building code requirements for structural concrete (ACI 318R-14)*. American Concrete Institute.

Ashraf, W., & Olek, J. (2016). *Investigation of the microstructure of concrete from the girders of the chase street overpass* (INDOT Internal Report).

Ashraf, W., Olek, J., & Jeong, H. (2016, June 30–July 1). Effects of high temperature on carbonated calcium silicate cement (CSC) and ordinary Portland cement (OPC) paste. *5th International Conference on Durability of Concrete Structures*, 1–7. https://doi.org/10.5703/1288284316153

BSI. (2002, November 26). *Eurocode 1: Action on structures: Part 1–2: General action–Actions on structures exposed to fire* (EN 1991-1-2:2002). British Standards Institution.

Graybeal, B. A. (2007, February). *Flexural capacity of fire-damaged prestressed concrete box beams* (Publication No. FHWA-HRT-07-024). Federal Highway Administration. https://www.fhwa.dot.gov/publications/research/infrastructure/structures/07024/07024.pdf

Griffin, B., & Beavis, M. (1992, March 6). *Fire resistance of prestressed concrete*. Retrieved July 18, 2019, from https://core.ac.uk/download/pdf/35470325.pdf

Hager, I. (2013, March). Behaviour of cement concrete at high temperature. *Bulletin of the Polish Academy of Sciences, Technical Sciences*, *61*(1), 145–154. https://doi.org/10.2478/bpasts-2013-0013

Harries, K. A. (2012, May). *Guide to recommended practice for the repair of impact-damaged prestressed concrete bridge girders*. National Cooperative Highway Research Program. http://onlinepubs.trb.org/onlinepubs/nchrp/docs/NCHRP20-07(307)_AppendixA-GUIDE.pdf

Hou, X., Kodur, V. K. R., & Zheng, W. (2014). Factors governing the fire response of bonded prestressed concrete continuous beams. *Materials and Structures*, *48*, 2885–2900. https://doi.org/10.1617/s11527-014-0365-9

Hurley, M. J., Gottuk, D., Hall, J. R., Jr., Harada, K., Kuligowski, E., Puchovsky, M., Torero, J., Watts, J. M., Jr., & Wieczorek, C. (Eds.) (2016). *SFPE handbook of fire protection engineering*. Society of Fire Protection Engineers. https://doi.org/10.1007/978-1-4939-2565-0

Indiana Department of Highways. (1987). *Bridge plans for spans over 20 feet on state road No. 24* (Project No. MAF-I70-1). Indiana Department of Highways.

INDOT. (2013). *Indiana design manual–2013*. Indiana Department of Transportation. https://www.in.gov/dot/div/contracts/design/IDM.htm

INDOT. (2016). *Standard specifications*. Indiana Department of Transportation. https://www.in.gov/dot/div/contracts/standards/book/sep15/2016Master.pdf

Ingham, J. P. (2009). Application of petrographic examination techniques to the assessment of fire-damaged concrete and masonry structures. *Materials Characterization*, *60*(7), 700–709. https://doi.org/10.1016/j.matchar.2008.11.003

ISO. (2002, October). *Fire-resistance tests—Elements of building construction—Part 8: Specific requirements for non-loadbearing vertical separating element* (International Standard ISO 834-8:2002). International Organization for Standardization.

Lee, J., Choi, K., & Hong, K. (2010, May). The effect of high temperature on color and residual compressive strength of concrete. *Proceedings of Fracture Mechanics of Concrete and Concrete Structures*, 1772–1775.

MacLean, K. J. N. (2007). *Post-fire assessment of unbonded post-tensioned concrete slabs: Strand deterioration and prestress loss* [Master Thesis, Queen's University]. QSPACE. https://qspace.library.queensu.ca/handle/1974/954

MacLean, K. J. N., Bisby, L. A., & MacDougall, C. C. (2008). Post-fire deterioration and prestress loss in steel tendons used in post-tensioned slabs [Symposium paper]. *American Concrete Institute–Designing Concrete Structures for Fire Safety Session at the ACI Spring Convention 2007*, *255*, 147–174.

Moore, W. L. (2008). *Performance of fire-damaged prestressed concrete bridges* [Master Thesis, Missouri University of Science and Technology]. Missouri University of Science and Technology Scholars' Mine. https://scholarsmine.mst.edu/masters_theses/6778/

NOAA. (2020). *Climate data online data tools* [Webpage]. National Oceanic & Atmospheric Administration. https://www.ncdc.noaa.gov/cdo-web/datatools

Stoddard, R. (2004, January 15). *Inspection and repair of a fire damaged prestressed girder bridge* (IBC-04-17). International Bridge Conference, Pittsburgh, PA.

Zheng, W., & Hou, X. (2008). Experiment and analysis on the mechanical behaviour of PC simply-supported slabs subjected to fire. *Advances in Structural Engineering*, *11*(1), 71–89.

APPENDICES

Appendix A. Non-Destructive Testing for Post-Fire Concrete Girder

Appendix B. Results of Microstructural Evaluation (SEM/EDS) of Concrete from Deck Specimens

Appendix C. Results of Microstructural Evaluation (SEM/EDS) of Concrete from Prismatic Specimens

Appendix D. Results of Microstructural Evaluation (SEM/EDS) of Concrete from Full-Scale AASHTO Type I Girders

APPENDIX A. NON-DESTRUCTIVE TESTING FOR POST-FIRE CONCRETE GIRDER

The damaging and spalling concrete may endanger vehicles and individuals nearby for the concrete bridges subjected to fire. To investigate the residual surface concrete strength of the prestressed beam experienced a severe fire event, INDOT performed a series of non-destructive testing on the Beam C7 after the pool fire test. The beam was separated into 1-ft long segments and a Schmidt hammer was used to measure the bottom concrete hardness at the endpoint of each segment. The hardness values were labeled at each measured point except the regions above the supporting blocks, as shown in Figure A.1(a). Afterward, the Ultrasonic Pulse Velocity (UPV) equipment was employed to measure the bottom surface's residual concrete strength (as presented in Figure A.1).

By measuring the speed and attenuation of an input ultrasonic wave, the concrete hardness value can be correlated to the compressive strength at a specific point; the results obtained from UPV can be summarized as Table A.1. It should be noted that the location listed in Table A.1 represents the point located at a specific distance from the end of Beam C7 (burned end). It can be noticed that the bottom concrete strengths were neglectable for the region between 7 ft to 12 ft from the end, suggesting that the concrete bottom surface in this region had almost lost all the strength due to the extremely experienced temperature. During the pool fire test, the 4-ft by 8-ft pool was placed under the Beam C7 at the location 8.5 ft. away from the end, indicating that the fire-induced damage on the bottom surface was most serious at the region close to the fire resource. Lastly, the concrete bottom surface's strengths at other regions were apparently higher, although accompanied with some variation (ranged from 1,119 psi to 4,352 psi), suggesting the impact introduced by the fire event was relatively insignificant in these regions.

Table A.1 Non-Destructive Testing Results

Location (ft)	Concrete Strength (psi)	**Location (ft)**	Concrete Strength (psi)	**Location (ft)**	Concrete Strength (psi)
1	2,164	**14**	1,413	**23**	2,407
2	2,262	**15**	2,811	**24**	3,718
7	0	**16**	3,558	**25**	2,885
8	0	**17**	2,000	**26**	4,004
9	0	**18**	4,352	**27**	4,176
10	0	**19**	3,096		
11	0	**20**	2,701		
12	0	**21**	2,110		
13	2,808	**22**	1,119		

(a) Labeled Concrete Hardness

(b) UPV Applied on the Bottom Surface

Figure A.1 Procedures of non-destructive testing.

APPENDIX B. RESULTS OF MICROSTRUCTURAL EVALUATION (SEM/EDS) OF CONCRETE FROM DECK SPECIMENS

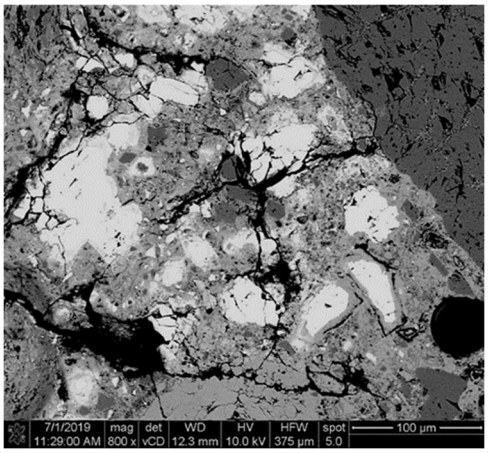

(a) Exposed Surface–0.25 in.: 897°F (481°C)

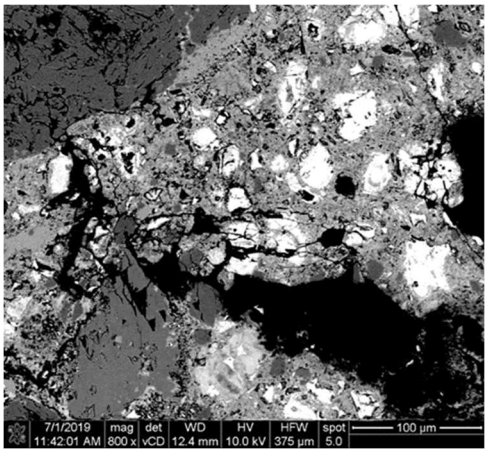

(b) 0.25 in.–0.5 in.: 782°F (417°C)

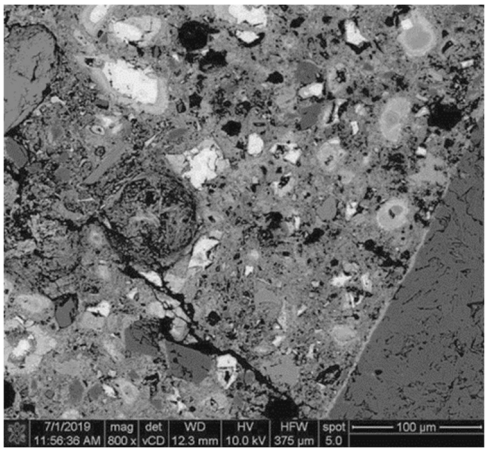

(c) 0.5 in.–0.75 in.: 667°F (353°C)

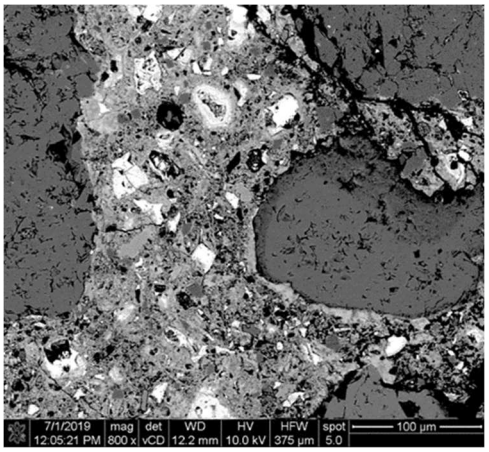

(d) 0.75 in.–1 in.: 553°F (289°C)

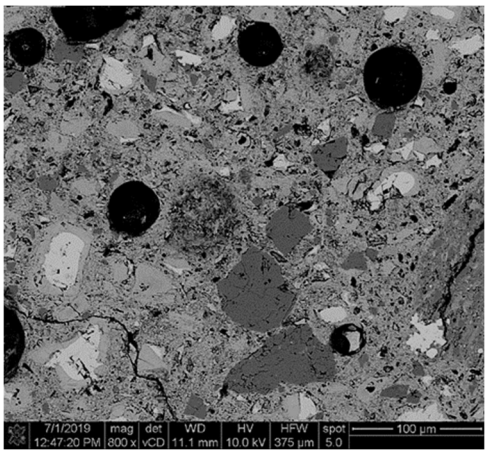

(e) 1 in.–1.5 in.: 390°F (199°C)

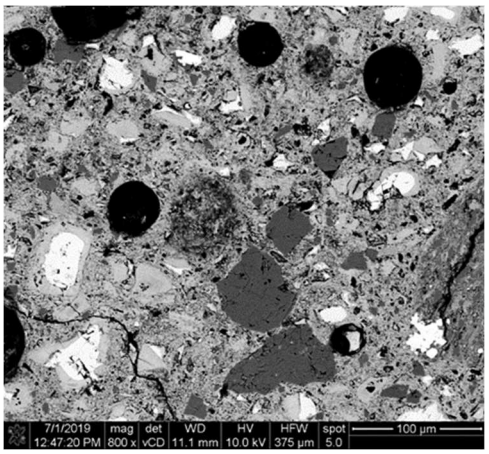

(f) 1.5 in.–2 in.: 284°F (140°C)

Figure B.1 SEM images of microstructure of heated–40 Specimen.

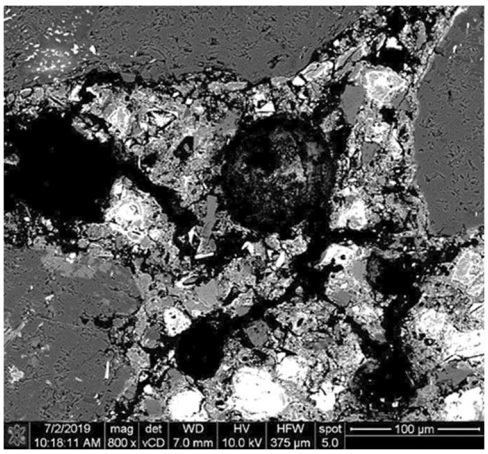

(a) Exposed Surface–0.25 in.: 1,186°F (641°C)

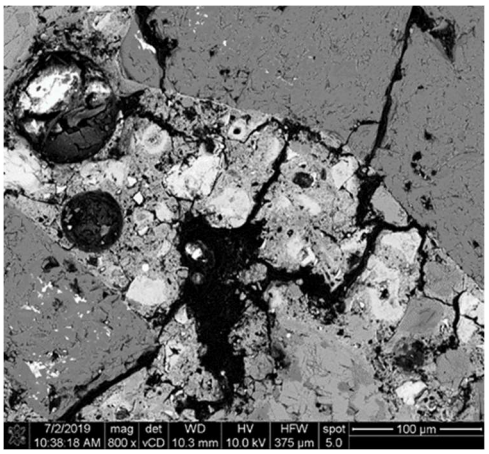

(b) 0.25 in.–0.5 in.: 1,080°F (582°C)

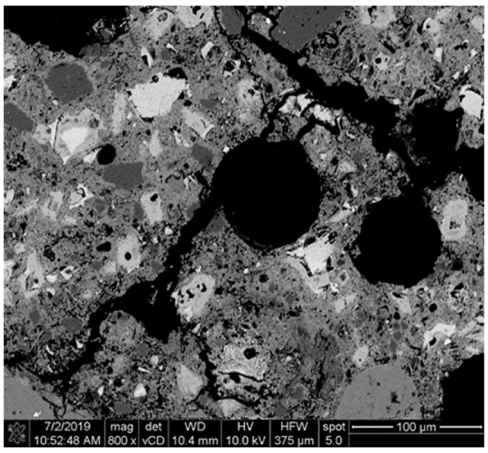

(c) 0.5 in.–0.75 in.: 974°F (523°C)

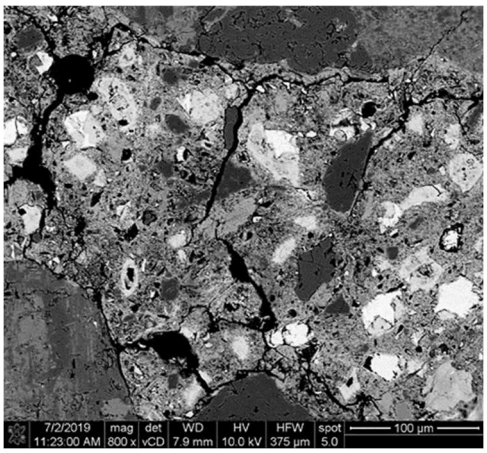

(d) 0.75 in.–1 in.: 880°F (471°C)

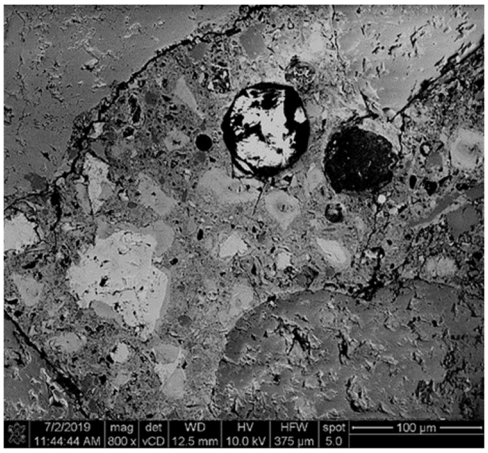

(e) 1 in.–1.5 in.: 692°F (367°C)

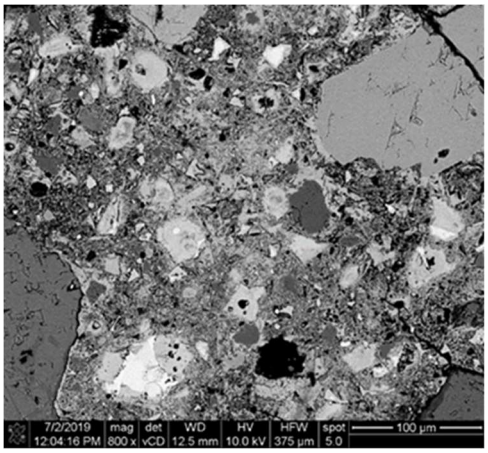

(f) 1.5 in.–2 in.: 553°F (289°C)

Figure B.2 SEM images of microstructure of heated–80 Specimen.

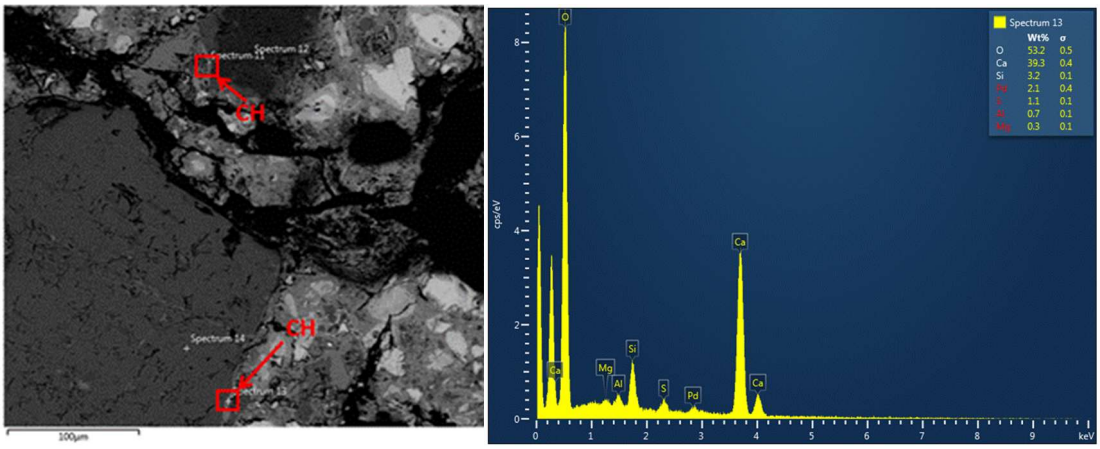

(a) Heated–40: 897°F (481°C)

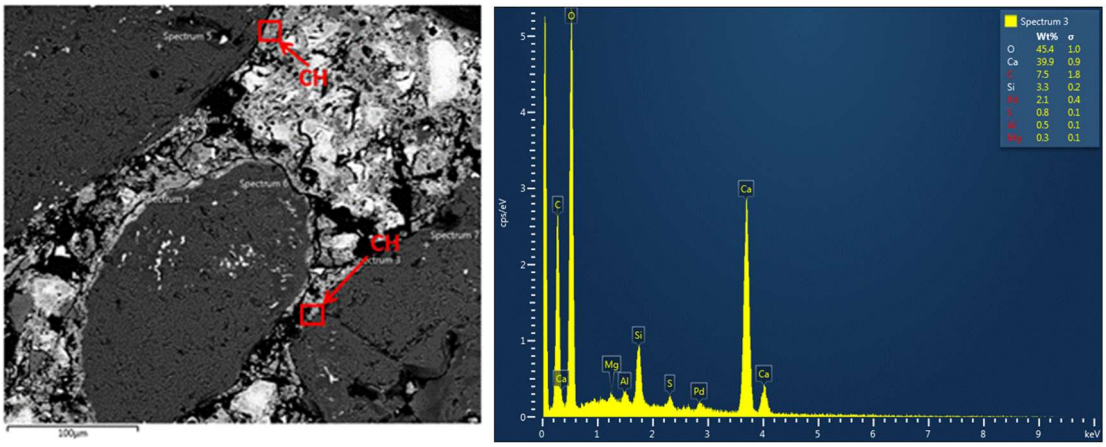

(b) Heated–80: 1186°F (641°C)

Figure B.3 Location of CH deposits as identified by the EDS signals collected at the depth of 0.25 in. from the heat-exposed surface.

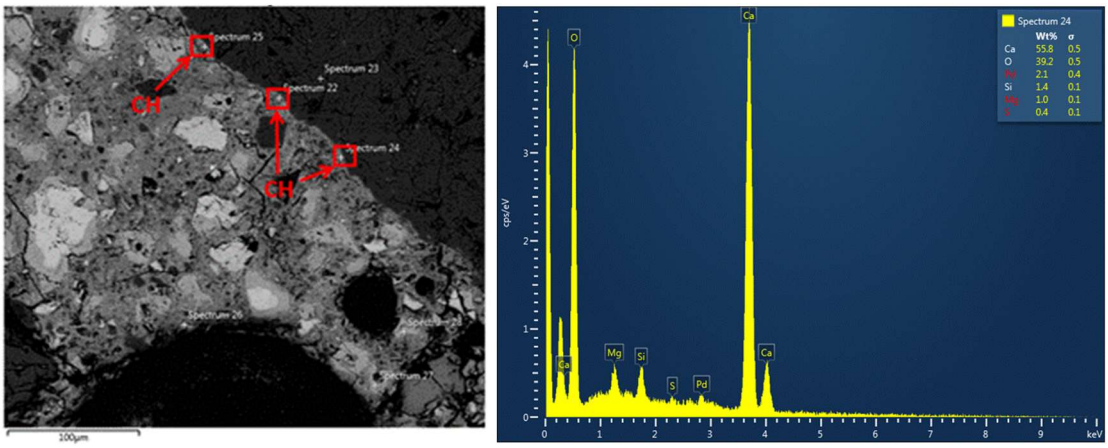

(a) Heated–40: 782°F (417°C)

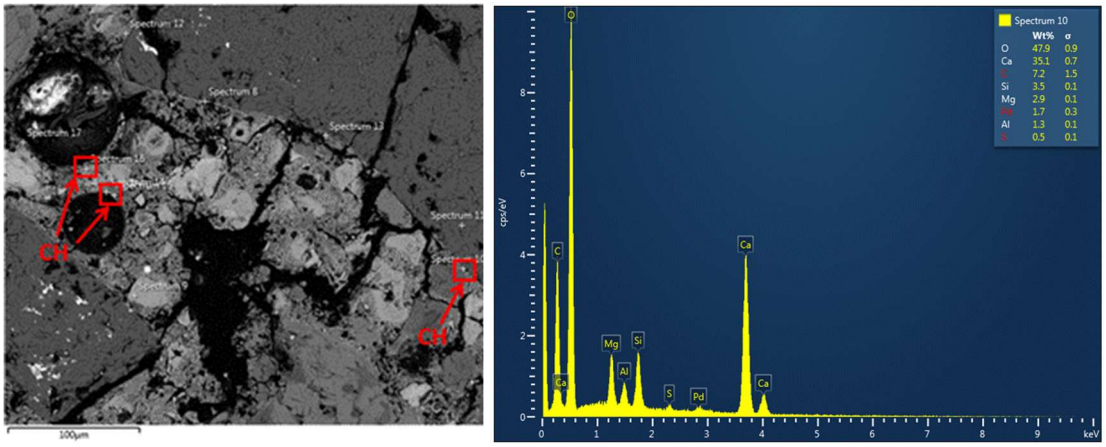

(b) Heated–80: 1,080°F (582°C)

Figure B.4 Location of CH deposits as identified by the EDS signals collected at the depth of 0.5 in. from the heat-exposed surface.

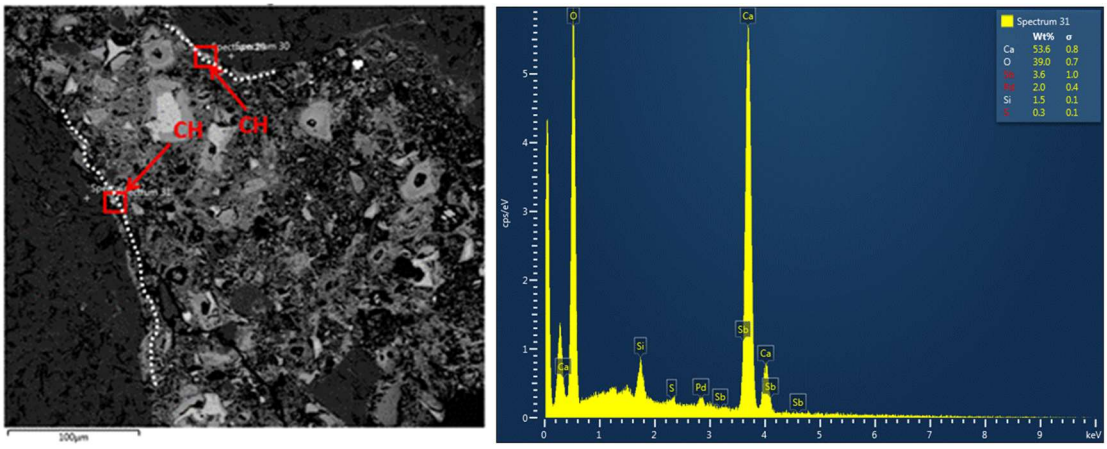

(a) Heated–40: 667°F (353°C)

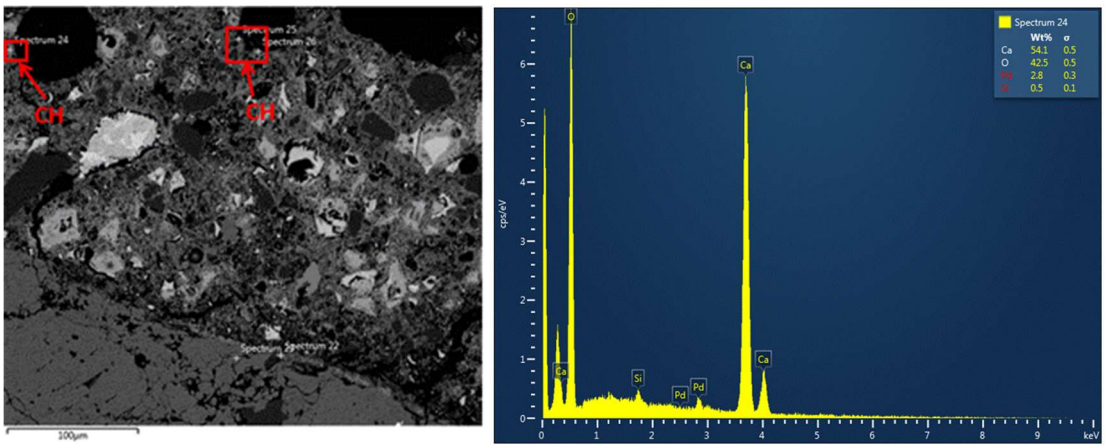

(b) Heated–80: 974°F (523°C)

Figure B.5 Location of CH deposits as identified by the EDS signals collected at the depth of 0.75 in. from the heat-exposed surface.

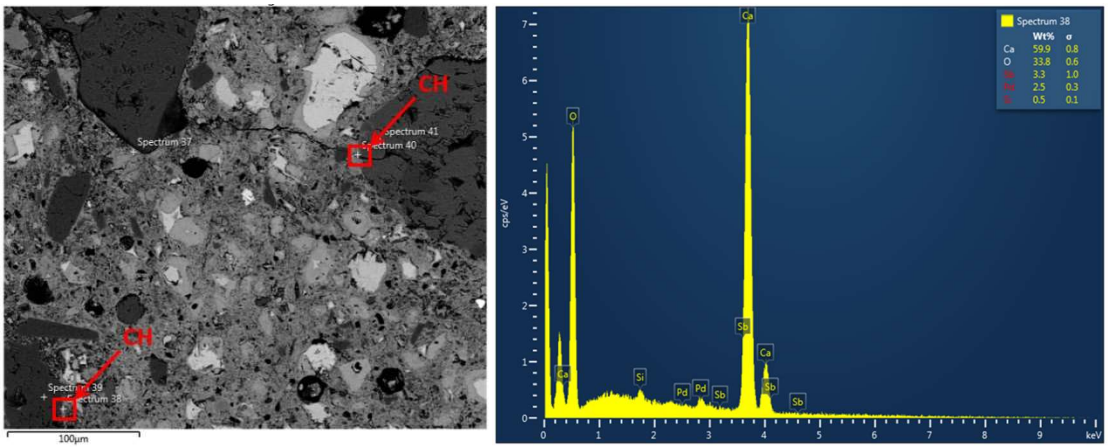

(a) Heated–40: 553°F (289°C)

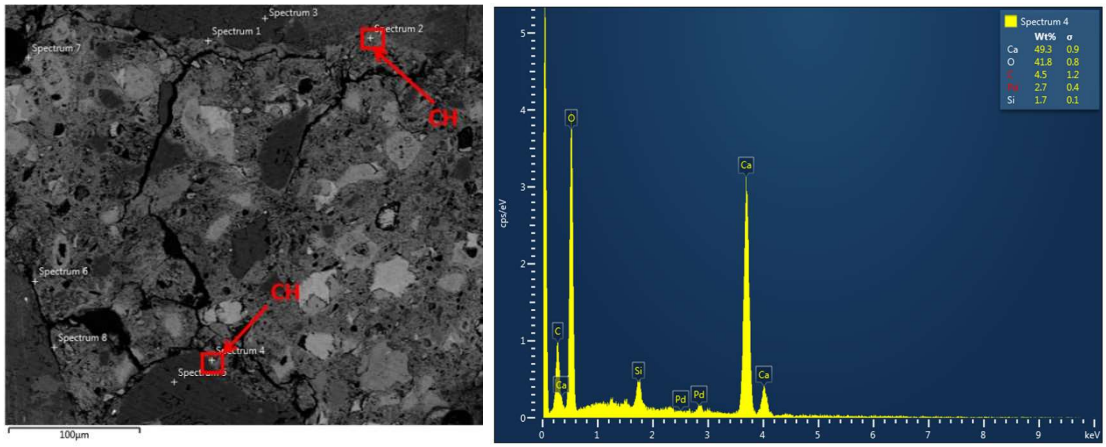

(b) Heated–80: 880°F (471°C)

Figure B.6 Location of CH deposits as identified by the EDS signals collected at the depth of 1.0 in. from the heat-exposed surface.

APPENDIX C. RESULTS OF MICROSTRUCTURAL EVALUATION (SEM/EDS) OF CONCRETE FROM PRISMATIC SPECIMENS

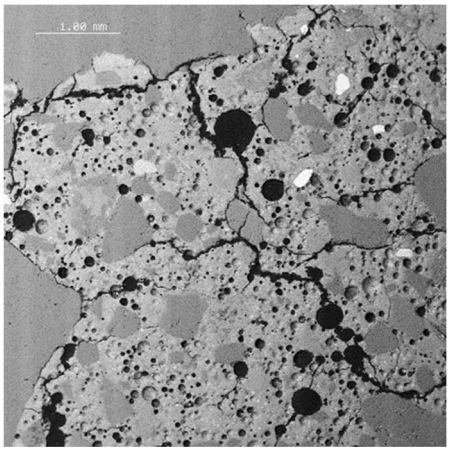

(a) PS1-40: 1,121°F to 796°F (605°C to 424°C)

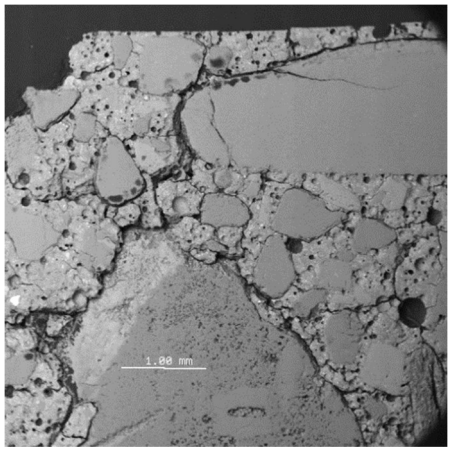

(b) PS2-80: 1,323°F to 1,123°F (717°C to 606°C)

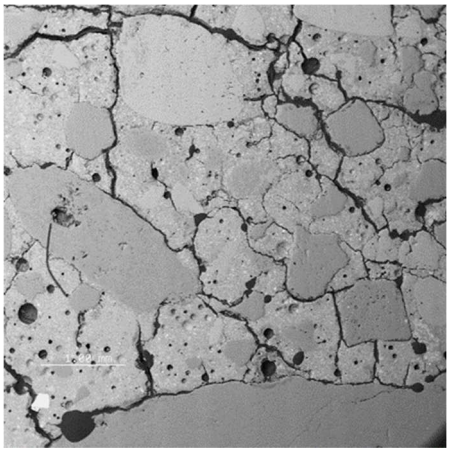

(c) PS3-80: 1,485°F to 976°F (807°C to 524°C)

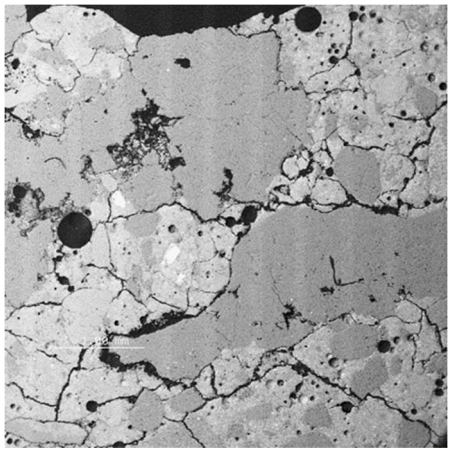

(d) PS4-30: 860°F to 628°F (460°C to 331°C)

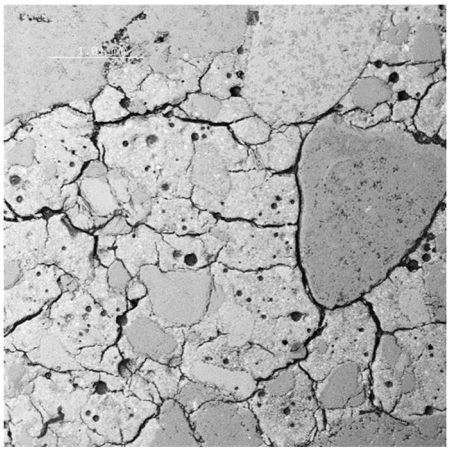

(e) PS5-48

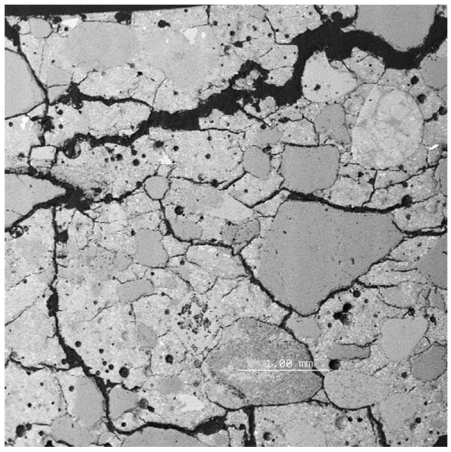

(f) PS6-48

Figure C.1 SEM images of the microstructure of concrete located within 0.0 in. to 0.25 in. from the heated surface.

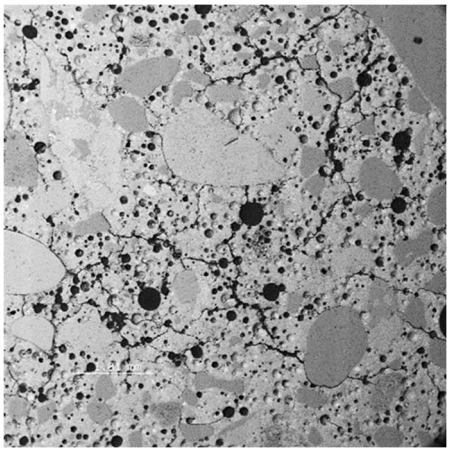

(a) PS1-40: 796°F to 531°F (424°C to 277°C)

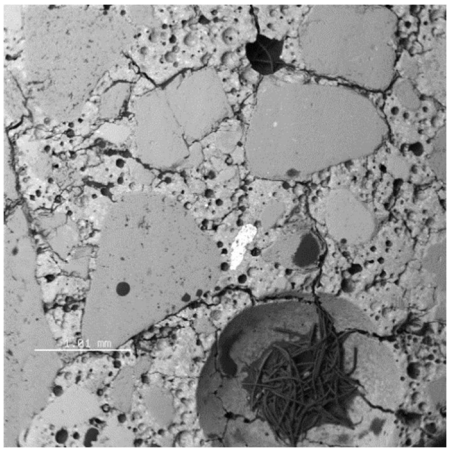

(b) PS2-80: 1,123°F to 871°F (606°C to 466°C)

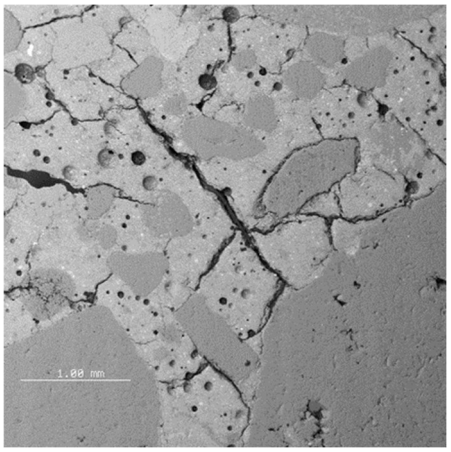

(c) PS3-80: 976°F to 842°F (524°C to 450°C)

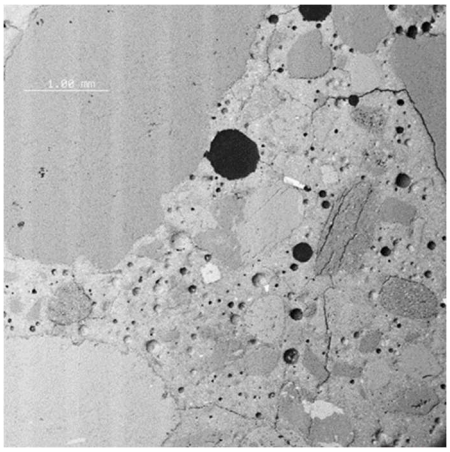

(d) PS4-30: 628°F to 489°F (331°C to 254°C)

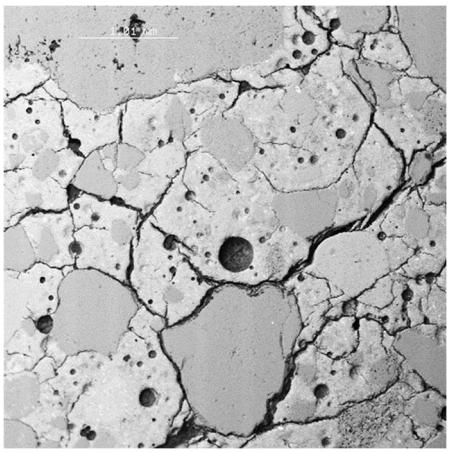

(e) PS5-48

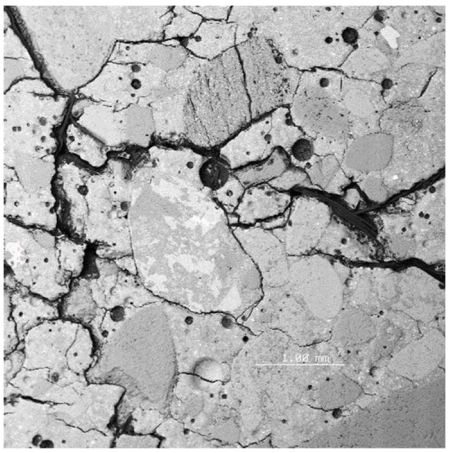

(f) PS6-48

Figure C.2 SEM images of the microstructure of concrete located within 0.25 in. to 0.5 in. from the heated surface.

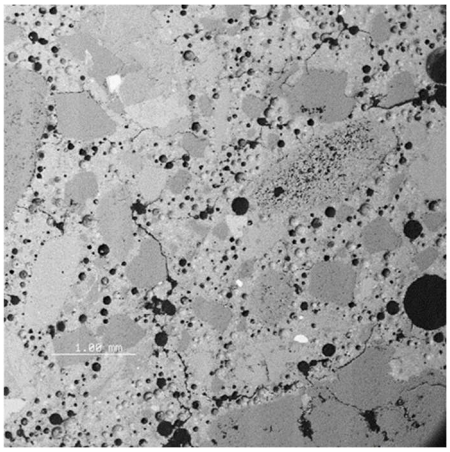

(a) PS1-40: 531°F to 446°F (277°C to 230°C)

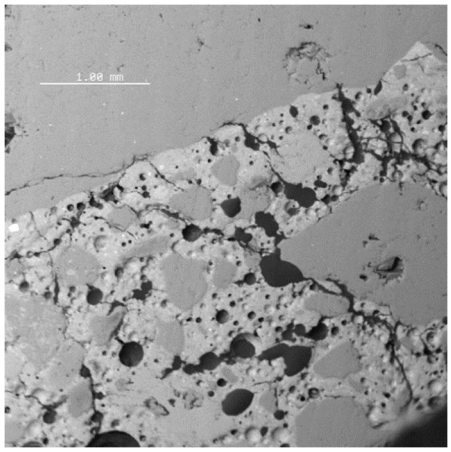

(b) PS2-80: 871°F to 823°F (466°C to 439°C)

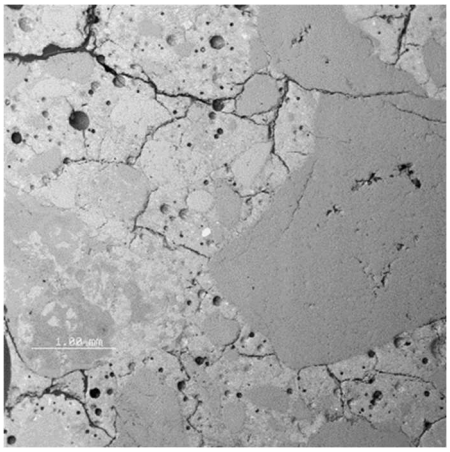

(c) PS3-80: 842°F to 799°F (450°C to 426°C)

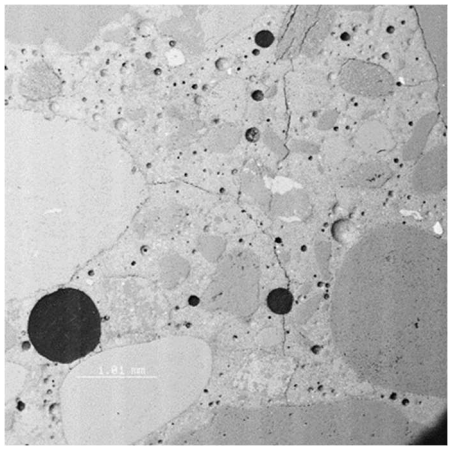

(d) PS4-30: 489°F to 427°F (254°C to 219°C)

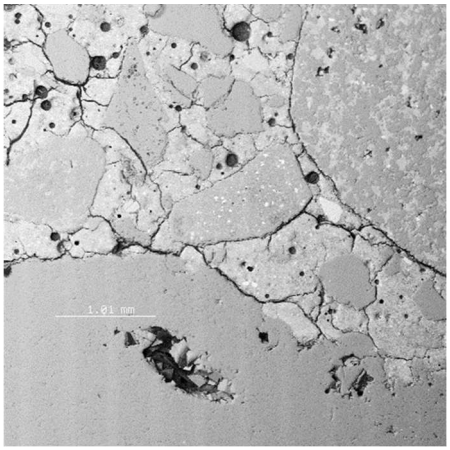

(e) PS5-48

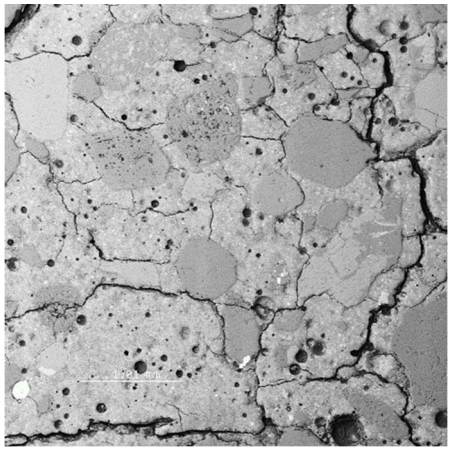

(f) PS6-48

Figure C.3 SEM images of the microstructure of concrete located within 0.5 in. to 0.75 in from the heated surface.

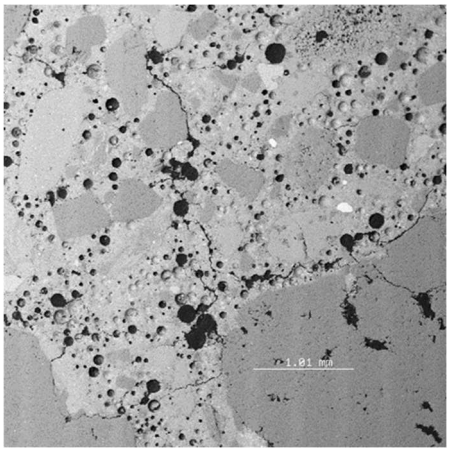

(a) PS1-40: 446°F to 414°F (230°C to 212°C)

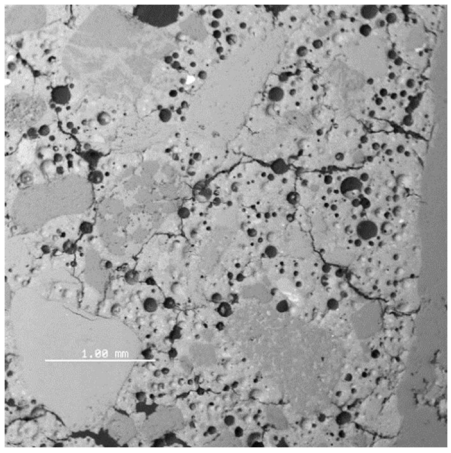

(b) PS2-80: 823°F to 702°F (439°C to 372°C)

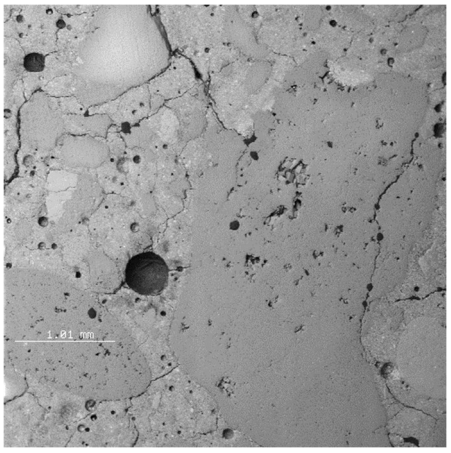

(c) PS3-80: 799°F to 700°F (426°C to 371°C)

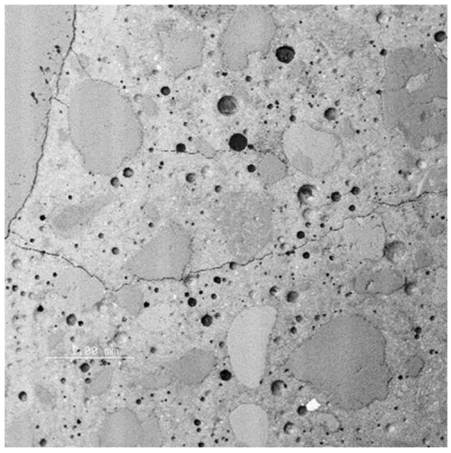

(d) PS4-30: 427°F to 372°F (219°C to 189°C)

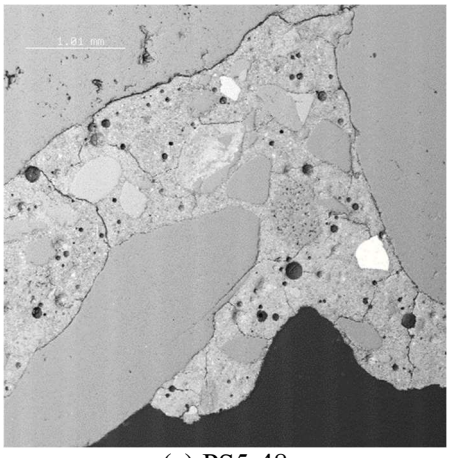

(e) PS5-48

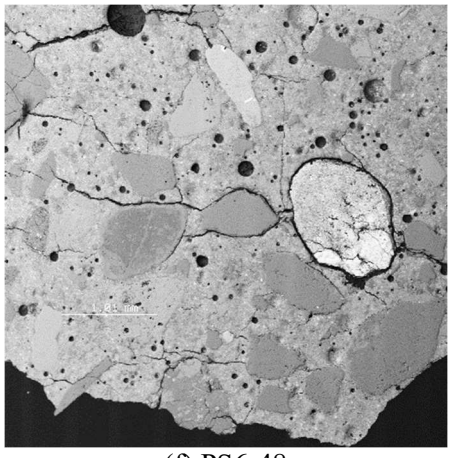

(f) PS6-48

Figure C.4 SEM images of the microstructure of concrete located within 0.75 in. to 1.0 in. from the heated surface.

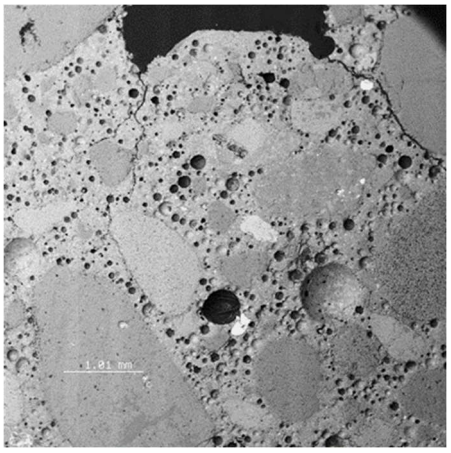

(a) PS1-40: 414°F to 339°F (212°C to 171°C)

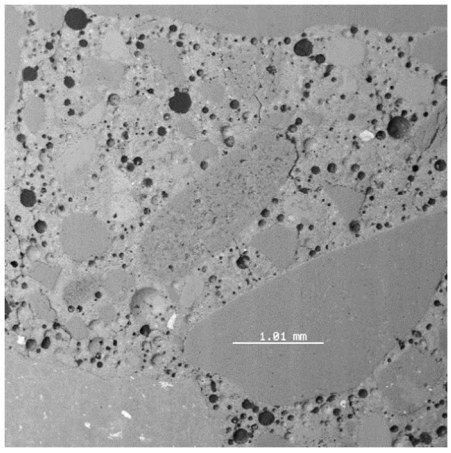

(b) PS2-80: 702°F to 577°F (372°C to 303°C)

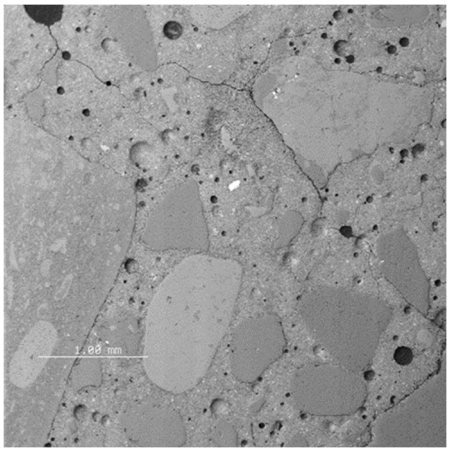

(c) PS3-80: 700°F to 598°F (371°C to 314°C)

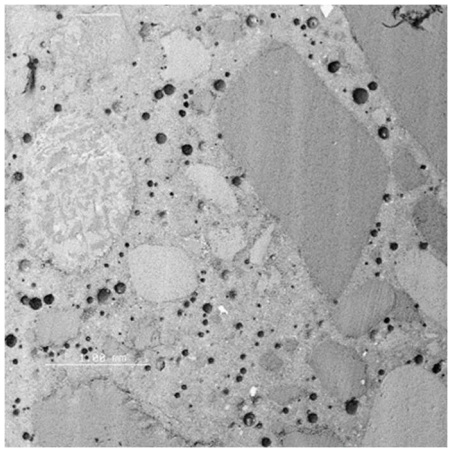

(d) PS4-30: 372°F to 298°F (189°C to 148°C)

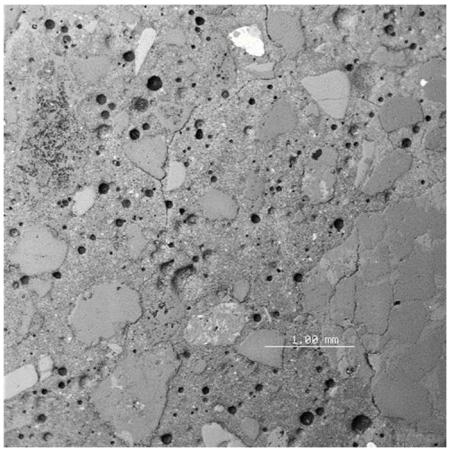

(e) PS5-48

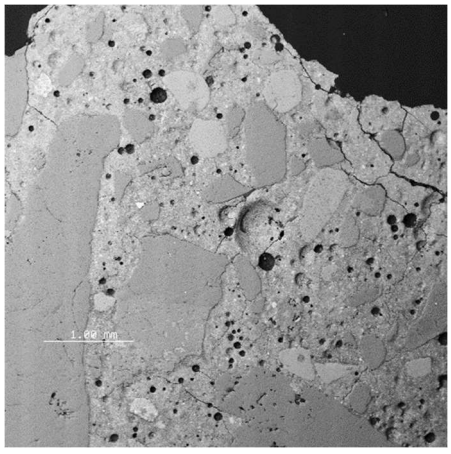

(f) PS6-48

Figure C.5 SEM images of the microstructure of concrete located within 1.0 in. to 1.5 in. from the heated surface.

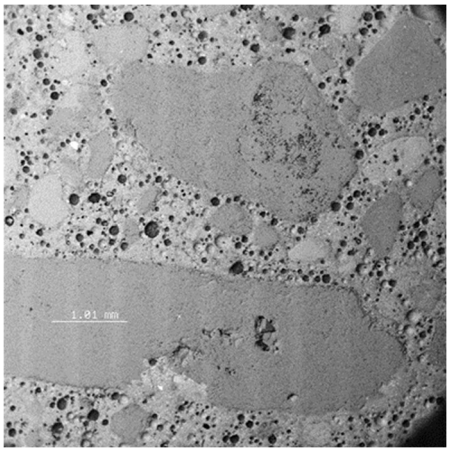

(a) PS1-40: 339°F to 287°F (171°C to 142°C)

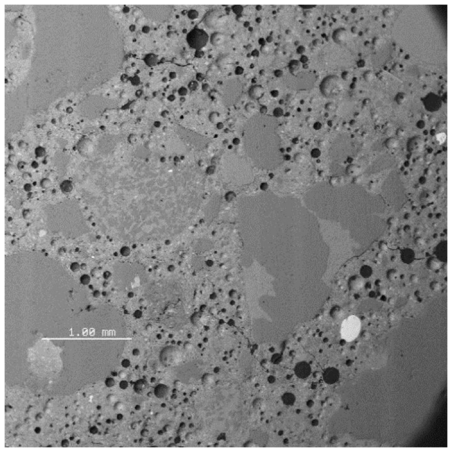

(b) PS2-80: 577°F to 473°F (303°C to 245°C)

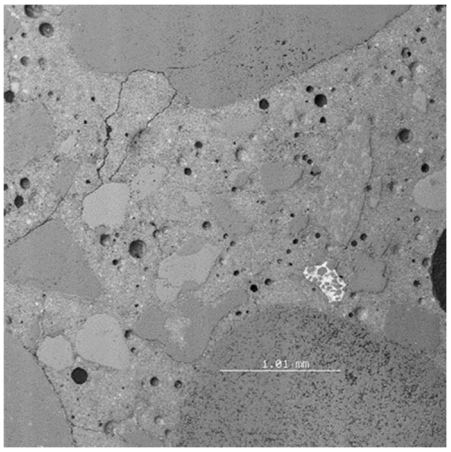

(c) PS3-80: 598°F to 510°F (314°C to 266°C)

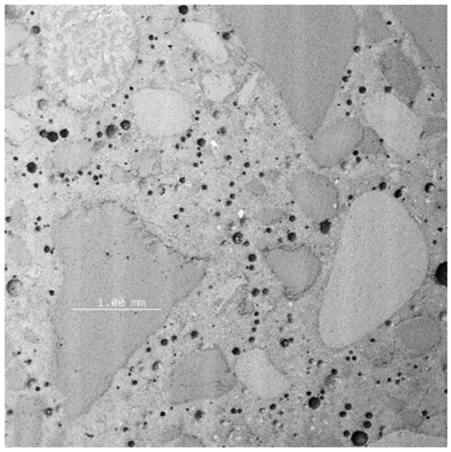

(d) PS4-30: 298°F to 290°F (148°C to 143°C)

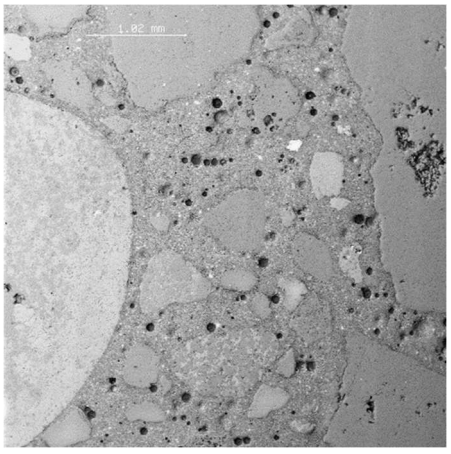

(e) PS5-48

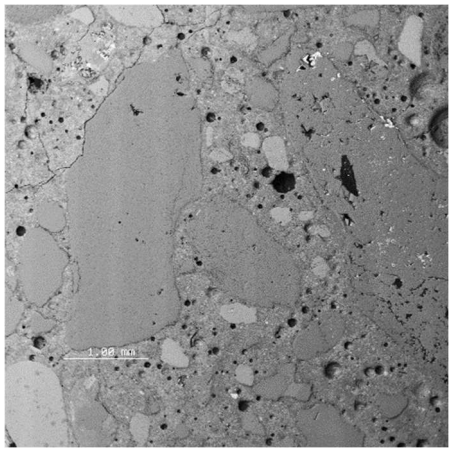

(f) PS6-48

Figure C.6 SEM images of the microstructure of concrete located within 1.5 in. to 2.0 in. from the heated surface.

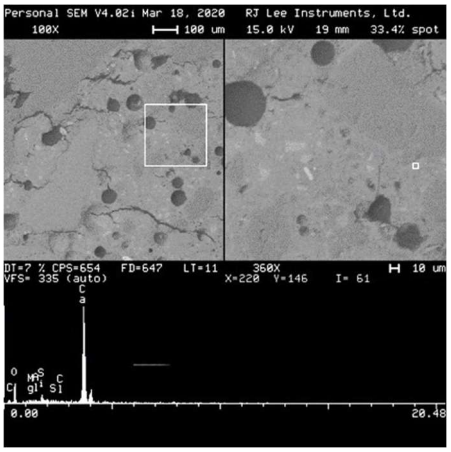

(a) PS1-40: 1,121°F to 796°F (605°C to 424°C)

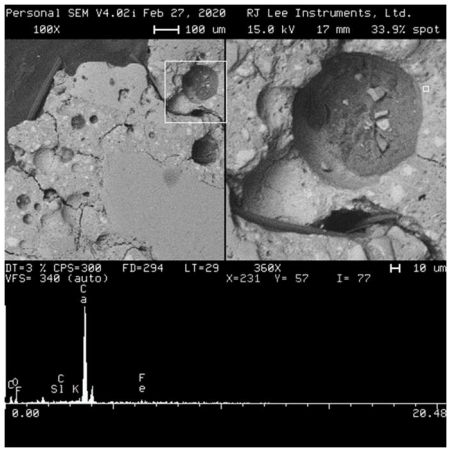

(b) PS2-80: 1,323°F to 1,123°F (717°C to 606°C)

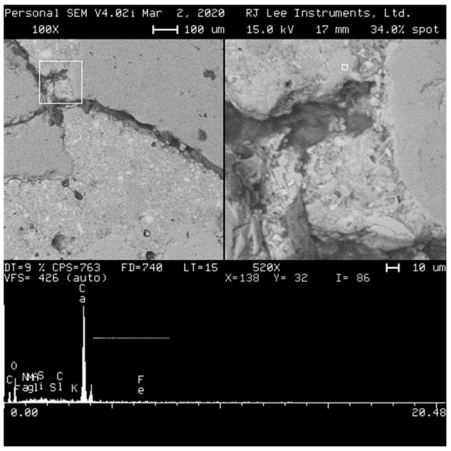

(c) PS3-80: 1,485°F to 976°F (807°C to 524°C)

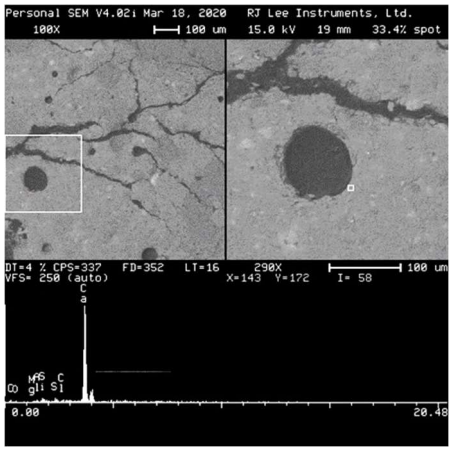

(d) PS4-30: 860°F to 628°F (460°C to 331°C)

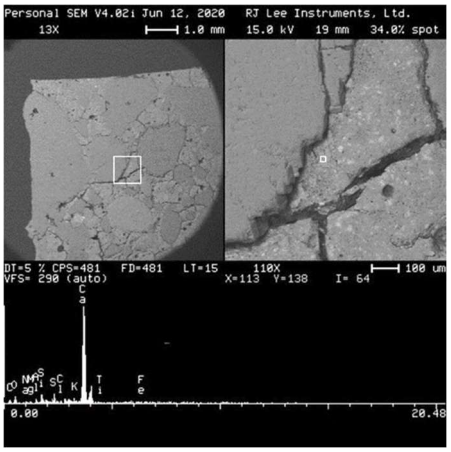

(e) PS5-48

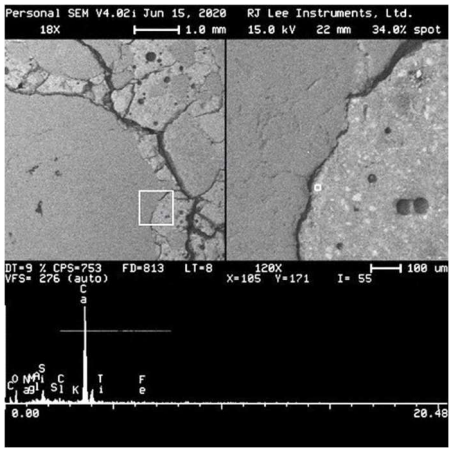

(f) PS6-48

Figure C.7 Deposits of calcium hydroxide (CH) in the microstructure of concrete located within 0.0 in. to 0.25 in. from the heated surface.

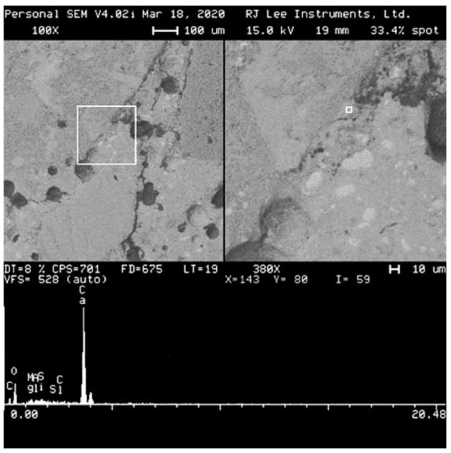

(a) PS1-40: 796°F to 531°F (424°C to 277°C)

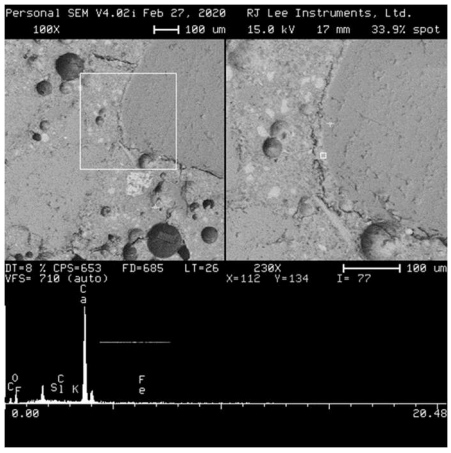

(b) PS2-80: 1,123°F to 871°F (606°C to 466°C)

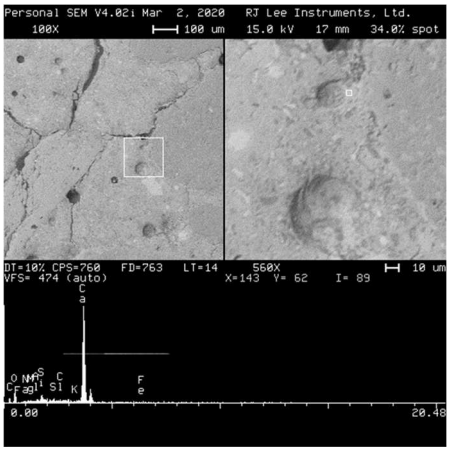

(c) PS3-80: 976°F to 842°F (524°C to 450°C)

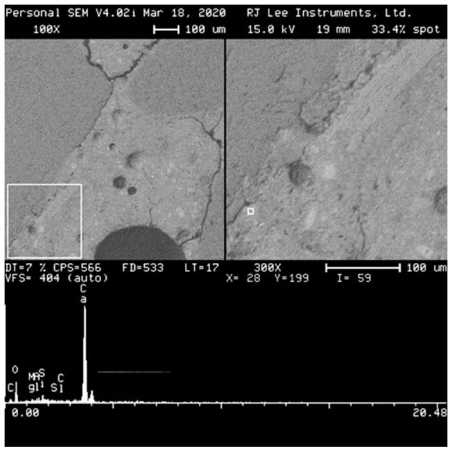

(d) PS4-30: 628°F to 489°F (331°C to 254°C)

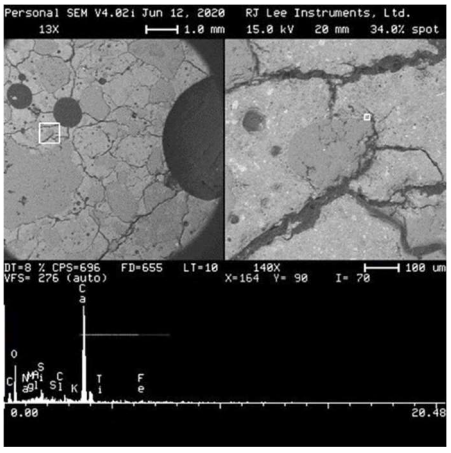

(e) PS5-48

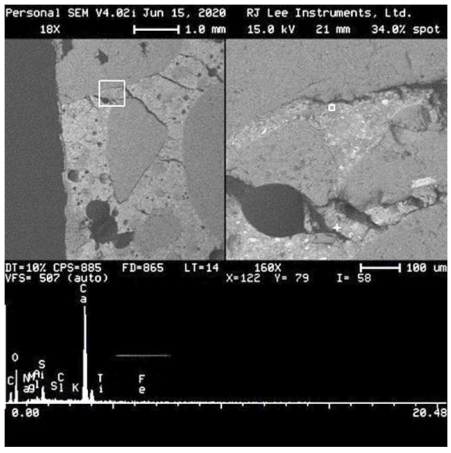

(f) PS6-48

Figure C.8 Deposits of calcium hydroxide (CH) in the microstructure of concrete located within 0.25 in. to 0.5 in. from the heated surface.

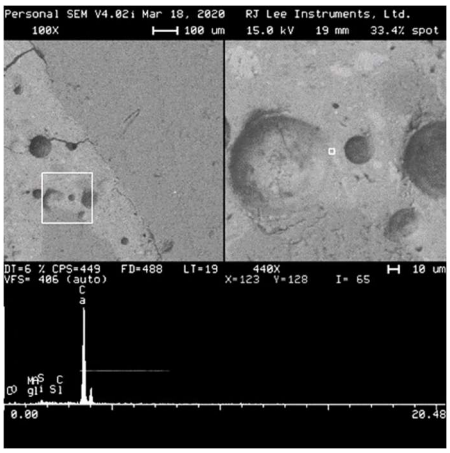

(a) PS1-40: 531°F to 446°F (277°C to 230°C)

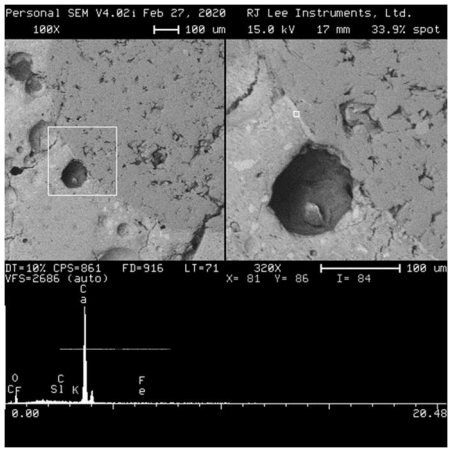

(b) PS2-80: 871°F to 823°F (466°C to 439°C)

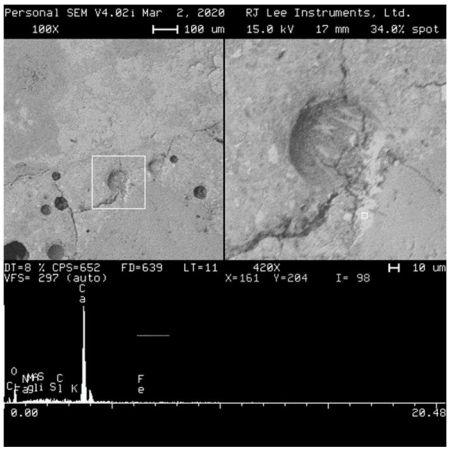

(c) PS3-80: 842°F to 799°F (450°C to 426°C)

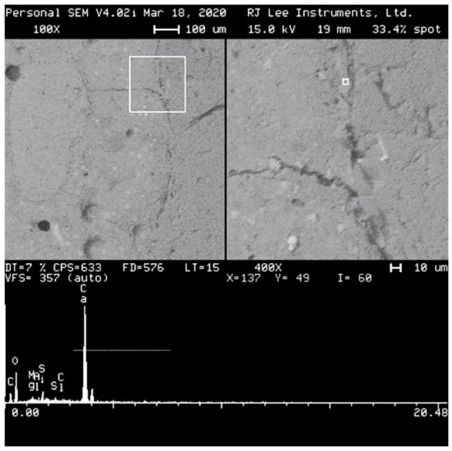

(d) PS4-30: 489°F to 427°F (254°C to 219°C)

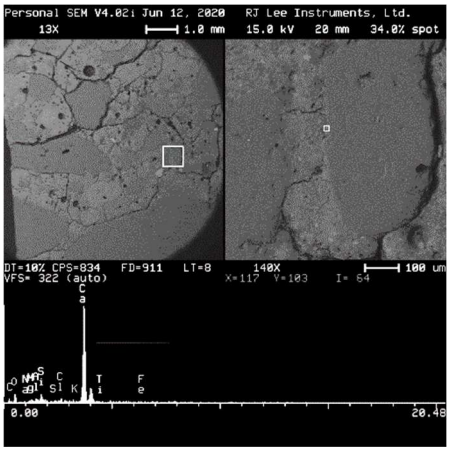

(e) PS5-48

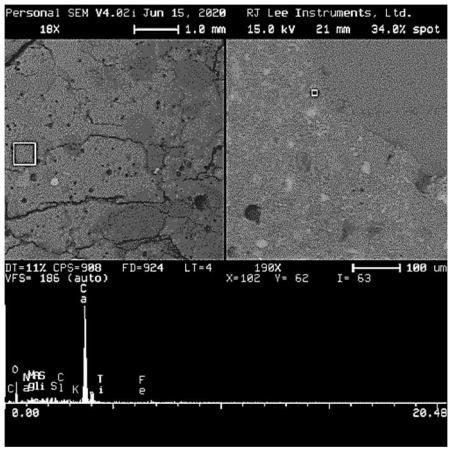

(f) PS6-48

Figure C.9 Deposits of calcium hydroxide (CH) in the microstructure of concrete located within 0.5 in. to 0.75 in. from the heated surface.

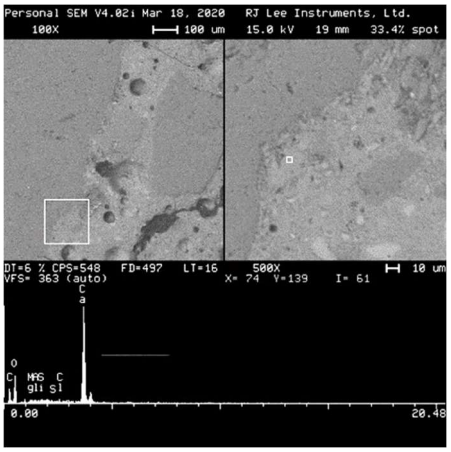

(a) PS1-40: 446°F to 414°F (230°C to 212°C)

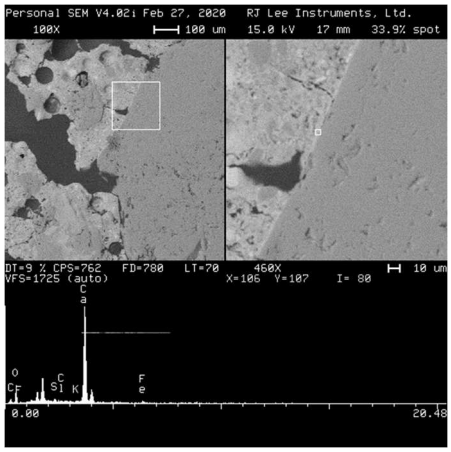

(b) PS2-80: 823°F to 702°F (439°C to 372°C)

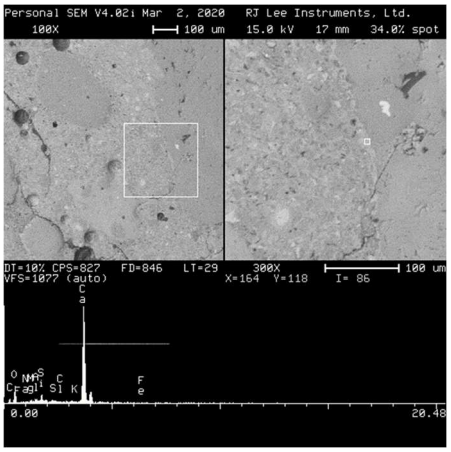

(c) PS3-80: 799°F to 700°F (426°C to 371°C)

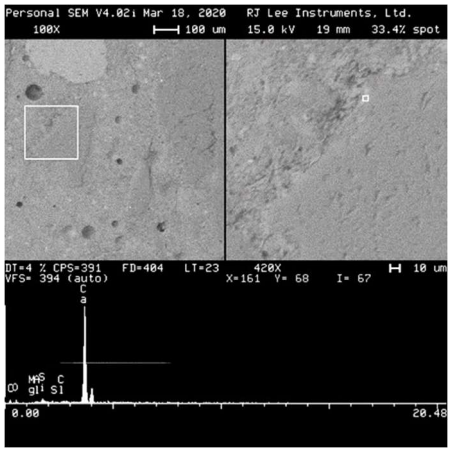

(d) PS4-30: 427°F to 372°F (219°C to 189°C)

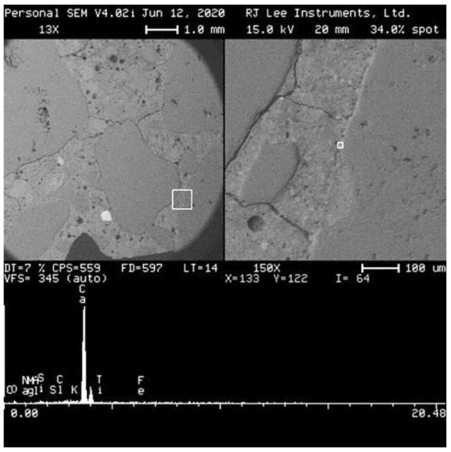

(e) PS5-48

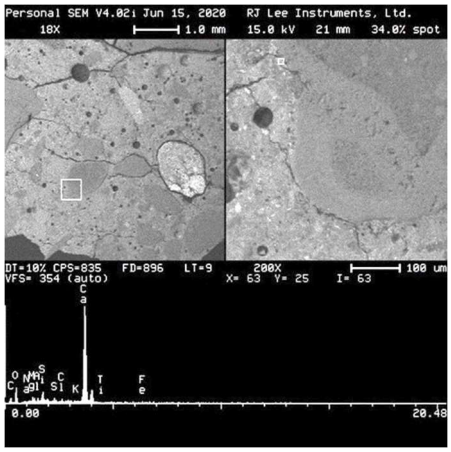

(f) PS6-48

Figure C.10 Deposits of calcium hydroxide (CH) in the microstructure of concrete located within 0.75 in. to 1.0 in. from the heated surface.

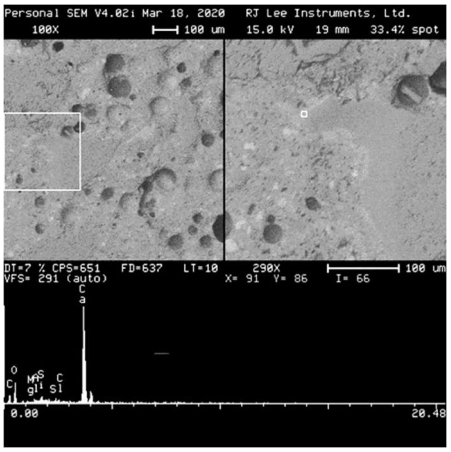

(a) PS1-40: 414°F to 287°F (212°C to 142°C)

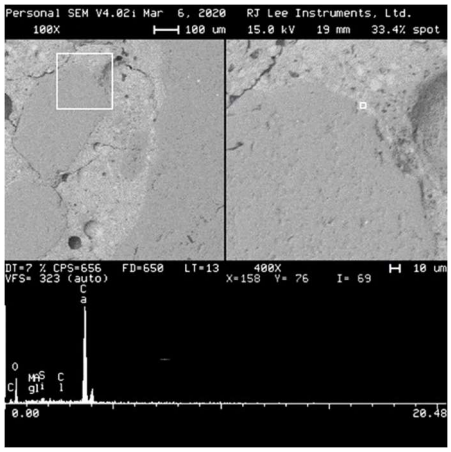

(b) PS2-80: 702°F to 473°F (372°C to 245°C)

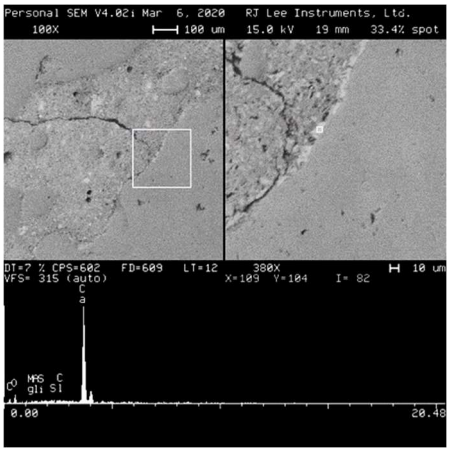

(c) PS3-80: 700°F to 510°F (371°C to 266°C)

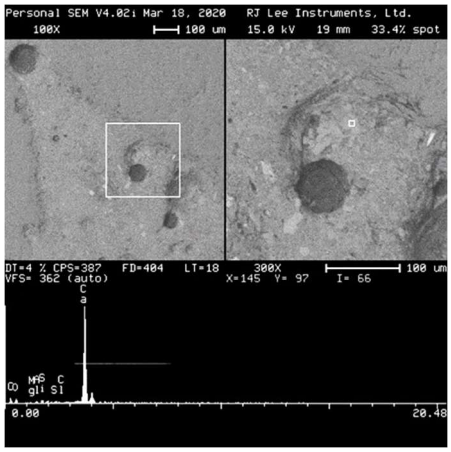

(d) PS4-30: 372°F to 290°F (189°C to 143°C)

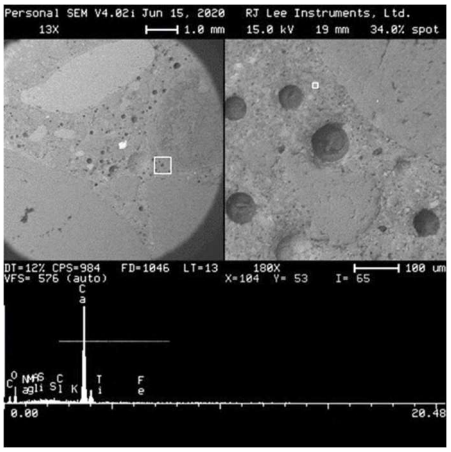

(e) PS5-48

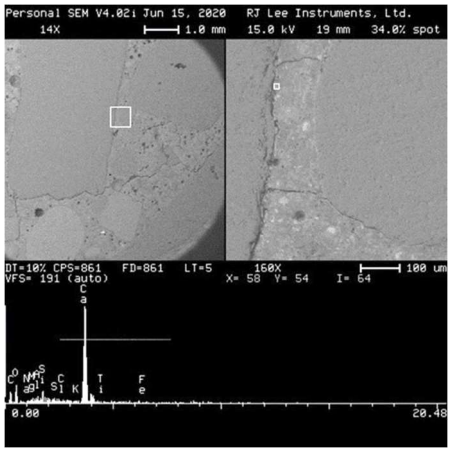

(f) PS6-48

Figure C.11 Deposits of calcium hydroxide (CH) in the microstructure of concrete located within 1.0 in. to 2.0 in. from the heated surface.

APPENDIX D. RESULTS OF MICROSTRUCTURAL EVALUATION (SEM/EDS) OF CONCRETE FROM FULL-SCALE AASHTO TYPE I GIRDERS

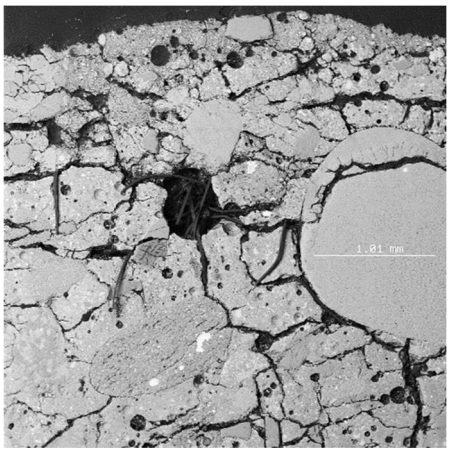

(a) Exposed Surface–0.25 in.

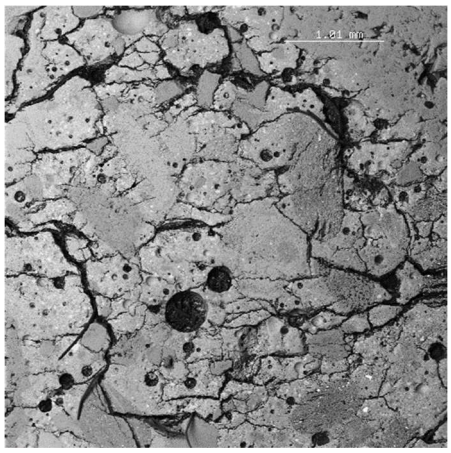

(b) 0.25 in.–0.5 in.

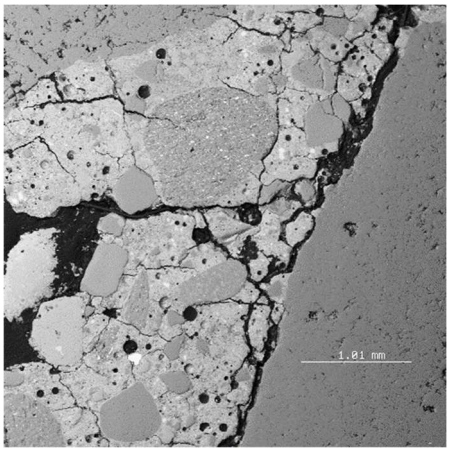

(c) 0.5 in.–0.75 in.

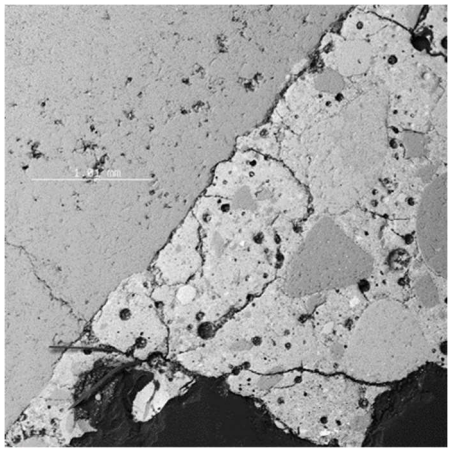

(d) 0.75 in.–1 in.

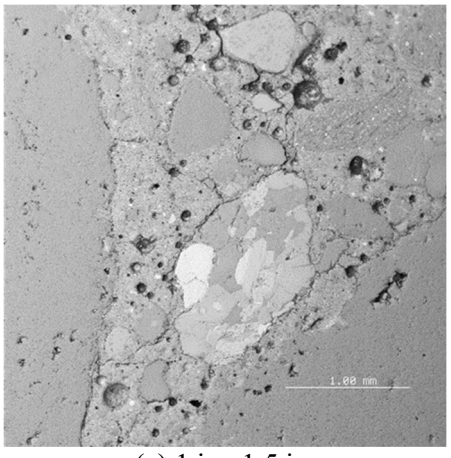

(e) 1 in.–1.5 in.

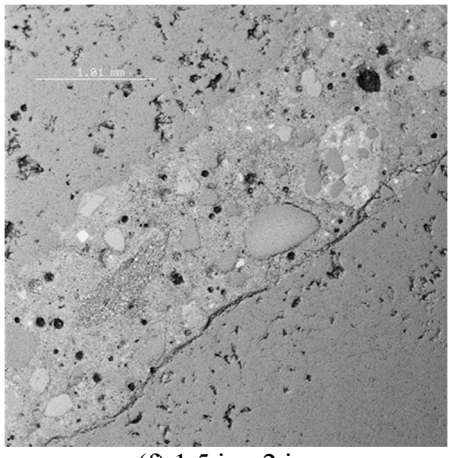

(f) 1.5 in.–2 in.

Figure D.1 SEM images of concrete microstructure from Beam C5.

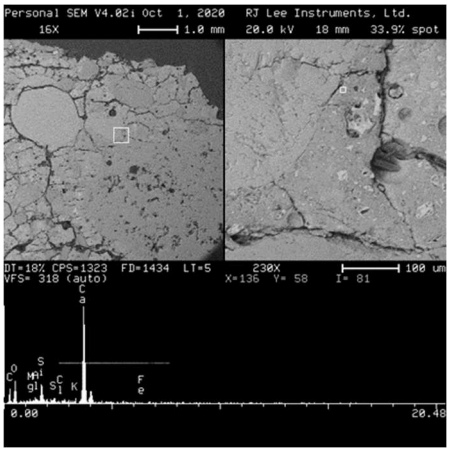

(a) Exposed Surface–0.25 in.

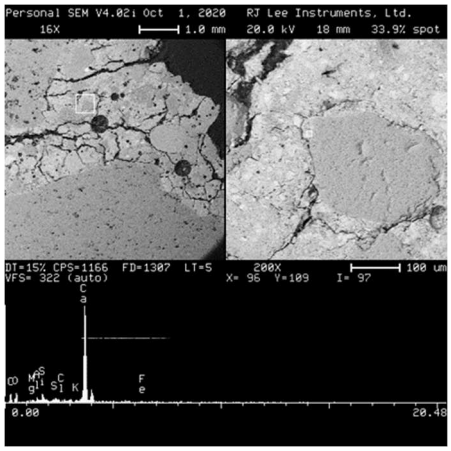

(b) 0.25 in.–0.5 in.

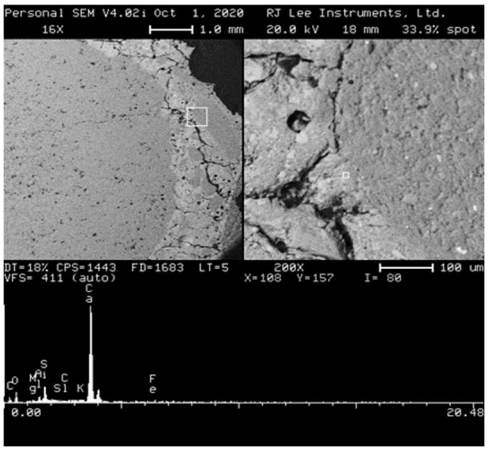

(c) 0.5 in.–0.75 in.

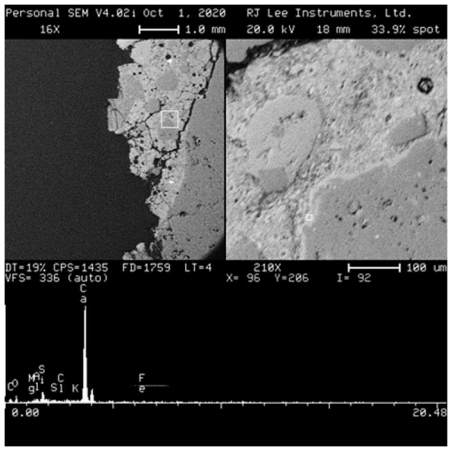

(d) 0.75 in.–1 in.

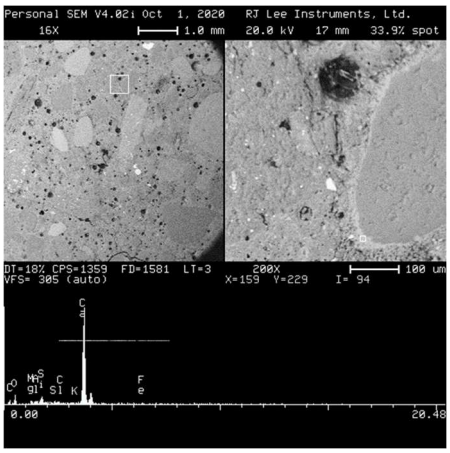

(e) 1 in.–1.5 in.

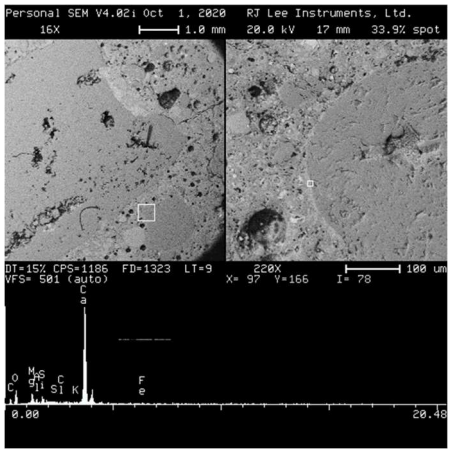

(f) 1.5 in.–2 in.

Figure D.2 Calcium hydroxide (CH) deposits in the microstructure of concrete from Beam C5.

About the Joint Transportation Research Program (JTRP)

On March 11, 1937, the Indiana Legislature passed an act which authorized the Indiana State Highway Commission to cooperate with and assist Purdue University in developing the best methods of improving and maintaining the highways of the state and the respective counties thereof. That collaborative effort was called the Joint Highway Research Project (JHRP). In 1997 the collaborative venture was renamed as the Joint Transportation Research Program (JTRP) to reflect the state and national efforts to integrate the management and operation of various transportation modes.

The first studies of JHRP were concerned with Test Road No. 1—evaluation of the weathering characteristics of stabilized materials. After World War II, the JHRP program grew substantially and was regularly producing technical reports. Over 1,600 technical reports are now available, published as part of the JHRP and subsequently JTRP collaborative venture between Purdue University and what is now the Indiana Department of Transportation.

Free online access to all reports is provided through a unique collaboration between JTRP and Purdue Libraries. These are available at http://docs.lib.purdue.edu/jtrp.

Further information about JTRP and its current research program is available at http://www.purdue.edu/jtrp.

About This Report

An open access version of this publication is available online. See the URL in the citation below.

Varma, A. H., Olek, J., Williams, C. S., Tseng, T.-C., Wang, S., Huang, D., & Bradt, T. (2021). *Post-fire assessment of prestressed concrete bridges in Indiana* (Joint Transportation Research Program Publication No. FHWA/IN/JTRP-2021/05). West Lafayette, IN: Purdue University. https://doi.org/10.5703/1288284317290